MODEL STUDIES ON THE MECHANISMS OF DIOXYGEN ACTIVATION AND OXYGENATION BY HEME-CONTAINING OXYGENASES

TATSUYA MURAKAMI

Department of Molecular Engineering
Graduate School of Engineering
Kyoto University

1998

PREFACE

Bioinorganic chemistry is a field of science which embraces the principles of biology and inorganic chemistry and which has grown tremendously in recent years. This field has important implications for many other sciences, ranging from medicine to the environment. Further, studies of the roles of metal ions in biological systems often involves the development of relevant chemistry, new methodologies of investigation, and the application of advanced physical techniques.

Metalloenzymes that can activate dioxygen by electron transfer from the metal to dioxygen and incorporate one of the oxygen atoms of the activated dioxygen into various substrates are designated as "monooxygenases." Especially, heme-containing-monooxygenases catalyze many chemical reactions *in vivo*. The function of these enzymes varies from case to case depending on the nature of the heme proximal ligand, the heme environment, and the substrate, though the same prosthetic group, heme, is shared.

This thesis contains collected papers and discussions of my studies at Department of Molecular Engineering, Graduate School of Engineering, Kyoto University during 1993 - 1998. The aim of this thesis is to clarify the relationship between structure and function of heme-containing monooxygenases and to elucidate the effects of the heme environmental structure determining the heme electronic structure on the O_2 activation. This thesis is divided in 6 parts. Part I contains a survey of the heme-containing monooxygenases and describes sufficient background and significance of these studies. Part II deals with the electronic structure and function of oxo-iron(V) porphyrin complexes as models for reaction intermediate in the catalytic cycle of P-450. In this part, effects of electron-withdrawing groups bound to the porphyrin ring and axial ligation on the electronic configuration of the reaction intermediate are examined. Part III provides studies for understanding the mechanism of the suicidal *meso*-hydroxylation of heme catalyzed by heme oxygenase. Part IV describes structures and functions of site-directed mutant myoglobins as models for heme-heme oxygenase complex. In Part V, the relationship between conformational change upon the substrate binding to heme oxygenase and its function has been studied. Finally, summary and general aspects of the present work are discussed in Part VI.

ACKNOWLEDGMENTS

I would like to express my gratitude to Professor Isao Morishima for his kind guidance, invaluable suggestions, and heartily encouragement throughout the course of the studies. It is also my great pleasure to thank Professor Yoshihito Watanabe for his excellent guidance and fruitful discussions. I am indebted to Associate Professor Koichiro Ishimori for helpful suggestions and comments. I also wish to thank Dr. Satoshi Takahashi for his valuable discussion and encouragement.

It should be emphasized that the studies in this thesis have required the collaboration in a number of investigations. I appreciate the help received from Professor Teizo Kitagawa and Dr. Tadashi Ogura with resonance Raman measurements, Dr. Hiroshi Hori, and Dr. Futoshi Masuya with ESR measurements, Dr Seiji Ogo with ESI mass measurements, and Mr. Yasuaki Hisamoto with FAB mass measurements.

This studies would not have been possible without help of the members of not only Molecular Design Group but also the groups in Institute for Molecular Science and Kurume University. I wish to thank Dr. Shinichi Ozaki and Mr. Toshitaka Matsui in Institute for Molecular Science and Professor Masato Noguchi, Dr. Yoshiaki Omata, and Dr. Hiroshi Sakamoto for providing me with the samples and for valuable advice. I gratefully acknowledge helpful discussions and collaboration of Dr. Kazuya Yamaguchi. I am also obliged to Masahiro Yamada for his generous collaboration. I also express my heartily thanks to Mr. Yoshio Goto for his help in various spectroscopic measurements. Grateful acknowledgment is given to Drs. Shinji Ozawa, Shingo Nagano, and Keisuke Wakasugi and Messrs. Masaaki Aoki, Eigo Sakamoto, Kenji Machii, Kenji Inaba, Takeshi Uchida, Taro Ichikawa, Michihiro Izuta, Motomasa Tanaka, Takaki Hatsui, Keiko Matsuda, Yoichi Sugiyama, Jin Nakatani, Shiro Yoshioka, Masanobu Ihara, Hirotaka Kataoka, Atsushi Morimoto, Mitsuru Murata, Shu-ji Akiyama, Haruto Ishikawa, Shino Kondo, Yoshiaki Furukawa, Jun Inoue, Hiroaki Tanioka, Manabu Teramoto, and Tetsushi Nakano. I am also grateful to Mr. Haruyuki Harada for his intruction and assistance in the NMR measurements.

Finally, I express my greatest gratitude to my parents and sister for their unfailing understanding and affectionate encouragement.

Tatsuya Murakami

LIST OF PUBLICATIONS

PART II

CHAPTER 1. A New Active Intermediate in Monooxygenations
Murakami, T.; Watanabe, Y.; Morishima, I. Submitted for publication (*Bull. Chem. Soc. Jpn.*)

PART III

CHAPTER 1. A Novel *Meso*-Oxygenation of an Iron Porphyrin Complex Related to *Meso*-Hydroxylation Catalyzed by Heme Oxygenase
Murakami, T.; Watanabe, Y.; Morishima, I. *Chem. Lett.* **1998**, 27-28.

CHAPTER 2. New Oxidation Reaction of a Iron Porphyrin Complex Related to Heme Catabolism.
Murakami, T.; Watanabe, Y.; Morishima, I. *J. Inorg. Biochem.* **1997**, *67*, 97.

Mechanistic Studies of Suicidal *meso*-Oxidation of Novel Iron Porphyrin Complexes as Models for the Formation of α-*Meso*-Hydroxyheme by Heme Oxygenase.
Murakami, T.; Watanabe, Y.; Morishima, I. Submitted for publication (*J. Am. Chem. Soc.*).

PART IV

CHAPTER 1. Effects of the Arrangement of a Distal Histidine on Regioselectivity of the Coupled Oxidation of Sperm Whale Myoglobin Mutants
Murakami, T.; Morishima, I.; Matsui, T.; Ozaki, S.; Watanabe, Y. *Chem. Commun.* in press.

Effects of the Arrangement of a Distal Catalytic Residue on Regioselectivity and Reactivity in the Coupled Oxidation of Sperm Whale Myoglobin Mutants
Murakami, T.; Morishima, I.; Matsui, T.; Ozaki, S.; Watanabe, Y. Submitted for publication (*J. Am. Chem. Soc.*).

CHAPTER 2. Alteration of Sperm Whale Myoglobin Distal Site Mimicking Heme Oxygenase.
Murakami, T.; Watanabe, Y.; Morishima, I. Submitted for publication (*Biochemistry*).

PART V

CHAPTER 1. Substrate-Induced Conformational Change in Heme Oxygenase.
Murakami, T.; Morishima, I.; Watanabe, Y; Sakamoto, H.; Omata, Y.; Noguchi, M. Submitted for publication (*J. Biol. Chem.*).

CONTENTS

PART I.

GENERAL INTRODUCTION

The enzymes that catalyze the introduction of oxygen atom(s) from dioxygen to organic molecules are designated as "oxygenases". The oxygenases can be further classified into two categories, monooxygenases and dioxygenases, depending on whether one or both oxygen atoms from

monooxygenase: $XH + {}^{*}O_2 + AH_2 \rightarrow X({}^{*}O)H + H_2{}^{*}O + A$

dioxygenase: $XH + {}^{*}O_2 \rightarrow X({}^{*}O_2)H$

dioxygen are incorporated into substrate,[1] where XH and AH_2 represent a substrate and an electron donor, respectively. Especially, monooxygenases require two electrons to reduce the second oxygen atom of dioxygen to water, and thus are sometimes called "mixed-function oxidase" or "mixed-function oxygenases" since they function as oxygenase and oxidase.

Examples of the monooxygenases containing heme, an iron porphyrin complex, as the prosthetic group include P-450, heme oxygenase (strictly the substrate-enzyme complex), and secondary amine monooxygenase. These enzymes reversibly bind O_2 to the ferrous heme iron, and yield a O_2-bound complex that is generally described as either $Fe^{II}O_2$ or $Fe^{III}O_2^{\bullet-}$ or a resonance hybrid of these two forms ($Fe^{II}O_2 \leftrightarrow Fe^{III}O_2^{\bullet-}$). The subsequent one-electron reduction of the bound oxygen to the heme iron forms an active intermediate responsible for each monooxygenation. Mechanisms of the activation of the bound oxygen to the heme iron and of the monooxygenation by the active intermediate are believed to be controlled and modulated by the heme environmental structures such as the axial ligand of the heme iron, arrangement of amino acid residues in the close vicinity of the heme, etc. Thus, numerous attempts have been conducted to characterize the active intermediates and to understand the detailed monooxygenation mechanisms. Unfortunately, these problems have not been fully clear yet, and remained open to further studies.

The barrier to detailed mechanistic studies of the enzymes is imposed by difficulties in detecting the active intermediate with very short lifetime, and by incomplete information about the active site structure which controls an enzyme function such as the reactivity and regioselectivity. Utilization of synthetic model complexes mimicking the active site of these enzymes is eminently suitable to investigate the electronic structure and formation mechanism of such unstable intermediates. Furthermore, myoglobin, which is one of the simplest heme proteins and reversibly binds molecular oxygen in its ferrous form for the storage, is a good

starting hemoprotein to mimic various heme enzymes because of large accumulation of the spectroscopic and crystallographic data. Therefore, active site mutants of myoglobin are also useful to elucidate structure-function relationships of the heme-containing monooxygenases.

In this thesis, I have mainly examined the mechanisms of O_2 activations and oxygenations by two heme-containing oxygenases, P-450 and heme oxygenase, by employing model systems constructed by both synthetic iron porphyrin complexes and active site mutants of myoglobin.

P-450 is generally membrane bound and have been found in virtually every mammalian tissue and organ as well as plants, animal, yeast, and bacteria.[2] The best characterized P-450 is soluble camphor-metabolizing $P\text{-}450_{cam}$ isolated from *Pseudomonas putida*.[3] P-450s share a common reaction cycle with four well-characterized intermediates (**1** → **4**, Scheme 1).[3,4] The resting form of the enzyme is a six-coordinate low-spin ferric state (**1**), with water (or hydroxide) as the exchangeable distal ligand trans to the proximal cysteinate. Substrate binding yields the five-coordinate high-spin ferric state (**2**), which has a vacant coordination site that will ultimately be available for dioxygen binding. Conversion of the ferric iron from low to high spin results in a significant increase in the redox

Scheme 1

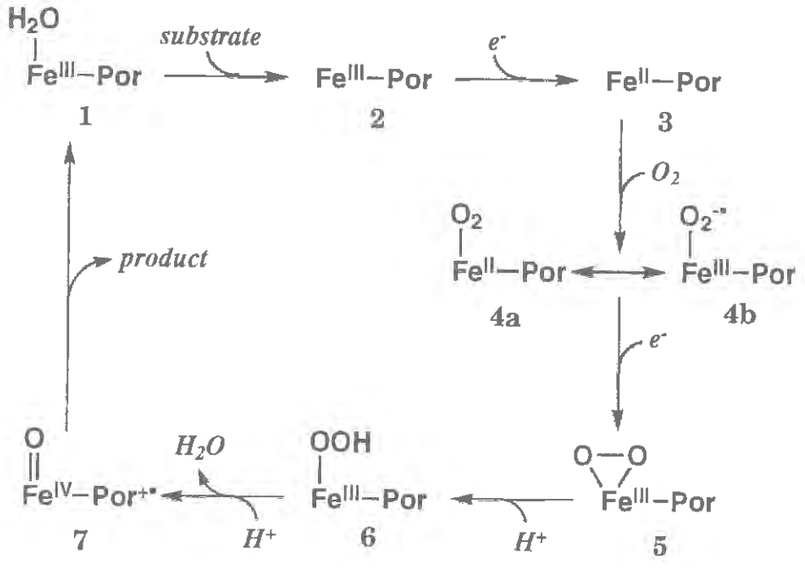

Por: porphyrin

potential ($E^{c'}$) of the enzyme heme (-330 to -173 mV vs NHE). Thus substrate binding facilitate electron transfer from reduced putidaredoxin ($E^{c'}$ = -193 mV) to the ferric P-450 heme to generate the five-coordinate high-spin deoxyferrous state (**3**). Dioxygen then binds to the ferrous enzyme heme iron to form the oxyferrous complex, whose valence structure can be represented either as the ferrous-O_2 (**4a**), or as the ferric-superoxide (**4b**) complex as described above. Addition of the second electron to **4**, the rate-limiting step in the cycle,[5] is proposed to yield a ferric peroxide adduct (**5a**), which can be protonated to give a hydroperoxide complex (**6**). A second protonation of the same oxygen then leads to heterolytic O-O bond cleavage releasing water and generating a proposed oxo-ferryl ($O=Fe^{IV}$) porphyrin radical intermediate (**7**) which is equivalent to the high-valent iron-oxo intermediate of peroxidase enzymes called compound I. The P-450 reaction cycle is completed when **7** transfers an oxygen via a rebound mechanism to give an oxygenated product and to regenerate **1**.[6]

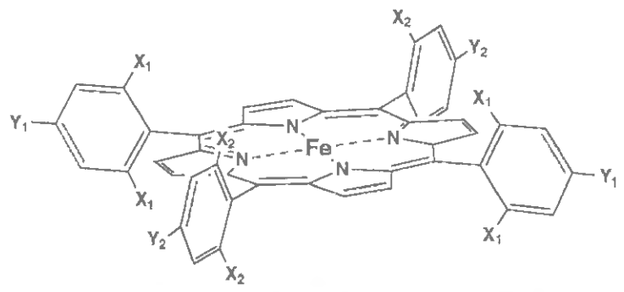

1a : $X = Y =$ Me
1b : $X =$ Cl, $Y =$ H
1c : $X_1 =$ H, $Y_1 =$ Cl, $X_2 = Y_2 =$ Me

Figure 1. Synthetic model complexes

The mechanism of oxygen activation by P-450 has been extensively studied; however, the crucial intermediate (**6**) in the catalytic cycle is too unstable to examine their electronic structure and reactivity.[5] Accordingly, model systems for P-450 with synthetic metalloporphyrins have illuminated the enzymic reaction mechanism. The first successful

application of synthetic iron porphyrins for the P-450-type oxidation was reported by Groves et al. in 1979.[7] Further, Groves et al. prepared an active intermediate responsible for the P-450-type oxidations by the reaction of Fe^{III}TMP(Cl) [TMP: 5,10,15,20-tetrakis(mesityl)porphyrin] (Figure 1a) with a peracid at low temperature and characterized it as an oxo-ferryl porphyrin cation radical, $O=Fe^{IV}Por^{+\bullet}$, which is formally two-electron oxidized from the iron(III) state.[8] The key development was the use of iron porphyrin with bulky mesityl groups at the *meso*-positions to prevent oxidative degradation of the complex. Since then, ferric porphyrin *N*-oxides[9] and ferric porphyrin dications[10] have been prepared as models for isoelectronic structures of the oxo-ferryl porphyrin cation radical, but they are not able to oxidize hydrocarbons and olefins. Only the oxo-ferryl species can oxidize hydrocarbons and olefins, indicative of the active intermediate in the catalytic cycle of P-450 being oxo-ferryl porphyrin cation radical, while an oxo-perferryl porphyrin complex ($O=Fe^{V}Por$) remains as an alternative candidate. In Chapter 1 of Part II, detailed electronic structure of the oxo-perferryl porphyrin complex prepared by using an iron porphyrin complex illustrated in Figure 1b is discussed by various spectroscopies. Further, monooxygenation activity of this new active intermediate is compared with that of the oxo-ferryl porphyrin cation radical.

Although a large number of mechanistic studies have been made on the oxo-ferryl porphyrin cation radical, little is known about the detailed mechanism of the oxo-perferryl porphyrin complex formation. Thus, we also describe a mechanism discriminating between oxo-perferryl porphyrin complex and oxo-ferryl porphyrin cation radical.

Heme oxygenase (HO), first characterized by Schmid and co-workers,[11] is a microsomal enzyme which catalyzes the first key step in heme catabolism, the oxidative degradation of heme (iron-protoporphyrin IX) to biliverdin and carbon monoxide.[12] The catalytic cycle consists of several steps involving two well-characterized intermediates: α-*meso*-hydroxyheme and verdoheme. The enzyme can be purified from several different organ sources including liver,[13] spleen,[14] brain,[15] and testis.[15] Though it has two known isoforms, referred to as HO-1 (33 kDa) and HO-2 (36 kDa),[15,16] it is generally assumed that they have similar active sites and share a similar mechanism of action. HO-1 is inducible and is highly expressed in the spleen and liver. HO-2 is constitutive and found

primarily in the brain. Recent studies suggest that CO liberated from heme by HO may act as a physiological messenger.[17]

HO by itself contains no prosthetic groups. Thus, unlike the other oxygen-activating enzymes, it is not a heme protein per se. It binds heme in a 1:1 ratio[13] and constrains it to an environment suitable for site specific O_2-dependent heme self-oxidation. It is therefore best described as a transient heme protein and is the only system currently known to utilize heme simultaneously as both a prosthetic group and substrate.[14] For a heme-HO complex, reducing equivalents are required to convert the heme iron in the reduced (Fe^{II}) state and to activate molecular oxygen for the heme degradation. According to the available information, normal catalytic turnover of the enzyme by utilizing NADPH and cytochrome P-450 reductase yields biliverdin *via* a sequence that is thought to involve α-*meso*-hydroxylation of the heme, aerobic fragmentation of the α-*meso*-hydroxyheme to verdoheme, and oxidative cleavage of verdoheme to biliverdin (Scheme 2).[18]

Scheme 2

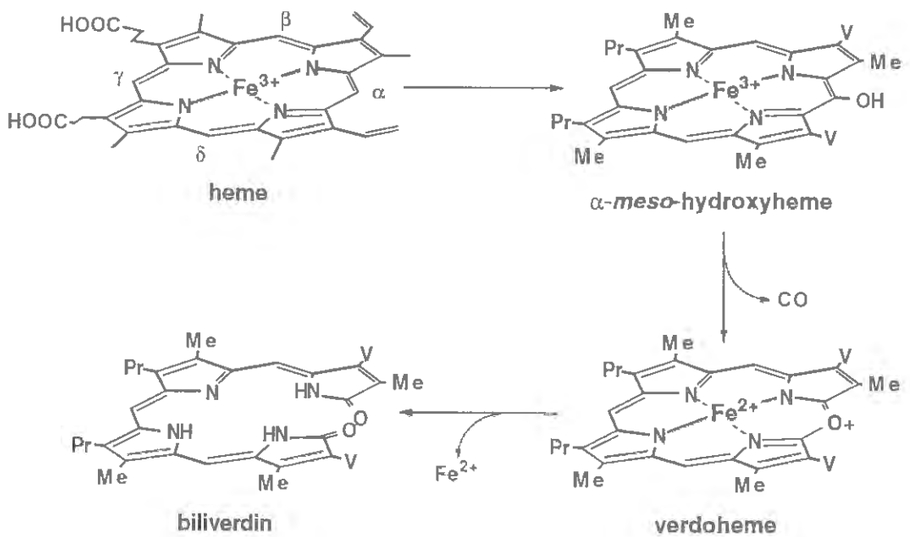

In the last few years, several articles have been devoted to the study of the molecular mechanism for the transfer of activated oxygen to α-*meso*-carbon in the first step. Involvement of an oxo-ferryl complex was

suggested on the basis of similarities between cytochrome P-450 and heme-HO complex in the O_2 activation on the heme iron However, Wilks et al. reported that the reaction of HO-heme and peracid only gave an oxo ferryl complex which was not converted to any metabolites including α-*meso*-hydroxyheme.[19] This result indicates that α-*meso*-hydroxylation, in contrast to most heme protein-catalyzed oxidation reactions, does not involve the oxo-ferryl species. Considering that the *meso*-hydroxylation by the bound oxygen is also the key step for the regiospecificity,[20] the first step is the best described as the unique function of HO.

The iron porphyrin complexes used in Part II require bulky substituents at the *meso*-positions to prevent heme degradation under the conditions. This result may imply that the introduction of one or two less hindered phenyl group(s) at *meso*-position(s) could allow me to examine details of heme degradation related to HO-catalyzed formation of α-*meso*-hydroxyheme. Thus, I have constructed a model oxidation reaction equivalent to the suicidal *meso*-hydroxylation to give α-*meso*-hydroxyheme by using an iron porphyrin complex shown in Figure 1c, and examined the detailed mechanism for the oxidation reaction (Chapter 1 and 2 of Part III).

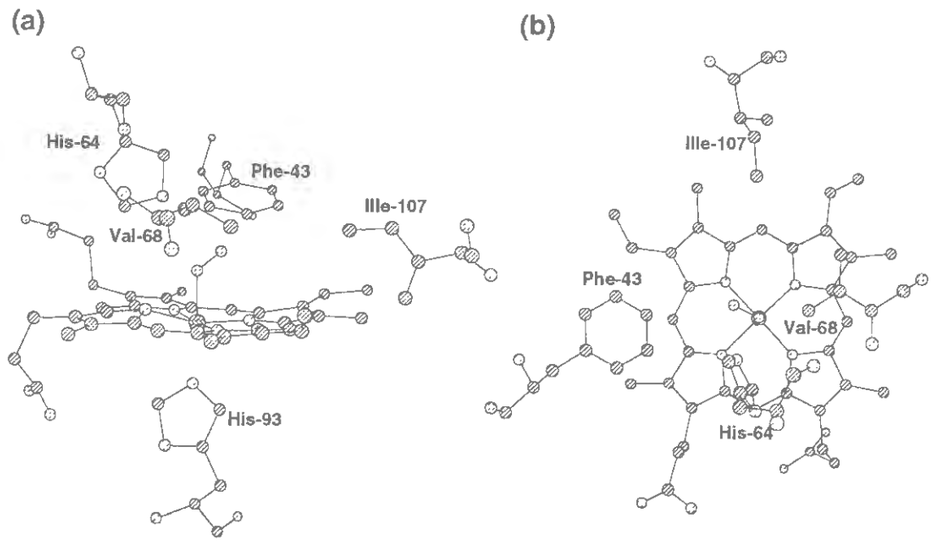

Figure 2. Heme environmental structure of myoglobin. Heme and some selected residues are shown. (a) Side view. (b) Top view.

As described before, heme is regioselectively converted to biliverdin IXα by HO.[20,21] Myoglobin also shows HO-type heme degradation activity and site-specificity at the α-*meso*-position even though the activity is much lower than HO.[22] The specific oxidation of the α-*meso*-position of myoglobin can be expected on the basis of its crystal structure of the O_2-bound myoglobin which shows less hindered α-*meso*-position (Figure 2). Brown et al. calculated the relative accessibility of the heme-bound oxygen to the four *meso*-carbons of myoglobin and concluded the α-*meso*-carbon to be the lowest energy.[23] Based on these observations, steric control was proposed for the reaction regioselectivity of the HO-catalyzed oxidation. However, there are many aspects to be investigated because the three dimensional structure have not been resolved yet.

Recent resonance Raman studies have suggested that the Fe–O–O unit of the O_2-bound heme-HO complex is highly bent enough to be in van der waals contact with the α-*meso*-carbon of the porphyrin ring.[24] In the case of myoglobin, the molecular oxygen bound to the heme is highly restricted by hydrogen bond with the distal histidine-64. These points lead me to construct the distal site of Mb by relocation or elimination of the distal histidine to evaluate whether or not the orientation of the bound oxygen regulates the regiospecificity of the HO-type reaction. Chapter 1 of Part IV describes a new mechanism capable of regulating the regioselectivity of the HO-type reaction by employing distal site mutants of myoglobin. The reactivity of the mutants is also discussed.

Heme-HO and myoglobin share neutral histidine as the axial ligand and similar electronic absorption spectra.[25] On the basis of a crystal structure of cytochrome CcP, Poulos et al suggested that anionic proximal histidine of peroxidases could serve as a strong internal electron donor to destabilize the O–O bond (push effect).[26] At the same time, distal histidine and polar amino acid residues such as arginine are expected to assist the O–O bond cleavage (pull effect).[26] This push-pull effect is illustrated in Figure 3a.[27] For P-450, strong "push" effect of the axial thiolate appears to be sufficient to cleavage the O–O bond without the assistance of the "pull" effect (Figure 3b).[28] On the other hand, the activation of O_2 including the O–O bond cleave of the iron bound peroxide in heme-HO is likely modulated by the distal site structure, since the proximal His in HO is neutral.[25]

Recently, an unusual pattern of spin density on the heme periphery of the CN-bound heme-HO complex has been suggested using isotope

labeling and 2D NMR.[29] The results indicate that the spin density is

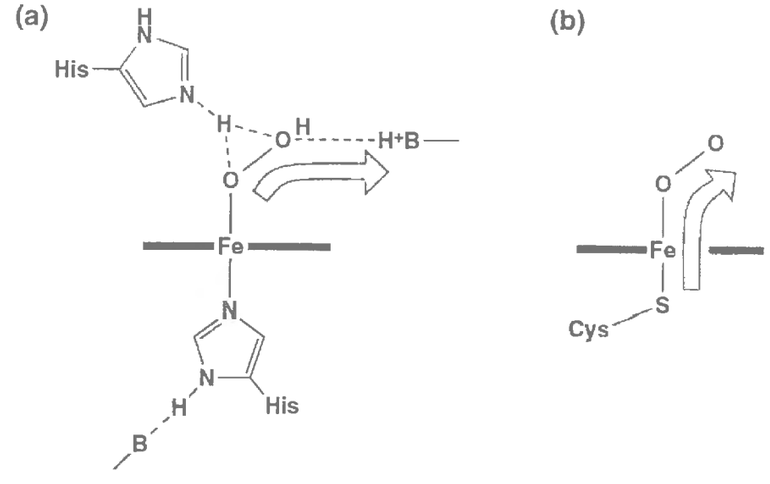

Figure 3. A schematic view of the "push-pull" mechanism for O-O bond cleavage of an iron-bound peroxide in (a) histidine-ligated and (b) thiolate-ligated system such as horseradish peroxidase and P-450, respectively.

localized primarily to the pyrrole carbons adjacent to the α, γ axis. This is attributed to a direct electronic effect of the protein on the heme as could occur through a perturbation of the α-*meso*-carbon by a nearby anionic side chain.[29] While this seems to be a reasonable mechanism of perturbation because the pattern attributed to the specific spin delocalization is lost at acidic pH,[29] no solid evidence has been provided due to a lack of the crystal structure of the heme-HO complex. According to the similarity of Mb to heme-HO, active site mutants of Mb may provide structural information of the heme-HO complex. As illustrated in Figure 2, the heme iron of Mb is surrounded by Ile-107, Phe-43, His-64, and Val-68 near the α, β, γ, and δ-*meso*-positions, respectively. Therefore, substitution of Ile-107 of Mb could perturb the electric field around the α-*meso*-carbon. Thus, I have examined effects of a carboxylate side chain near the α-*meso*-position of a mutant myoglobin on the active site structure and the reactivity in the HO-type reaction (Chapter 2 of Part IV).

The heme-HO complex has properties analogous to those of hemoproteins as described before. Although the amino acid sequences of some of HO are now available, no crystal structure of HO has been

reported; consequently, very little is known of their secondary and tertiary structures of the enzymes and enzyme-substrate complexes. Especially, a substrate-induced conformational change of enzymes is generally of considerable importance because it is related to the function.[30] In Part V, a unique conformational change associated with the substrate binding to heme oxygenase are discussed by using proton NMR, circular dichroism, and fluorescence spectroscopies and urea-denaturation.

References

(1) Dawson, J. H.; Eble, K. S. *Cytochrome P-450: Heme iron coordination structure and mechanisms of action*, Adv. Inorg. Bioinorg. Mech. 4: pp1-64, 1986.

(2) (a) Katagiri, M.; Ganguni, B. N.; Gunsalus, I. C. . *J. Biol Chem.* **1968**, *243*, 3543. (b) Poulos, T. L.; Finzel, B. C.; Gunsalus, I. C.; Wagner, G. C.; Kraut, J. *J. Biol. Chem.* **1984**, *260*, 16122. (c) Poulos, T. L.; Finzel, B. C.; Howard, A. J. *Biochemistry* **1986**, *25*, 5314.

(3) Dawson, J. H.; Sono, M. *Chem. Rev.* **1987**, *87*, 1255.

(4) *Cytochrome P-450: Structure, Mechanism, and Bilchemistry, 2nd ed.*; Ortiz de Montellano, P. R., Ed.; Plenum: New York, 1995.

(5) (a)Brewer, C. B.; Peterson, J. A. *J. Biol. Chem.* **1988**, *263*, 791. (b) Pederson, T. C.; Austin, R. H.;Gunsalus, I. C. *In Microsomes and Drug Oxidations*; Ullrich, V., Roots, I., Hildebrandt, A., Estabrook, R. W., Conney, A. H., Eds.; Pergamon Press: Oxford, England, 1977; pp275-283.

(6) Holm, R. H. *Chem. Rev.* **1987**, *87*, 1401.

(7) Groves, J. T.; Nemo, T. E.; Myers, R. S. *J. Am. Chem. Soc* . **1979**, *101*, 1032-1033.

(8) Groves, J. T.; Haushalter, R. C.; Nakamura, M.; Nemo, T. E.; Evans, B. J. *J. Am. Chem. Soc.* **1981**, *103*, 2884-2886.

(9) Groves, J. T.; Watanabe, Y. *J. Am. Chem. Soc.* **1986**, *108*, 7836-7837.

(10) (a)Tsurumaki, H.; Watanabe, Y.; Morishima, I. *J. Am. Chem. Soc.* **1993**, *115*, 11784-11788. (b)Watanabe, Y.; Takehira, K.; Shimizu, M.; Hayakawa, T.; Orita, H.; Kaise, M. *J. Chem. Soc., Chem. Commun.* **1990**, 1262-1264. (c)Watanabe, Y.; Takehira, K.; Shimizu, M.; Hayakawa, T.; Orita, H.; Kaise, M. *Transformation of Fe(III)TMP N-oxide to a two electron oxidized equivalent of Fe(III)TMP complex*; Watanabe, Y.; Takehira, K.; Shimizu, M.; Hayakawa, T.; Orita, H.; Kaise, M., Ed.; Elsevier Science Publishers B.V : Amsterdam, 1991; Vol. 66, pp 213-220.

(11) (a) Tenhunen, R.; Marver, H. S.; Schmid, R. J. *Proc. Natl Acad. Sci. U.S.A.* **1968**, *61*, 748. (b) Tenhunen, R.; Marver, H. S.; Schmid, R. *J. Biol. Chem.* **1969**, *244*, 6388-6394.

(12) (a) O'Carra, P. *Porphyrins and Metaloporphyrins*; Elsevier: Amsterdam, 1975. (b)Kikuchi, G.; Yoshida, T. *Mol. Cell. Biochem.* **1983**, *53/54*, 163-183. (c) Maines, M. D. *FEBS Lett.* **1988**, *2*, 2557-2568.

(13) (a) Yoshida, T.; Kikuchi, G. *J. Biol. Chem.* **1979**, *254*, 4487-4491. (b) Bonkovsky, H. L.; Healy, J. F.; Pohl, J. *Biochem. J.* **1990**, *189*, 155.

(14) (a) Yoshinaga, T.; Sassa, S.; Kappas, A. *J. Biol. Chem.* **1982**, *257*, 7778. (b) Yoshida, T.; Kikuchi, G. *J. Biol. Chem.* **1978**, *253*, 4224-4229.

(15) Maines, M. D.; Trakshel, G. M.; Kutty, R. K. *J. Biol. Chem.* **1986**, *261*, 411-419.

(16) (a) Muller, R. M.; Taguchi, H.; Shibahara, S. *J. Biol. Chem.* **1987**, *262*, 6795. (b) Cruse, I.; Maines, M. D. *J. Biol. Chem.* **1988**, *263*, 3348.

(17) (a) Brune, B.; Ullrich, V. *Mol. Pharmacol.* **1987**, *32*, 497. (b) Verma, A.; Hirsch, D. J.; Glatt, C. E.; Ronnett, G. V.; Snyder, S. H. *Science* **1993**, *259*.

(18) Beale, S. I. *Chem. Rev.* **1993**, *93*, 785-802.

(19) Wilks, A.; Ortiz de Montellano, P. R. *J. Biol. Chem.* **1993**, *268*, 22357-22362.

(20) (a) Kondon, T.; Nicholson, D. C.; Jackson, A. H.; Kenner, G. W. *Biochem. J.* **1971**, *121*, 601-607. (b) Jackson, A. H.; Kenner, F. W.; McGillivrav, G.; Smith, K. M. *J. Chem. Soc., Chem. Commun.* **1968**, 294-302. (c) Jackson, A. H.; Lee, M. G.; Jenkins, R. T.; Brown, S. B.; Chaney, B. D. *Tetrahedron Lett.* **1978**, *51*, 5135-5138.

(21) (a) Yoshida, T.; Kikuchi, G.; Sano, S. *J. Biochem. (Tokyo)* **1981**, *90*, 125-131. (b) Yoshinaga, T.; Sudo, Y.; Samo, S. *Biophys. J.* **1990**, *270*, 659-664.

(22) O'Carra, P.; Colleran, E. *FEBS Lett.* **1969**, *5*, 295-298.

(23) Brown, S. B.; Chabot, A. A.; Enderby, E. A.; North, A. C. T. *Nature* **1981**, *289*, 93-95.

(24) Takahashi, S.; Ishikawa, K.; Takeuchi, N.; Ikeda-Saito, M.; Yoshida, T.; Rousseau, D. L. *J. Am. Chem. Soc.* **1995**, *117*, 6002-6006.

(25) (a) Takahashi, S.; Wang, J.; Rousseau, D. L.; Ishikawa, K.; Yoshida, T.; Host, J. R.; Ikeda-Saito, M. *J. Biol. Chem.* **1994**. *269*, 1010-1014. (b) Takahashi, S.; Wang, J.; Rousseau, D. L.; Ishikawa, K.; Yoshida, T.; Takeuchi, N.; Ikeda-Saito, M. *Biochemistry* **1994**, *33*, 5531-5538.1)Sun, J.; Loehr, M.; Wilks, A.; Ortiz de Montellano, P. R. *Biochemistry* **1994**,

33, 13734-13740 (c) Ito-Maki, M.; Ishikawa, K.; Mansfield Matera, K.; Sato, M.; Yoshida, T. *Arch. Biochem. Biophys* **1995**, *317*, 253-258. (d) Ishikawa, K.; Sato, M.; Ito, M.; Yoshida, T *Biochem. Biophys. Res. Commun.* **1992**, *182*, 981-986.

(26) (a) Finzel, B. C.; Poulos, T. L.; Kraut, J. *J. Biol. Chem.* **1984**, *259*, 13027-13036. (b) Poulos, T. L.; Freer, S. T.; Alden, R. A.; Edwards, S. L.; Skogland, U.; Takio, K.; Eriksson, B.; Xuong, N.-H.; Yonetani, T.; Kraut, J. *J. Biol. Chem.* **1980**, *255*, 575-580. (c) Poulos, T. L. *Adv. Inorg. Biochem.* **1987**, *7*, 1.

(27) Dawson, J. H. *Science* **1988**, *240*, 433-439.

(28) (a) Dawson, J. H.; Holm, R. H.; Trudell, J. R.; Barth, G.; LinderR.E.;; Bunnenberg, E.; Djerassi, C.; Tang, S. C. *J. Am. Chem. Soc.* **1976**, *98*, 3707. (b) Sono, M.; Andersson, L. A.; Dawson, J. H. *J. Biol. Chem.* **1982**, *257*, 8308.

(29) Hernández, G.; Wilks, A.; Paolesse, R.; Smith, K. M.; Ortiz de Montellano, P. R.; La Mar, G. N. *Biochemistry* **1994**, *33*, 6631-6641.

(30) (a) Anderson, C. M.; Zucker, F. H.; Steitz, T. A. *Science* **1979**, *204*, 375-380. (b) Bennett, J. W. S.; Steitz, T. A. *Proc. Natl. Acad. Sci. U.S.A.* **1978**, *75*, 4848-4852. (c) Koshland, D. *The Enzyme*, E.Boyer, P. D.; Lardy, H.; Myrbäck, K, Ed.; Academic Press: New York, 1959; Vol. 1, pp 305-346.

PART II.

ELECTRONIC STRUCTURES AND FUNCTIONS OF THE REACTION INTERMEDIATE IN THE CATALYTIC CYCLE OF P-450

CHAPTER 1.

A New Active Intermediate in Monooxygenations.

Abstract

A new type of high-valent oxo-iron porphyrin (**3b**), has been prepared by the reaction of Fe^{III}TDCPP (**1b**) [TDCPP: 5,10,15,20-tetrakis(2,6-dichlorophenyl)porphyrin] with *p*-nitroperbenzoic acid (*p*NPBA) or pentafluoroiodosylbenzene (F_5-PhIO) in dichloromethane at -90°C *in the presence of methanol*. The UV-vis spectrum of **3b** (λ_{max} at 418 and around 550 nm) is similar to that of O=Fe^{IV}TDCPP (**4b**, λ_{max} 419, 543 nm). However, titration of **3b** by iodide ion indicates the oxidation state of **3b** being two-electron oxidized from the ferric state. Further, **3b** catalyzes epoxidation of olefins such as styrene even at -90°C at the rate constant of 0.11 $M^{-1}s^{-1}$. While UV-vis spectrum of **3b** is completely different from that for the corresponding oxo-iron(IV) porphyrin π-cation radical (**2b**), possible formulation of **3b** as π-cation radical is readily ruled out by deuterium NMR observation. EPR spectrum (g = 4.33, 3.69, 1.99 at 4.2 K) and solution magnetic susceptibility (μ_{eff} = 4.0 ± 0.2 μ_B) of **3b** indicate that **3b** possesses three unpaired electrons. These results indicate the formal description of **3b** being a high spin complex of either an O=Fe(V) porphyrin or •O-Fe(IV) porphyrin. The same oxidation of **1b** *in the absence of methanol* gave **2b**. We attribute the ligation of methanol to cause the destabilization of iron d orbitals and it eventually turns upside down the energy levels between the iron d_{xz}, d_{yz} orbitals and porphyrin HOMO orbital (a_{2u}) since the a_{2u} orbital is stabilized by the introduction of electron-withdrawing groups on the porphyrin ring.

Introduction

Synthetic iron porphyrin complexes in high oxidation states have been served as models for the active species of peroxidase, catalase, and cytochrome P-450. Among them, two-electron oxidized iron porphyrin complexes have been extensively studied to understand biological utilization and manipulation of reactive intermediates. For example, oxo-iron(IV) porphyrin π-cation radical,[1] iron(III) porphyrin *N*-oxide,[2] and iron(III) porphyrin dication,[3] which are formally two-electron oxidized from the ferric state, are now known. Especially, the oxo-iron(IV) porphyrin π-cation radicals are closely related to compound I of peroxidases[4] and catalases.[5] The formation of compound I in the catalytic cycles of these heme enzymes is supported on the basis of electronic,[6] EPR,[7] NMR,[8] ENDOR,[4f,4g] resonance Raman,[9] and Mössbauer spectral measurements.[10]

The active species responsible for the oxidative metabolism of foreign compounds by P-450 has been considered to be similar to compound I of peroxidases[11] since many types of monooxygenation by P-450 have been mimicked by oxo-iron(IV) porphyrin π-cation radicals of synthetic iron porphyrin complexes.[12] Unfortunately, any higher valent intermediates in the catalytic cycle of P-450 have never been characterized. Very recently, Egawa et al. have reported the observation of compound I as a transient intermediate by rapid scan absorption spectrometry in the reaction of *m*-chloroperbenzoic acid (*m*CPBA) with P-450_{cam},[13] however, the observed spectrum is a mixture of several species and a spectrum obtained by the subtraction of undesired species is still controversial. Thus, the efforts on the elucidation of the active species of P-450 are quite important. Especially, an oxo-iron(V) porphyrin complex is an attractive candidate for the active species in the P-450 reactions. In 1989, Champion proposed favorable formulation of an iron(IV) porphyrin oxy radical (one extreme resonance structure of oxo-iron(V) porphyrin) over compound I due to strong electron donating ability of the thiolate ligand and non-polar environment of the heme pocket of P-450 (eq. 1).[14]

(1)

Very recently, we have reported the transformation of O=Fe^{IV}TDCPP$^{+\bullet}$ (**2b**, TDCPP: 5,10,15,20-tetrakis(2,6-dichlorophenyl)-porphyrin) to an alternative intermediate, most likely, O=Fe^{V}TDCPP (**3b**) by *introducing MeOH* as a sixth ligand.[15] However, Jayaraj et al. also reported the oxidation of Fe^{III}TDCPP in the presence of MeOH to give O=Fe^{IV}TDCPP$^{+\bullet}$ under similar conditions.[16] Thus, we would like to show experimental evidence for the rationalization of these different observations. In addition, we have successfully prepared **3b** by the reaction of Fe^{III}TDCPP(ClO_4) and pentafluoroiodosylbenzene under mild condition. Two independent preparations of **3b** allows us to examine detailed reactivities of **3b** under various conditions. More importantly, we have shown herein the manipulation of the electronic structure of the two electron oxidized oxo-iron porphyrin complexes, **2** and **3**, by introducing a series of electron-withdrawing substituents on the porphyrin ring.

Experimental Section

Materials. Dichloromethane was refluxed over CaH_2 and distilled under Ar just before use. $TDCPPH_2$, $TCMPPH_2$ [TCMPP: 5,10,15,20-tetrakis(2-chloro-6-methylphenyl)porphyrin], $TCFPPH_2$ [TCFPP: 5,10,15,20-tetrakis(2-chloro-6-fluorophenyl)porphyrin], and $TTCPPH_2$ [TTCPP: 5,10,15,20-tetrakis(2,3,6-trichlorophenyl)porphyrin] were prepared by the methods reported.[17] Pyrrole-deuterated $TDCPPH_2$ was prepared as described previously.[18] *Meso*-substituents-deuterated $TDCPPH_2$ was prepared by treating $TDCPPH_2$ with concentrated $^2H_2SO_4$ at room temperature.[19] Iron was inserted into $TDCPPH_2$ to form Fe^{III}TDCPP(Cl) by a standard method.[20] Fe^{III}TDCPP(OH) was prepared by passing a dichloromethane solution of Fe^{III}TDCPP(Cl) through an alumina column. Addition of 1 equiv of *m*-chlorobenzoic acid (*m*CBA) to Fe^{III}TDCPP(OH) gave Fe^{III}TDCPP(*m*CB) (**1b**-*m*CB) (*m*CB: *m*-chlorobenzoate). Fe^{III}TDCPP(ClO_4) (**1b**-ClO_4) was prepared as described earlier.[21] Pentafluoroiodosylbenzene (F_5-PhIO)[22] and *p*-nitroperbenzoic acid (*p*NPBA)[23] were prepared and purified by literature procedures. *m*-Chloroperbenzoic acid (*m*CPBA) was purchased from Wako Chemicals and purified as described earlier.[23] Silver perchlorate and tetrabutylammonium iodide (TBAI) were purchased from Aldirich and Wako, respectively. TBAI was purified by recrystallization from dichloromethane/hexane and dried *in vacuo*. Norbornylene, styrene, *p*-chlorostyrene, *p*-methylstyrene, and α-methylstyrene were purchased from Aldrich and used without further purification.

Physical Measurements. Absorption spectra were recorded on a Hitachi 330 spectrometer. Low-temperature absorption spectra were obtained by using a DN 1704 variable-temperature liquid nitrogen cryostat (Oxford Instruments). Proton NMR and deuterium NMR spectra were recorded on a GE Omega-500 spectrometer and Nicolet NT-300 spectrometer. Chemical Shifts were referenced to tetramethylsilane (TMS), and downfield shifts were given a positive sign. EPR spectra were recorded on a JEOL JES-3X spectrometer operating with 100 kHz magnetic field modulation. GLC analyses were performed on a Shimadzu GC-14A fitted with a Shimadzu CBP1 (25 m) capillary column. Electrochemical measurements were carried out with a three-electrode potentiostatic system. The working electrode was a $Ag/AgNO_3$ saturated calomel electrode (SCE) separated from the bulk solution by fine glass frits. Cyclic voltammogram was obtained on a BAS CV-50W.

Preparation of 3b and 3b'. A dichloromethane solution of **1b**-*m*CB [2.2×10^{-5} M] in UV-cuvette was cooled to -90°C. To the resulting solution was added 8 equiv of *m*CBA, 1.8 equiv (a small excess amount for the complete oxidation) of *p*NPBA, and *4 equiv of methanol*, to give a red species, **3b**. Complete formation of **3b** was confirmed by the UV-vis spectral changes at -90°C. The reaction of 1.8 equiv of F_5-PhIO and **1b**-ClO_4 [1.0×10^{-4} M] in dichloromethane in the presence of 200 equiv of methanol at -90°C also yielded a red species, **3b'**.

NMR and EPR samples of **3b** [3.0×10^{-3} M] and **3b'** [1.0×10^{-3} M] were prepared at -90°C according to the stoichiometry described above. The samples prepared in EPR tubes were examined by NMR to make sure the formation of **3b** and **3b'** before the EPR measurement at 4K.

Preparation of Oxo-Iron(IV) Porphyrin π-cation radicals (2). Oxo-iron(IV) porphyrin π-cation radical (**2b-d**) were synthesised by the addition of 8 equiv of *m*CBA and 1.8 equiv of *p*NPBA to Fe^{III}TDCPP(*m*CB) [2.2×10^{-5} M] *in dichloromethane* at -90°C.[15] Oxo-iron(IV) porphyrin π-cation radicals (**2a-d**) were also prepared by the reaction of **1**-ClO_4 (**a-d**) [1.0×10^{-5} M] with 1.8 equiv of *m*CPBA in dichloromethane at -90°C.[24] Characterization of the products was made on the basis of a less intense

Soret band and gentle absorption around 600~700 nm as well as a large upfield shift of the pyrrole β-protons of **2** on the NMR spectroscopy.

Preparation of Oxo-Iron(IV) Porphyrin (4b). As reported by Gold et al.,[25] Fe^{III}TDCPP(OH) [1.0×10^{-5} M] was oxidized by mixing with 4 equiv of *m*CPBA at -60°C in dichloromethane solution containing 0.1% ethanol as preservative. The formation of an oxo-iron(IV) porphyrin complex (**4b**) was confirmed by comparison of its UV-vis spectrum (λ_{max} 419 and 543 nm) to that reported.[25]

Reaction of 2 and 3 with Olefins. In a typical run, a dichloromethane solution of **2** or **3** [ca. 2×10^{-5}M] was prepared by the addition of one equiv of the oxidants at -90°C. Completion of the reaction was confirmed by monitoring absorbance spectral changes at -90°C. Then, 500 equiv of norbornylene, 1000 equiv of styrene, or 1000 equiv of *p*-chlorostyrene at -90°C was introduced to initiate the epoxidation. The rate constants for each reaction were calculated on the basis of the time-dependent spectral changes.

Results

p-Nitroperbenzoic acid (*p*NPBA) and pentafluoroiodosyl benzene (F_5-PhIO) have been used as convenient stoichiometric oxidants for the preparation of oxo-iron(IV) porphyrin π-cation radicals (**2**). The rate for the formation of **2** is known to be dependent on the reaction conditions and the nature of porphyrin ligands.[26] For example, introduction of electron-withdrawing groups such as halogens on the porphyrin periphery discourage the rate while the reaction can be accelerate by the addition of acid since the O-O bond cleavage in acylperoxo-iron(III) porphyrin complexes is catalyzed by acid.[2b,27] Thus, we have to employ an excess amount of *m*-chlorobenzoic acid (*m*CBA) for the preparation of **2b** by the reaction of Fe^{III}TDCPP(*m*CB) (**1b**-*m*CB) and *p*NPBA.[15] On the other hand, *m*-chloroperbenzoic acid (*m*CPBA) can be used if Fe^{III}TDCPP(ClO_4) was used as a starting material.[24]

UV-vis Spectra of High Valent Intermediates. The reaction of **1b**-*m*CB with 1.8 equiv of *p*-nitroperbenzoic acid (*p*NPBA) in the presence of 8 equiv of *m*CBA was examined at -90°C by UV-vis spectroscopy. The

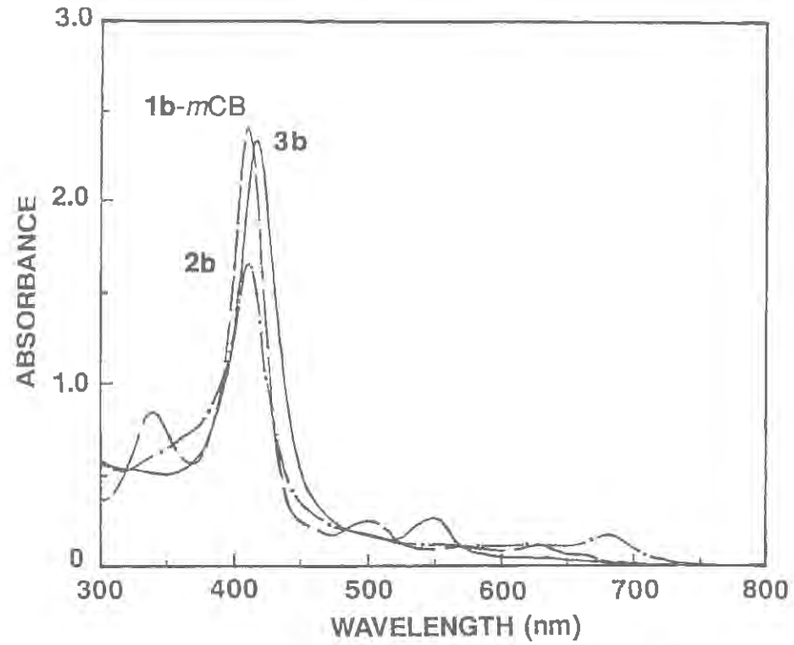

Figure 1. UV-vis spectra of **1b**-*m*CB, **2b**, and **3b** [2.2×10^{-5} M] in dichloromethane at -90°C. **2b** was obtained by the addition of 1.8 equiv of *p*NPBA to **1b**-*m*CB. **3b** was obtained by the addition of 4 equiv of methanol to **2b**.

oxidation product was readily assigned to O=Fe^{IV}TDCPP$^{+\bullet}$ (**2b**) on the basis of its characteristic UV-vis spectrum (Figure 1). As reported in our preliminary communication,[15] addition of 4 equiv of methanol to the dichloromethane solution of **2b** afforded a red species **3b**, whose UV-vis spectrum (Figure 1) is similar to those of oxo-iron(IV) porphyrin complexes[25] (**4**) but very different from complexes of iron(III) porphyrin dication[3] and iron(III) porphyrin *N*-oxide.[2] **3b** can be directly prepared if the reaction of **1b**-*m*CB and *p*NPBA was carried out in the presence of a small amount of methanol. In most of spectroscopic studies including Figure 1, we have employed a small excess of oxidants to complete the formation of **2b** and **3b**. However, **2b** and **3b** can be prepared by the

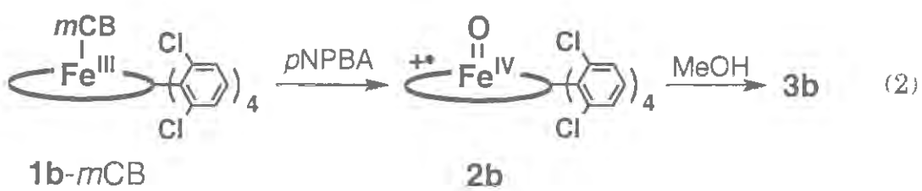

(2)

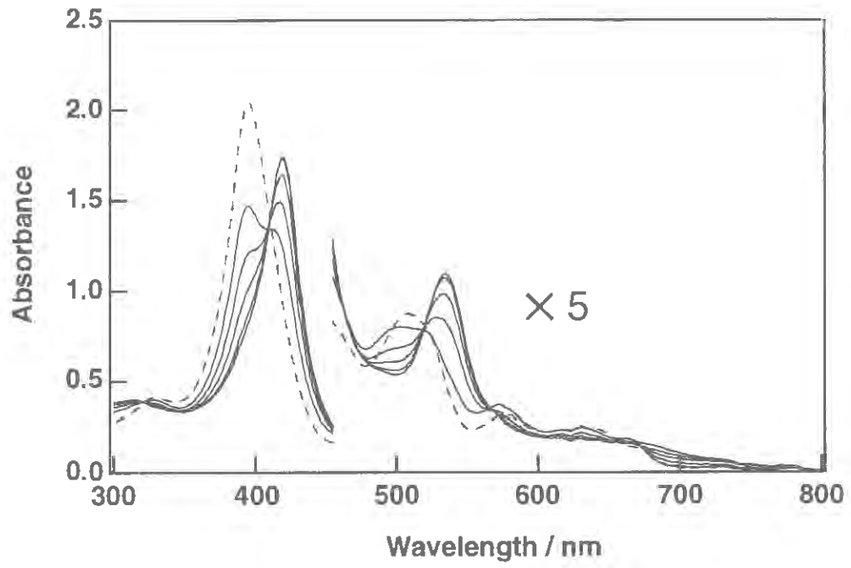

Figure 2. UV-vis spectral changes upon the addition of 1.8 equiv of F_5-PhIO to Fe^{III}TDCPP(ClO_4) (**1b**-ClO_4) [1.0×10^{-4} M] (---) in dichloromethane containing 200 equiv of methanol at -90°C at 7-min intervals (first scan was immediate after the addition of F_5-PhIO).

stoichiometric reactions of **1b** and *p*NPBA in 90% yield.

In the previous report,[15] we have assigned **3b** as oxo-iron(V) porphyrin on the basis of iodometric titration and EPR and NMR spectroscopic observations, however, the solution of **3b** contains additives such as *m*CBA, and *p*NBA to prevent us to examine detailed structure of **3** and roles of methanol. Therefore, we have exploited another synthetic procedure of **3** under neutral condition. Figure 2 shows time dependent spectral changes upon the addition of pentafluoroiodosylbenzene (F_5-PhIO) to a dichloromethane solution (including 200 equiv of MeOH) of **1b**-ClO_4 at -90°C. The UV-vis spectrum of the product (**3b'**) is similar to that of **3b**, though absorption maximum of **3b** at 546 nm is different from **3b'** by

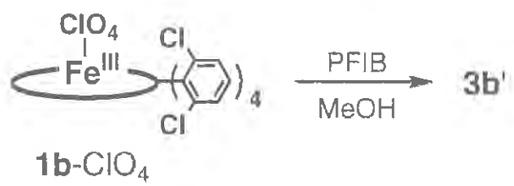

(3)

14 nm (Table 1). Like the reaction of **3b** with olefins, addition of norbornylene to the solution of **3b'** in an UV cuvette at -90°C caused the

spectral changes to afford **1b** even at -90°C, while independently prepared O=Fe^{IV}TDCPP (**4b**) did not react with olefins under similar conditions. That both **3b** and **3b'** react with olefins even at -90°C to afford **1b** suggests these complexes being two electron oxidized ones from **1b**.

In order to confirm these considerations, we have examined the oxidation state of **3b** and **3b'** along with **2b** by iodometric titration.

Table 1. UV-vis and Proton NMR Spectral Data of **3b**, **3b'** and **2b**.

		Chemical Shift (ppm from TMS)	
porphyrin	UV-vis spectra (nm)	pyrrole-H	*meta*-H
3b[a]	418, 546	-35.1	8.0
3b'	418, 532	-22.9	8.8
2b[a]	409, 681	-46.2	44.0

[a] Yamaguchi et al. *J. Chem. Soc., Chem. Commun.*, **1992**, 1721-1723.

Formal Oxidation State of 2b, 3b, and 3b'. Ten equiv of tetra-*n*-butylammonium iodide (TBAI) and *m*-chlorobenzoic acid (*m*CBA) were added at -90°C to a dichloromethane solution of **2b** prepared by 1.8 equiv of *p*NPBA. The reaction was directly monitored by UV-vis spectroscopy as shown in Figure 3a. The final spectrum is the superimposition of iron(III) porphyrin complexes and I_3^-, which is generated by the oxidation of I^-. Figure 3a (*inset*) displays a difference spectrum of the resulting solution and **1b**-*m*CB. The difference spectrum exhibits absorption maximum at 363 nm, showing the formation of I_3^-. The addition of 10 equiv of TBAI to the solution of **3b** prepared by 1.8 equiv of *p*NPBA exhibited superimposed spectrum of **1b**-*m*CB and I_3^- (Figure 3b (*inset*)). The same amount of I_3^- was also observed for **3b'** prepared by 1.8 equiv of F_5-PhIO. The total amounts of I_3^- observed should include the amounts of I_3^- formed by the reaction of I^- with free oxidants, since we have used 1.8 equiv of the oxidant to complete the formation of **2b**, **3b**, and **3b'**. Therefore, the titration of 1.8 equiv of *p*NPBA by I^- was carried out and the same amount of I_3^- formation was observed. In this case, *p*NPBA is also reduced to *p*NBA by two electrons. These results indicate that **2b**, **3b**, and **3b'** are in the same oxidation state, which is formally two-electron oxidized from the

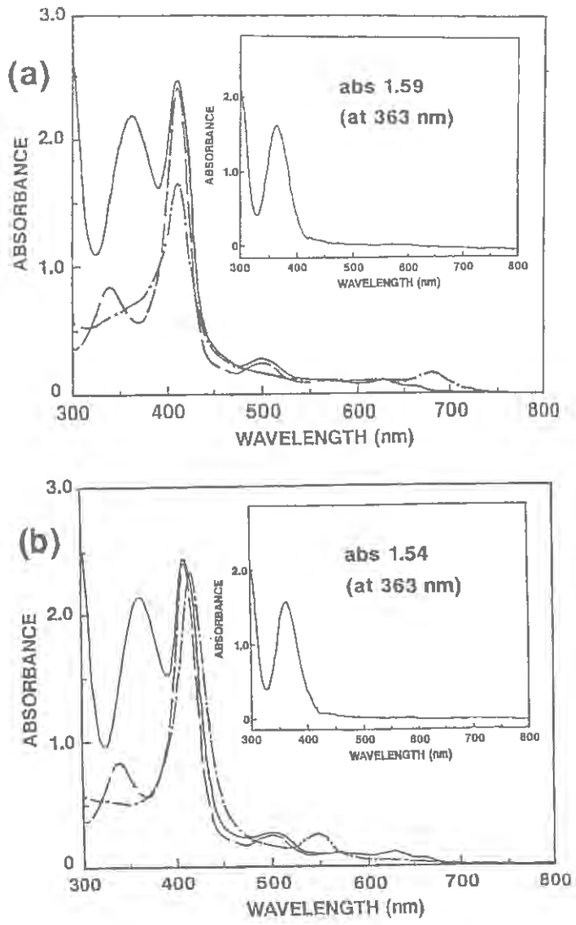

Figure 3. (a) UV-vis spectra of **1b**-*m*CB (---), **2b** (-•-), and **1b**-*m*CB and I_3^- (—), which was obtained by the addition of 10 equiv of TBAI to **2b**. (*inset*) UV-vis spectrum of I_3^-, which was given by subtracting the spectrum of **1b**-*m*CB from that of **1b**+I_3^-. (b) UV-vis spectra of **1b** (---), and **3b** (-•-), and **1b**+I_3^- (—), which was obtained by the addition of 10 equiv of TBAI to **3b**. (*inset*) UV-vis spectrum of I_3^-, which was given by subtracting the spectrum of **1b** from that of **1b**+I_3^-.

ferric state. Thus, we concluded that **3b** and **3b'** are essentially the same species and a small shift of the Q band in **3b'** from **3b** could be induced by different reaction conditions (see Discussion).

EPR Spectra. The EPR spectrum of **3b** shows three absorptions at g = 4.33, 3.69, and 1.99 at 4.2 K in frozen dichloromethane as shown in Figure

4. The EPR spectrum corresponds to S = 3/2 system with a large value of the zero field splitting parameter (D) to give E/D of 0.04. These spectroscopic characteristics are very close to those of $O=Fe^{IV}(TMP)^{+\bullet}$ [TMP: 5,10,15,20-tetramesitylporphyrin] that shows three EPR absorptions at g = 4.5, 3.5, 2.0 arisen from ferromagnetically coupled state.[28a]

The magnetic susceptibility of **3b** determined by the Evans method[29] was 4.0 ± 0.2 μ_B, which fits to the spin-only value expected for S = 3/2 system and is consistent with the EPR data. These results also suggest **3b** to be isoelectronic to oxo-iron(IV) porphyrin π-cation radical.

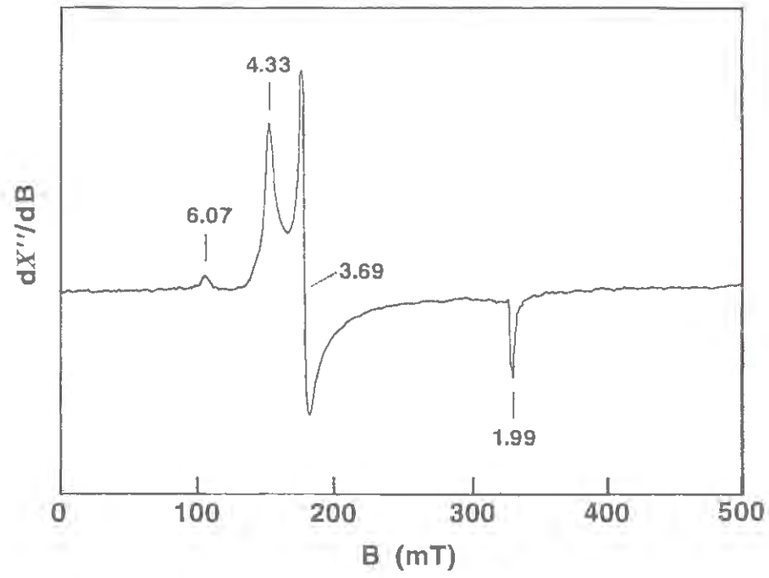

Figure 4. X-band EPR spectrum of **3b** [3.0×10^{-3} M] as a frozen dichloromethane solution at 4.2 K, 9.2289 GHz, 0.5 mW microwave power.

NMR Spectra of 2b, 3b, and 3b'. The reaction of pyrrole-d_8-**1b**-*m*CB with 1.8 equiv of *p*NPBA in the presence of 8 equiv of *m*CBA was also examined at -95°C. Upon addition of *p*NPBA to a dichloromethane solution of pyrrole-d_8-**1b**-*m*CB, the pyrrole β-deuterium resonance of pyrrole-d_8-**1b**-*m*CB at 130 ppm (signal i, Figure 5a) shifted to -46.2 ppm (signal ii, Figure 5b) due to the formation of **2b**.[1,15,28] Addition of methanol to the solution of **2b** at -95°C caused solution color change from green to red with the replacement of the pyrrole β-deuterium resonance by a new resonance of **3b** at -35.1 ppm (signal iii, Figure 5c) which is in the

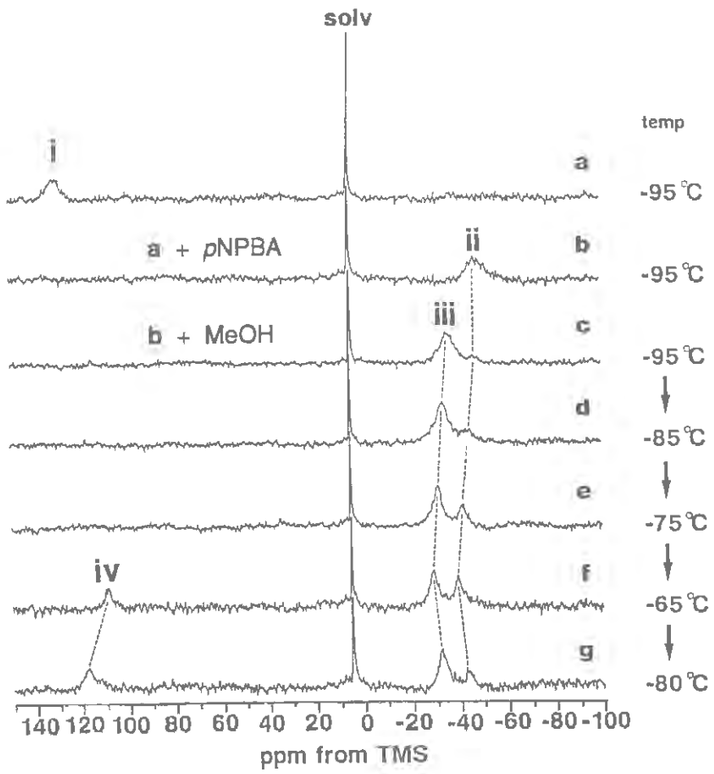

Figure 5. Deuterium NMR spectra of (a) pyrrole-d_8-**1b**-*m*CB [3.0×10^{-3} M]; (b) **2b** prepared by the addition of 1.8 equiv of *p*NPBA to **1b**-*m*CB; (c) **3b** formed by the addition of 2 equiv of **2b** in dichloromethane at -95°C; (d)-(f) temperature dependence of deuterium NMR spectra of solution (c) at -85°C, -75°C, and -65°C; (g) a NMR spectrum of solution (f) at -80°C.

region associated with the unpaired electron occupation in d_{xy}, d_{xz}, and d_{yz} orbitals.[30] The signal iii shows Curie law behavior from -95 to -40°C. During the deuterium NMR measurements, we have found reversible appearance of signal ii upon raising temperature (Figure 5, c-f). The temperature-dependent interconversion between **2b** and **3b** is the further demonstration of **3b** being in the same oxidation state of **2b**. Upon warming the solution to -65°C, **3b** was reduced to **1b**-*m*CB (signal iv, Figure 5f) in several hours.

Figure 6 shows the deuterium NMR spectra of pyrrole-d_8-*meta*-d_8-**1b**-ClO_4 and its oxidized product (**3b'**). Upon addition of F_5-PhIO to a dichloromethane solution of pyrrole-d_8-*meta*-d_8-**1b**-ClO_4, the pyrrole β-deuterium and *meta*-deuterium resonances of **3b'** appeared at -22.9 and 8.8 ppm from TMS at -90°C, respectively. The signals were assigned

based upon the result of the oxidation of pyrrole-d_8-**1b**-ClO_4. The appearance of the *meta*-deuterium resonance in the diamagnetic region readily eliminates possible formulation of **3b'** as a porphyrin π cation radical[30] (see Discussion). The signals at ~110 ppm and ~-50 ppm could be assigned to the pyrrole β-deuterium of decomposed products of **3b'**, ferric and ferryl species, respectively, since the intensity of these signals gradually increased during NMR measurement. Finally, the disappearance of the signal at ~-50 ppm with concomitant increase of the signal at ~110 ppm was observed. Further, addition of olefin to the solution of **3b'** at -90°C caused the pyrrole β-deuterium resonance shift to 108 ppm, which is typical for pyrrole β-protons of high spin iron(III)

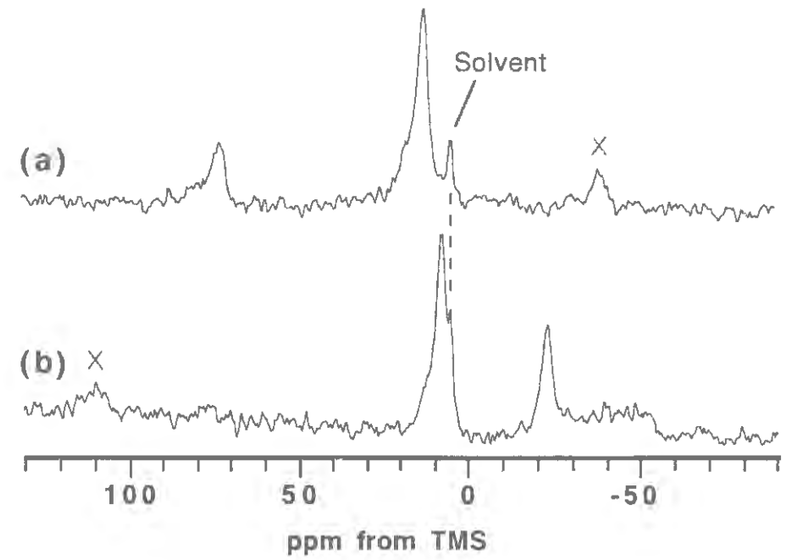

Figure 6. Deuterium NMR spectra of (a) pyrrole-d_8-*meta*-d_8-**1b**-ClO_4 [1.0×10^{-3} M] and (b) **3b'** formed by the addition of 1.8 equiv of F_5-PhIO in dichloromethane containing 200 equiv of methanol at -90°C. In (a), the signal at ~40 ppm is assigned to pyrrole β-^{2}H of ferric low spin species.

porphyrin complexes.[30] NMR spectral data of **2b**, **3b**, and **3b'** are summarized in Table 1 As observed in the UV-vis spectra of **3b** and **3b'**, the chemical shifts of the pyrrole β-protons of **3b** and **3b'** are different.

Upon the addition of a small amount of methanol-d_4 to a dichloromethane solution of pyrrole-d_8-**2b**, additional deuterium NMR signal at 25.6 ppm was observed at -95°C, together with free methanol signals at 3.4 (CD_3)and 4.8 (OD) ppm and the pyrrole deuterium signal for **3b** at -35.1 ppm. Disappearance of the signal at 25.6 ppm by replacement of methanol-d_4 to methanol allows us to assign it to methyl deuterium of methanol (or methoxide) ligated to **3b**. On the basis of these observations, we assigned **3b** and **3b'** as O=Fe(V) (or •O-Fe(IV)) porphyrin complexes having methanol or methoxide as a 6th ligand.

Reactivity of 3b with Olefins. Reactions of olefins with **2b** or **3b** were studied by following the time-dependent UV-vis spectral changes of **2b** or **3b**. In these cases, **2b** and **3b** were prepared by the use of *one equiv* of oxidants to avoid reproduction of **2b** and **3b** by the reaction of an excess amount of oxidants. Upon addition of 500 equiv of norbornylene at -90°C, disappearance of **2b** (or **3b**) was found to be first order both in [olefin] and in [**2b** (or **3b**)] (eq. 4). The same reactions with 1000 equiv of styrene and *p*-chlorostyrene were also examined. The rate constants obtained are listed in Table 2. In all cases, **3b** was less reactive than **2b**.

$$d[\mathbf{1b}]/dt = k_2[\text{olefin}][\mathbf{2b}\ (\text{or}\ \mathbf{3b})] = k_{obs}[\mathbf{2b}\ (\text{or}\ \mathbf{3b})] \qquad (4)$$

Competitive epoxidation of norbornylene and α-methylstyrene by **2b** or **3b** was also carried out to examine steric effect of substrates. Oxidation of a mixture of norbornylene and α-methylstyrene (1:1, 20 equiv with respect to the porphyrin) took place at -90 °C for 30 minutes. The amount

Table 2. Comparison of k_2 ($10^{-2}M^{-1}s^{-1}$) for Reaction of **2b**, **3b** and **3b'** with Olefins in dichloromethane at -90°C.

Olefin	**2b**[a]	**3b**[a]	**3b'**
Norbornylene	120	13	3.3
Styrene	120	11	2.9
p-Chlorostyrene	22	2.3	0.62

[a] Yamaguchi et al. *J. Chem. Soc., Chem. Commun.*, **1992**, 1721-1723.

of oxidized products was determined by GC. The total yields of styrene oxide and α-methylstyrene oxide based on **2b** and **3b** were 71.5 % and 53.0 %, respectively. Both **2b** and **3b** exhibited preferable epoxidation of norbornylene over α-methylstyrene with the selectivity (norbornylene oxide : α-methylstyrene oxide) of 100:30 and 100:35 by **2b** and **3b**, respectively.

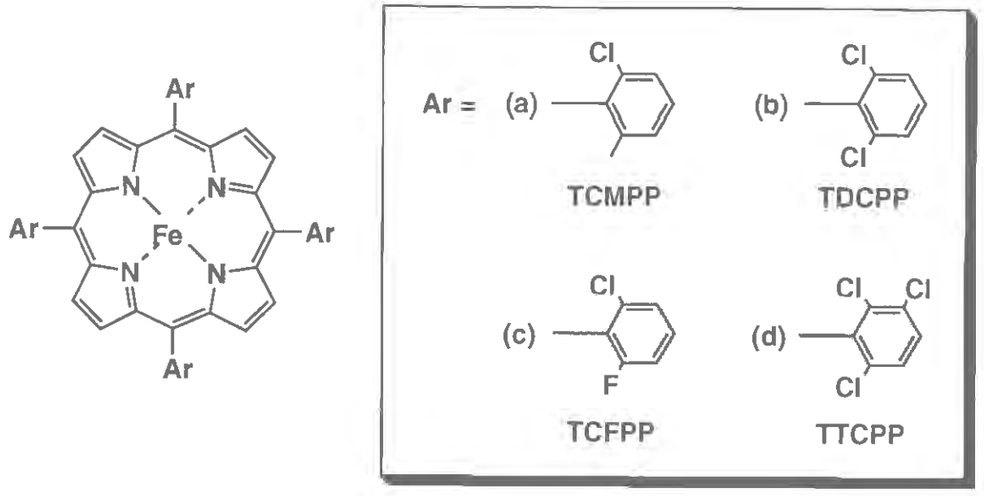

Figure 7. Structure of the porphyrin core of various substituted iron porphyrin complexes (**a**-**d**) employed in this study. Axial ligands have been omitted for simplicity.

Effect of Electron-Withdrawing Substituents Bound to the Porphyrin Ring on the Formation of 3'. Groves et al. showed in the first time that the oxidation of Fe^{III}TMP by *m*CPBA in dichloromethane/methanol affords the corresponding oxo-iron(IV) porphyrin π-cation radical.[1] In the present study, however **3b** was formed by the oxidation of Fe^{III}TDCPP (**1b**) *in the presence of methanol*. In our preliminary report, we have assigned **3b** as O=Fe^{V}TDCPP due to its relatively lower HOMO of the porphyrin ring over the HOMO of methanol coordinated heme iron, since the introduction of electron-withdrawing chlorides on the porphyrin periphery.[15] If our assumption is correct, we could control the electronic structure of two-electron oxidized oxo-iron porphyrin complexes between **2** and **3** by changing the porphyrin substituents. Therefore, we have

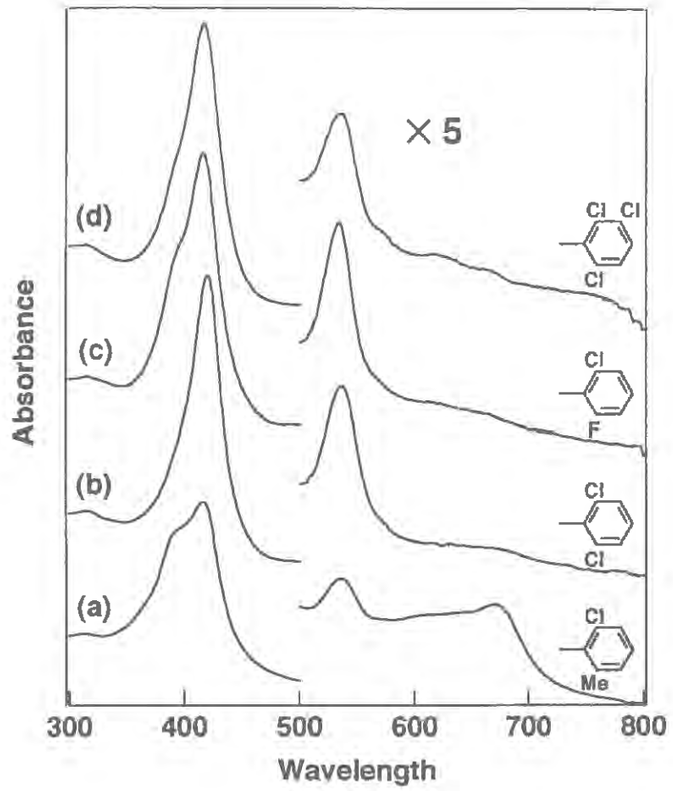

Figure 8. UV-vis spectra of (a) **2a/3a'**, (b) **3b'**, (c) **3c'**, and (d) **3d'** in dichloromethane containing 200 equiv of methanol at -90°C.

prepared aseries of iron porphyrins having substituents at the *meso*-position of the porphyrin ring (Figure 7). Figure 8 shows the UV-vis spectra of the oxidation products of **1**-ClO_4 (**a**-**d**) by F_5-PhIO in dichloromethane containing *200 equiv of methanol* at -90°C. Apparently spectra of **3c'** and **3d'** are essentially the same to that of **3b'**. By contrast, the UV-vis spectrum obtained by the reaction of **1a**-ClO_4 and F_5-PhIO is quite unusual. A less intense Soret band at ca. 395 nm and gentle absorption around 600~700 nm are the indication of oxo-iron(IV) porphyrin π-cation radical (**2a**) formation, and a red shifted Soret band at 420 nm and a Q band around 540 nm are the spectrum expected for oxo-iron(V) porphyrin (**3a'**). Thus, we conclude that the oxidation of **1a**-ClO_4 by F_5-PhIO gave a mixture of two oxidation products **2a** and **3a'**. This assignment was further supported by the interconversion of two oxidation products upon temperature changes (Figure 9).

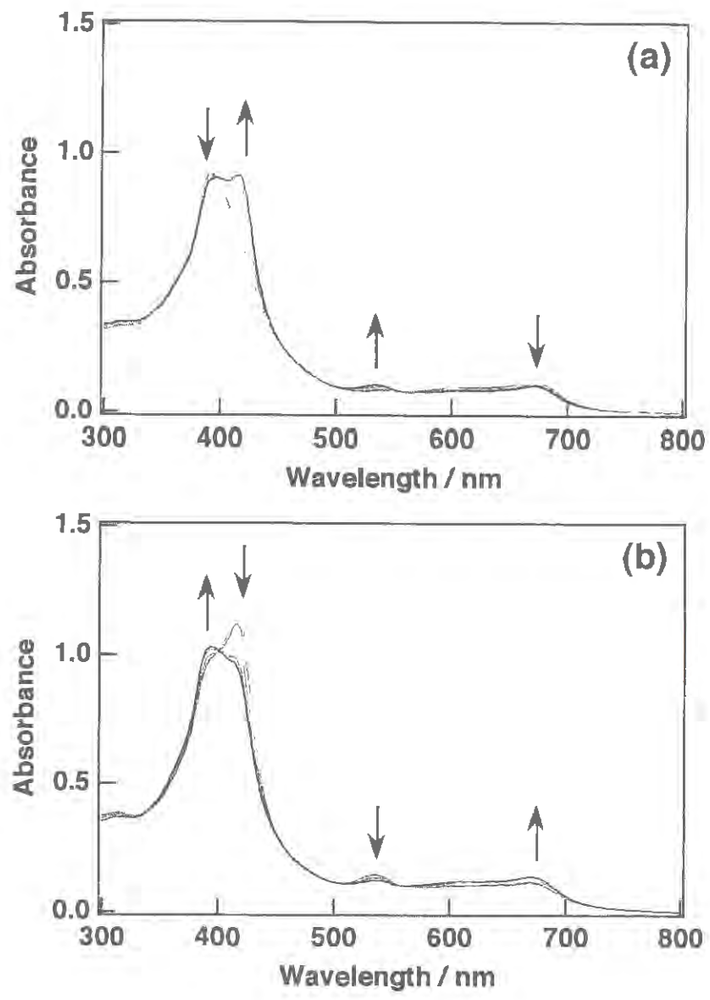

Figure 9. UV-vis spectral changes of **2a/3a'** for (a) lowering temperature from -80°C to -100°C and (b) raising temperature from -95°C to -85°C.

Figure 10 shows ^{1}H NMR spectra of the oxidation products of **1**(**a**-**d**)-ClO_4 prepared by F_5-PhIO in dichloromethane-d_2 containing 200 equiv of methanol-d_4 at -90°C. The oxidation products of **1** gave well-resolved hyperfine-shifted proton NMR spectra that are different from those of the parent iron(III) porphyrins. Signals were assigned based on the selective deuteration. Appearances of the resonances of the pyrrole β-protons and *meta*-protons of **3c'** and **3d'** around -21 and 9 ppm, respectively, suggest the electronic structures of **3c'** and **3d'** are very similar to **3b'**. Under the NMR conditions, formation of a small amount of **2b** and **2c** was observed

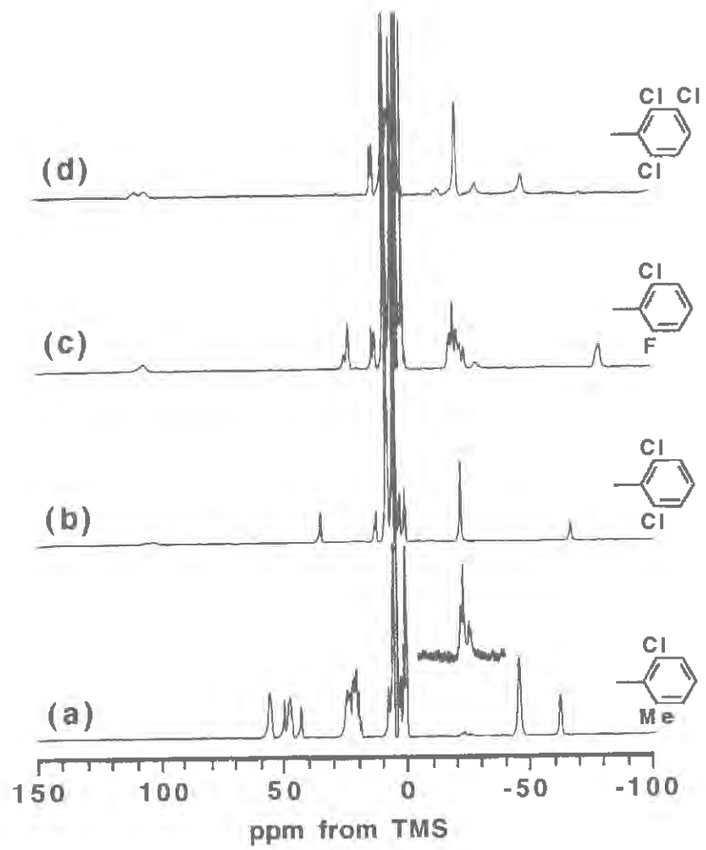

Figure 10. Proton NMR spectra of (a) **2a/3a'**, (b) **3b'**, (c) **3c'**, and (d) **3d'** in dichloromethane-d_2 containing 200 equiv of methanol-d_4 at -90°C. In (a), the signals at ~50 and ~20 ppm are assigned to the *meta*-H and *ortho*-methyl H of **2a'**, respectively.[22] In (b), (c), and (d), the signals of the pyrrole β-H and *meta*-H for ferric porphyrins can be seen at ~110 and ~10 ppm, respectively. The signals in high field region in (d) except -21 ppm are now not assigned.

(pyrrole β- and *meta*-proton resonances: -67 ppm and 35 ppm for **2b** and -80 ppm and 24 ppm for **2c**[24]). Though the increase of electron-withdrawing ability of the porphyrin substituents has been shown to cause upfield shift of the pyrrole β-proton and *meta*-proton signals of oxo-iron(IV) porphyrin π-cation radicals[24], the chemical shifts of the pyrrole β-protons and *meta*-

protons of **3b'-d'**, are almost the same regardless of the electron-withdrawing ability of the porphyrin substituent.

On the other hand, observation of two pyrrole β-proton resonances at -44[24] and -21 ppm (Figure 10a) upon the oxidation of **1a** indicates the formation of two products, **2a** (major product) and **3a'** (minor product), consistent with the UV-vis spectroscopic study. In a separate experiment, **2a** prepared *in the absence of methanol* gave the pyrrole β-proton resonance at -62 ppm[24]. Upon the addition of methanol, the signal at -62 ppm became less intense with concomitant appearance of signals at -44 ppm. Thus, the resonance at -44 ppm could have appeared as a major component due to an interaction of **2a** with methanol.

In a previous report, we attributed to the coordination of MeOH (or MeO^-) to **2b** to afford **3b**.[15] If this is the case, observation of **2a** and **3a'** even in the presence of methanol could be rationalized by the equilibrium between methanol-bound oxo-iron(V) porphyrin and methanol-unbound oxo-iron(IV) porphyrin π-cation radical (eq. 5). However, as shown in Figure 10a, we have observed two different resonances assignable to pyrrole β-protons of **2a** in the presence of methanol. Moreover, the resonance at -62 ppm was also observed for **2a** in the absence of methanol as described above. These results do not fit to a simple binding mechanism shown in eq. (5).

(5)

In order to understand detailed roles of methanol for the transformation of **2** to **3**, NMR spectra of **2a** and **3a'** in the presence of methanol-d_4 were examined[31]. Figure 11a depicts the deuterium NMR spectrum of a mixture of **2a** and **3a'** in the presence of methanol-d_4. Appearance of the paramagnetically shifted resonance at 20 ppm allows us to assign it as methyl deuterium of methanol (or methoxide) ligated to the paramagnetic complex, **3a'**. We have applied the same systems to$O=Fe^{IV}(TMP)^{+\bullet}$ prepared by F_5-PhIO, since $O=Fe^{IV}(TMP)^{+\bullet}$ is known to form even in the presence of methanol.[1] A resonance at 17.2 ppm in Figure 11b is readily assigned to the methyl signal of methanol bound to $O=Fe^{IV}(TMP)^{+\bullet}$ as an axial ligand. The coordination of methanol to $O=Fe^{IV}(TMP)^{+\bullet}$ without changing its electronic structure is indicative of

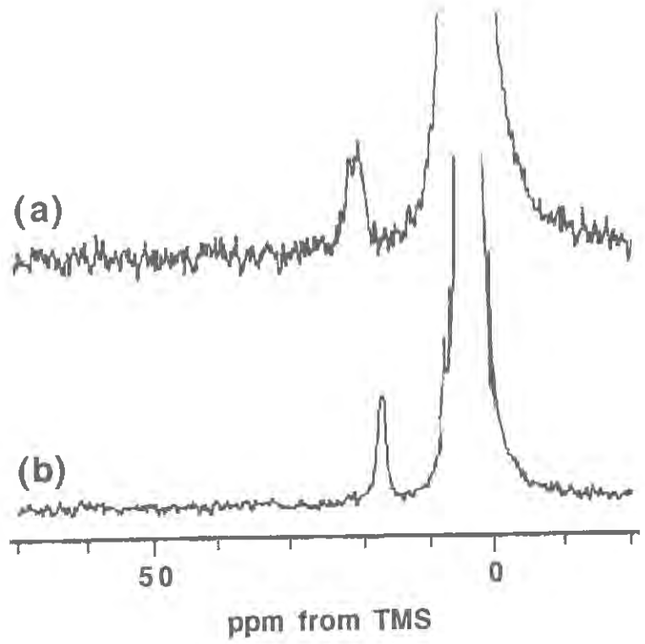

Figure 11. Deuterium NMR spectra of (a) **2a/3a'** in the presence of methanol-d_4, (b) O=Fe^{IV}(TMP)$^{+\bullet}$ in the presence of methanol-d_4.

similar binding of methanol to **2a**, consistent with our tentative assignment of the -44 ppm resonance to **2a** interacting with methanol. These observations can be rationalized if one assumes the coordination of

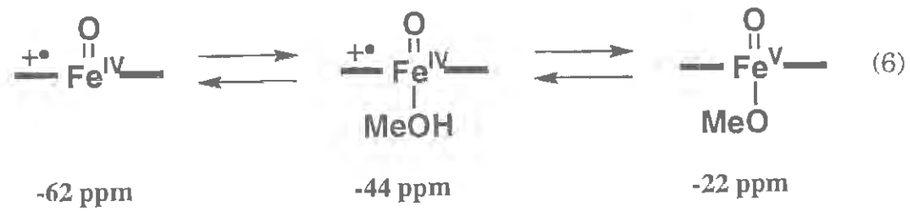

(6)

methoxide anion (MeO^-) to **3a'**, while **2a** can be observed as methanol ligated and unligated forms (eq. 6).

Effect of Electron-Withdrawing Substituents on the Reactivity of 3'. The effect of electron-withdrawing substituents bound to the *meso*-phenyl groups of the porphyrin ring on the reactivity of oxo-iron(IV) porphyrin π-cation radical complexes has been studied by using various *meso*-substituted porphyrins.[24] The results indicate that the reactivity of the oxo-iron(IV) porphyrin π-cation radicals is dependent on their oxidation potentials. Therefore, we have examined the substituent effect on the epoxidation of styrene by **3'** formed by the addition of one equiv of F_5-PhIO. As mentioned earlier, the use of one equiv of the oxidant to prepare **3'** prevents reproduction of active species during the epoxidation. At the same time, we have also examined the epoxidation by oxo-iron(IV) porphyrin π-cation radicals (**2a-d**) which were synthesised by the reaction of **1**-ClO_4 with one equiv of *m*CPBA *in the absence of methanol*.

On the other hand, the first oxidation potentials of **1a-d** were measured by cyclic voltammogram in dichloromethane containing 0.1 M TBAP. Reversible oxidation peaks for **1a-d** were observed in the range from 1.0 to 1.5 V vs SCE. The half-wave oxidation potentials of **1a-d** along with the rate constants of the styrene epoxidation by **2** and **3'** are summarized in Table 3.

Table 3. $E_{ox.}$ of Chloro Iron(III) Porphyrins and k_2 for Styrene Epoxidation by High-Valent Oxo-Iron Porphyrins.

		k_2 ($10^{-2}M^{-1}s^{-1}$)	
porphyrin	$E_{ox.}$ (V)	**3'**	**2**
TCMPP (**a**)	1.29[a]	—	—
TDCPP (**b**)	1.35[a]	2.9	550
TCFPP (**c**)	1.39	4.4	800
TTCPP (**d**)	1.44	4.7	1300

[a] Fujii. *J. Am.Chem. Soc.*, **1993**, *115*, 4641-4648.

Discussion

Electronic Structure of New Active Intermediates, 3 and 3'. Iron(III) porphyrin *N*-oxides, iron(III) porphyrin dications, and oxo-iron(IV) porphyrin π-cation radicals have been reported as high-valent iron porphyrins formally two-electron oxidized from the ferric state. In the present study we have described the formation of new two-electron oxidized oxo-iron porphyrins, **3** and **3'**, by the chemical oxidation of iron(III) porphyrins in the presence of methanol under acidic and

neutral conditions. The formulation of **3** is supported by iodometric titration, UV-vis, NMR, and EPR spectroscopic measurements, thermal interconversion between **2** and **3**, and ability for epoxidation at -90°C.

The UV-vis spectra of **3b** and **3b'** (Figure 1 and 2, λ_{max} : 418 and 546, and 418 and 532 nm, respectively) are different from those of iron(III) porphyrin *N*-oxides (λ_{max} : 441 and 547 nm in toluene for Fe^{III}TMP *N*-oxide), iron(III) porphyrin dications (λ_{max} : 412 nm in toluene for Fe^{III}TMP dication), and also different from both of a_{2u} oxo-iron(IV) porphyrin π-cation radicals (λ_{max} : 409 and 681 nm in dichloromethane for O=Fe^{IV}TDCPP$^{+\bullet}$ (**2b**)) and a_{1u} type complexes[24]. Though the spectrum of oxo-iron(IV) porphyrin (**4b**) (λ_{max} : 419 and 543 nm in dichloromethane) is rather similar to those of **3b** and **3b'**, epoxidation activity at -90°C, thermal stability, and oxidizing equivalents determined by iodometric titration readily discriminate **3b** and **3b'** from **4b**. Especially, **4b** is observable even at 0°C and does not react with olefins at low temperature. These results suggest that **3b** and **3b'** are two-electron oxidized complexes from the resting state and may not be the π-cation radicals, such as **2b**.

The resonance of *meta*-deuterium in **3b** was observed in a

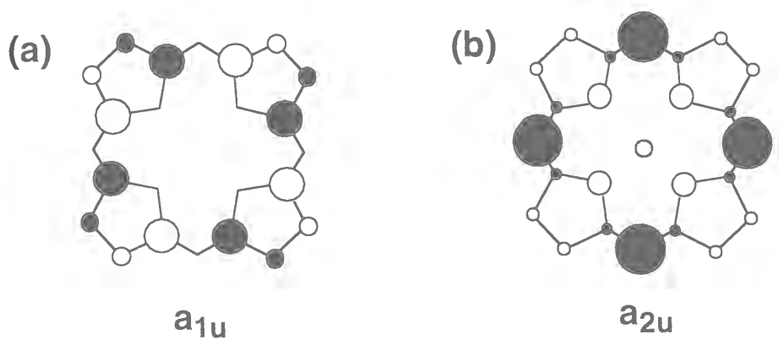

Figure 12. Electron spin distribution of porphyrin HOMO: (a) a_{1u}, (b) a_{2u}.

diamagnetic region (8.8 ppm). If **3b** was a a_{2u} radical species such as **2b**, a large downfield shift for the *meta*-deuterium should be observed because of the large negative π-spin density on the *meso*-carbons in the a_{2u} radical orbital, as shown in Figure 12b. While the signal in a diamagnetic region reminds us of the a_{1u} radical species having node at the *meso*-carbons (Figure 12a), the UV-vis spectrum of **3b** is inconsistent with a_{1u} oxo-

iron(IV) porphyrin π-cation radicals, as already mentioned[24] Similar considerations are also applicable for **3b'**. Furthermore, the pyrrole β-deuterium signals of **3b** at -35.1 ppm and **3b'** at -22.9 ppm are less paramagnetically shifted than that of **2b** (-46.2 ppm) and rather similar to **4b** (-33.1 ppm). These results also suggest that **3b** and **3b'** have a neutral porphyrin ring. Finally, the EPR spectrum (g = 4.33, 3.69, 1.99) and magnetic moment (μ_{eff} = 4.0 μ_B) of **3b** provide conclusive evidence for the presence of 3 unpaired electrons in **3b**. Thus, the most likely description for **3b** is high spin complexes of either O=Fe^{V}TDCPP or •O-Fe^{IV}TDCPP. At this moment, we are not able to differentiate the O=Fe^{V} complex from •O-Fe^{IV} complex, thus we describe them as the O=Fe^{V} complex for simplicity. To gain a further insight, resonance Raman and Mössbauer measurement are under investigation.

Figure 5 depicts temperature dependent interconversion between **2b** and **3b**. Favorable formation of **3b** at lower temperature and observation of the paramagnetically shifted methyl deuterium of methanol at 25.6 ppm (data not shown) indicate that the ligation of methanol (or methoxide) to **2b** altered its electronic structure to **3b**[31]. Though appreciable UV-vis spectral change was not observed upon the introduction of methanol to a dichloromethane solution of O=Fe^{IV}(TMP)$^{+\bullet}$, ligation of methanol has been confirmed by the appearance of the methyl resonance at 17.2 ppm. Therefore, formation of both **2a** and **3a'** in the same solution containing methanol may not be simply attributed to the exclusive ligation of methanol in **3a'**. Ligation of methanol both to **2a** and **3a'** but in a different manner as shown in eq. (6) seems to be rather likely.

On the basis of these considerations, both **3b** and **3b'** can be formulated as oxo-iron(V) high spin porphyrin having the methoxide ligand. So far, we could not explain why small differences in UV-vis and NMR spectra were observed for **3b** and **3b'**. These differences are also reflected on the epoxidation activities of **3b** and **3b'** (Table II). One of the major differences between **3b** and **3b'** is that perchloric acid must be formed in the course of **3b'** formation (eq. 7) while very weak *m*-

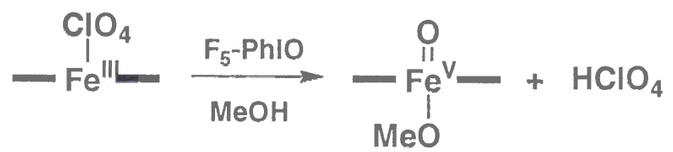

(7)

chlorobenzoic acid is present in a solution of **3b**. Therefore, one may expect a hydrogen bond between the oxo-oxygen and/or methanol-oxygen of the axial ligand in **3b'** and perchloric acid, because such a small difference in the reaction condition is known to cause spectral changes.[32] Further investigation is needed on effects of acid.

Recently, Jayaraj et al. reported the influence of *meso*-substituents on the electronic states of oxo-iron(IV) porphyrin π-cation radicals.[16] In the report, oxo-iron(IV) porphyrin π-cation radicals were the sole oxidation products even though the oxidations were performed under the condition similar to ours, where iron(III) porphyrins having electron-withdrawing substituents were oxidized by peracid in the presence of methanol. Therefore, we have carried out the same reactions by using UV-vis spectroscopy. Figure 13(a) shows the spectrum of the oxidation product given under almost the same conditions reported by Jayaraj et al. ([Fe^{III}TDCPP($OCOCF_3$)] = 1 mM; **4 equiv of *m*CPBA**; CH_2Cl_2 : CD_3OD = 10 : 1; -90°C). Since the oxidation product exhibits the same spectral characteristics reported by Jayaraj et al., the formation of oxo-iron(IV) porphyrin π-cation radical (**2b**) is apparent. As described in experimental, we have prepared high-valent oxo species *with a small excess amount of oxidants* (*1 ~ 1.8 equiv*). Therefore, we have examined the reaction of Jayaraj et al. by **1.5 equiv of *m*CPBA** (Figure 13(b)). In this case, the absorbance at 678 nm clearly decreased with concomitant appearance of absorption at ~520 nm. Then, we performed the oxidation *in the presence of only 100 equiv of CD_3OD* with 1.5 equiv of *m*CPBA (Figure 13(c)). Surprisingly, the new absorption was observed around 540 nm. The addition of 100 equiv of styrene to the solution caused the conversion of 540 nm species to iron(III) porphyrin as well as oxo-iron(IV) porphyrin π-cation radical at -90°C. Judging from these results, we concluded that 540 nm species was oxo-iron(V) porphyrin (**3b**) and **3b** was not formed in the presence of a large amount of peracid. We attribute the suppression of the oxo-iron(V) porphyrin formation to the coordination of peracid (acid) or methanol instead of methoxide whose coordination is crucial for the formation of oxo-iron(V) porphyrin. As shown in Figure 13(d), the oxidation of Fe^{III}TDCPP(OH) afforded **3b** as the sole product by the addition of 1.5 equiv of *m*CPBA in CH_2Cl_2 containing 100 equiv of CD_3OD at -90°C, since the resulting solution is almost neutral. Furthermore, the conversion of **3b** to oxo-iron(IV) porphyrin π-cation radical (**2b**) was observed by the addition of 2 equiv of trifluoroacetic acid (TFA) to the solution of (d) (Figure 13(e)). These results were

summarized in Table IV, and indicate that the formation of **2** and **3** (and **3'**) is very dependent on the condition of the reaction solutions, especially the nature of the 6th ligand and acid.

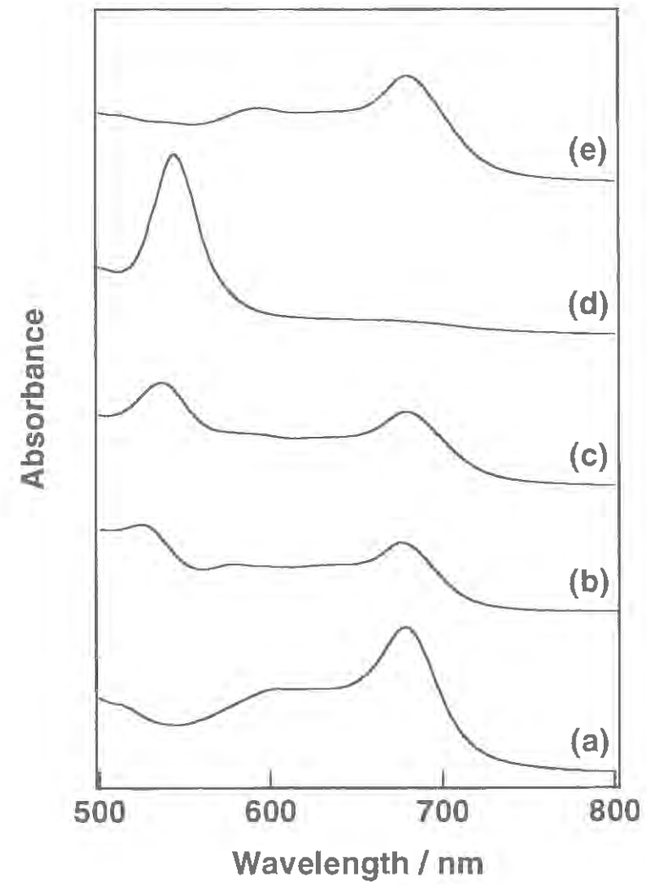

Figure 13. UV-vis spectra of the oxidation products under various conditions: (a) Fe^{III}TDCPP(trifluoroacetate) + 4 equiv of *m*CPBA in CH_2Cl_2/CD_3OD (10:1) at -90°C, (b) + 1.5 equiv of *m*CPBA, (c) +1.5 equiv of *m*CPBA in CH_2Cl_2 containing 100 equiv of CD_3OD at -90°C, (d) Fe^{III}TDCPP(OH) +1.5 equiv of *m*CPBA in CH_2Cl_2 containing 100 equiv of CD_3OD at -90°C, (e) (d) + 2 equiv of TFA.

Table 4. Summary of Figure 13.

symbol[a]	axial ligand of ferric complex	quantity of added *m*CPBA	reaction condition	products (total 100%) **2b** (%)	**3b** (%)
ref.16	$CF_3SO_3^-$	8 equiv	in CH_2Cl_2:MeOH = 10:1 at -80°C	100	
(a)	CF_3COO^-	4 equiv	in CH_2Cl_2:MeOH = 10 1 at -90°C	100	
(c)	CF_3COO^-	1.5 equiv	in CH_2Cl_2/100 equiv of MeOH at -90°C[b]	~50[c]	~50[c]
(d)	OH^-	1.5 equiv	in CH_2Cl_2/100 equiv of MeOH at -90°C[b]		100
(e)	———	———	(d) + 2 equiv of TFA	~90[c]	~10[c]

[a] Symbols for the spectra in Figure 13.

[b] CH_2Cl_2/100 equiv of MeOH approximately corresponds to CH_2Cl_2:MeOH = 300:1.

[c] These ratios were determined by the decomposition of each spectrum into **2b** (a) and **3b** (d).

Possible Mechanism for the Formation of Oxo-iron(V) Porphyrins. On the basis of the various spectroscopic data for **3**, it is clear that this complex has three unpaired electrons on the iron-oxo unit (possibly only iron), not the porphyrin ring. We attribute the electron-withdrawing substituents on the porphyrin ring and the axial ligand for the formation of **3** instead of **2**. Introduction of electron-withdrawing groups on the porphyrin ring is known to lower the porphyrin orbital energy. For instance, a higher oxidation potential of $[Fe^{II}TDCPP]^+/[Fe^{II}(TDCPP)^{+\bullet}]^{2+}$ (1.35 V) than that of $[Fe^{II}TMP]^+/[Fe^{II}(TMP)^{+\bullet}]^{2+}$ (1.11 V)[24] suggests that HOMO (a_{2u}) energy of the chloro substituted complex ($Fe^{II}TDCPP$) is 0.24 V lower than that of the methyl substituted complex ($Fe^{II}TMP$) as shown in Figure 14a,b. Ligation of methoxide to **2b** raises the d_{xz} and d_{yz} orbitals as well as the d_{z^2} orbital. These effects eventually turn upside down the energy levels between the a_{2u} orbital and the d_{xz} and d_{yz} orbitals to form **3b** (Figure 14c). The idea is supported by the result of the oxidation of **1(b-d)**-ClO_4 by F_5-PhIO in the presence of methanol. While the preferable formations of **3b'-d'** are observed, the oxidation of a less electron deficient complex (**1a**-ClO_4) afforded a mixture of **2a** (major) and **3a'** (minor). These results suggest that the electron-withdrawing substituents on the porphyrin ring play two roles in the formation of **3**. One is lowering the π energy level of the porphyrin ring, and the other is encouragement of methoxide ligation rather than methanol to raise iron *d* orbitals. Once the energy level between the a_{2u} orbital of the porphyrin ring and the d_{xy} and d_{yz} orbitals of the iron are turned upside down, transformation of **2** to **3** will be observed. In the case of **2a** and **3a'**, less electron-withdrawing ability of the substituents failed to complete the ligation of methoxide as shown in Figure 14d. So far, this proposed mechanism can explain all the results obtained in this study without contradiction.

Reactivity of Oxo-iron(V) Porphyrins and Oxo-iron(IV) Porphyrin π-Cation Radicals. It has been known that oxo-metalloporphyrin complexes are able to oxidize various substrates observed in P-450 catalyzed reactions such as epoxidation of olefins (eq. 8).[33] Although kinetic studies of the epoxidation catalyzed by metalloporphyrins have been carried by many groups, the direct comparison of reactivities between oxo-iron(V) porphyrins (**3**) and oxo-iron(IV) porphyrin π-cation radicals (**2**) has never been carried out except for our preliminary study. Preparation of **2** and **3** now allows us to examine roles of porphyrin π-cation radicals in **2** on the olefin epoxidation.

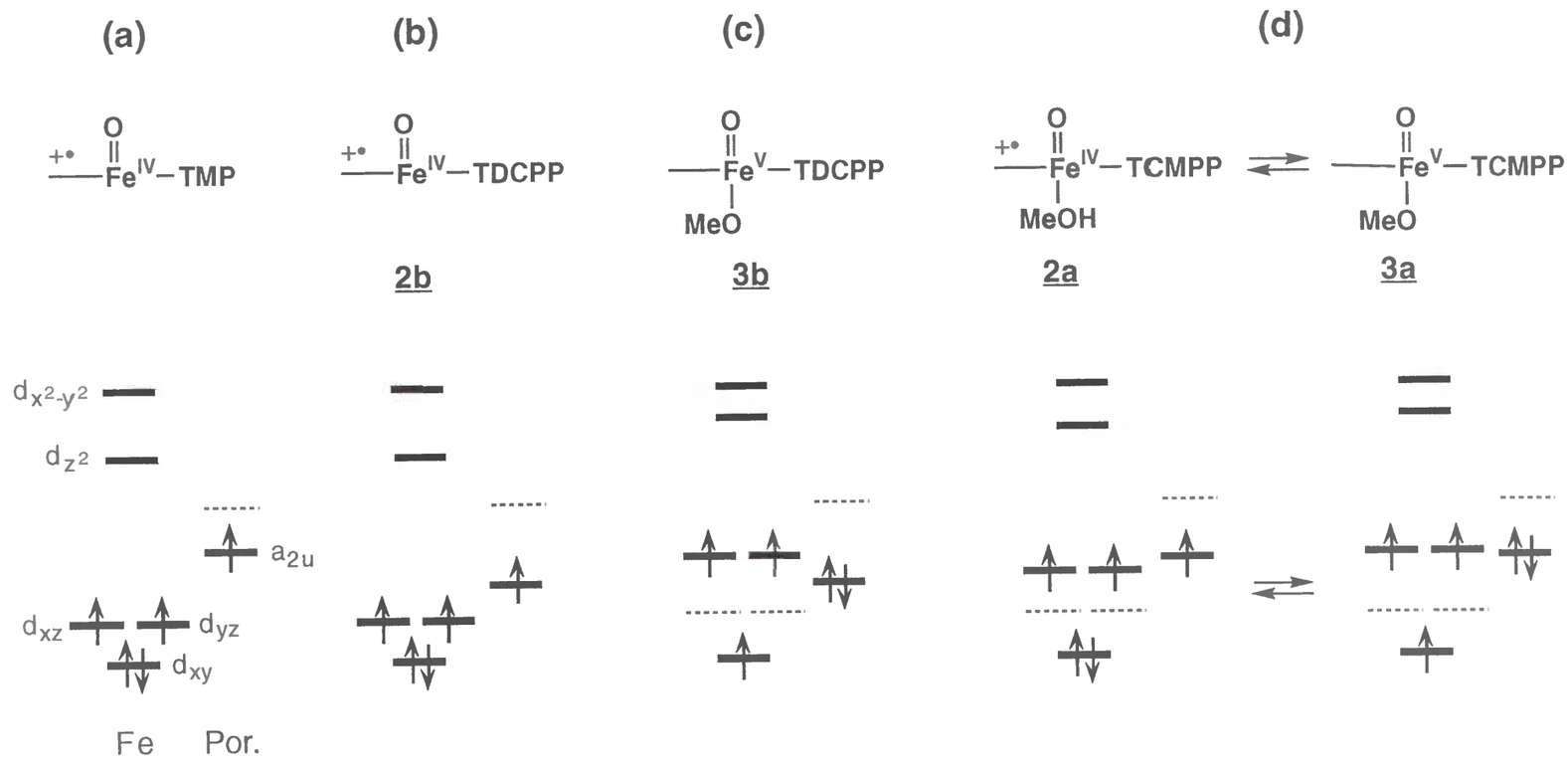

Figure 14. Orbital energy diagram for high-valent iron porphyrins: (a) O=FeIV(TMP)+•, (b) 2b, (c) 3b, (d) 2a and 3a.

(8)

Thus, we have determined the rate constants of the epoxidation reactions by stoichiometric oxidation of olefins by **2** and **3** at -90°C (Tables II and III). Interestingly, **3** is found to be less reactive than **2** in the epoxidation of olefins. That one electron oxidation of either the porphyrin ring or the central iron in an O=Fe^{IV} complex (**4**) exhibits different reactivity could be explained as follows: while the π-cation radical orbital (a_{2u}) in **2** interacts with p_z orbital of the oxo ligand through an iron p_z orbital as well as the interactions between iron d_{xz} (d_{yz}) and p_x (p_y) of the oxo ligand, iron d_{xy} orbitals of **3** does not interact with any of the oxo ligand orbitals.[24,34] It implies that the radical character of the oxo ligand in **3** is similar to that of **4**, even though the missing of one electron from the d_{xy} orbital makes **3** less electron rich than **4**. Therefore, the reactivity of **3** is expected to be between **2** and **4**. The observations indicate that the presence of porphyrin radical is crucial for the activation of the oxo ligand.

That **3** having higher oxidation potential porphyrin is more reactive as shown in Table III indicates the mechanism for epoxidation reaction by **3** involves electrophilic character as observed in the epoxidation by oxo-iron(IV) porphyrin π-cation radicals. Thus, *p*-chlorostyrene is less reactive than styrene. Interestingly, relative rates of olefin epoxidation by **2b** and **3b** are very close (Table II). In addition, competitive epoxidation of norbornylene and α-methylstyrene by **2b** and **3b** showed preferable oxidation of less hindered norbornylene with almost identical selectivity (100: 30 - 35), suggesting very similar epoxidation mechanisms by **2** and **3**.[35]

Implication of Biological Use of Porphyrin π-Cation Radicals. Heme enzymes such as peroxidase and catalases are known to utilize two-electron oxidized intermediates so called compound I. Many spectroscopic studies support the formulation of compound I as an oxo-ferryl porphyrin π-cation radical.[6-10] In the case of P-450, the active species responsible for the monooxygenations are still obscure and the subject of intensive investigations.[11] While Champion pointed out possible description of •O-Fe(IV) (one extreme structure of O=Fe(V)) as

the active species of P-450,[14] Egawa et al. suggested formation of compound I type intermediate on the basis of their rapid scan measurements.[13] There are two important conclusions from our studies; i) UV-vis spectra of the $O=Fe^{V}$ complexes are almost identical to those of O=Fe(IV) species, compound II. Therefore, one must be very careful to assign compound II on the basis of UV-vis spectroscopy. ii) O=Fe(V) porphyrins are less reactive than the corresponding O=Fe(IV) porphyrin π-cation radicals. The results are suggestive of the biological role of porphyrin π-cation radicals in compound I of peroxidases, catalases, and possibly in the active species of P-450.

References

(1) Groves, J. T.; Haushalter, R. C.; Nakamura, M.; Nemo, T. E.; Evans, B. J. *J. Am. Chem. Soc.* **1981**, *103*, 2884-2886.

(2) (a) Groves, J. T.; Watanabe, Y. *J. Am. Chem. Soc.* **1986**, *108*, 7836-7837. (b) Groves, J. T.; Watanabe, Y. *J. Am. Chem. Soc.* **1988**, *110*, 8443-8452. (c) Mizutani, Y.; Watanabe, Y.; Kitagawa, T. *J. Am. Chem. Soc.* **1994**, *116*, 3439-3441.

(3) (a) Tsurumaki, H.; Watanabe, Y.; Morishima, I. *J. Am. Chem. Soc.* **1993**, *115*, 11784-11788. (b) Watanabe, Y.; Takehira, K.; Shimizu, M.; Hayakawa, T.; Orita, H.; Kaise, M. *J. Chem. Soc., Chem. Commun.* **1990**, 1262-1264.

(4) (a) Dolphin, D.; Forman, A.; Borg, D. C.; Fajar, J.; Felton, R. H. *Proc. Natl. Acad. Sci. USA.* **1971**, *68*, 641. (b) Traylor, T. G.; Lee, W. A.; Stynes, D. V. *J. Am. Chem. Soc.* **1984**, *106*, 755-764. (c) Schulz, C. E.; Rutter, R.; Sage, J. T.; Debrunner, P. G.; Hager, L. P. *Biochemistry* **1984**, *23*, 4743-4754. (d) La Mar, G. N.; de Roppe, J. S. *J. Am. Chem. Soc.* **1980**, *102*, 395-397. (e) La Mar, G. N.; De Roppe, J. S.; K.M., S.; Langry, K. *J. Biol. Chem.* **1981**, *256*, 237-243. (f) Roberts, J. E.; Hoffman, B. M.; Rutter, R.; Hager, L. P. *J. Biol. Chem.* **1981**, *256*, 2118-2121. (g) Roberts, J. E.; Hoffman, B. M.; Rutter, R.; Hager, L. P. *J. Am. Chem. Soc.* **1981**, *103*, 7654-7656. (h) Patterson, W. R.; Poulos, T. L.; Goodin, D. B. *Biochemistry* **1995**, *34*, 4342-4345. (i) Makino, R.; Uno, T.; Nishimura, Y.; Iizuka, T.; Tsuboi, M.; Ishimura, Y. *J. Biol. Chem,* **1986**, *261*, 8376-8382.

(5) (a) Robert, A.; Loock, B.; Momenteau, M.; Meunier, B. *Inorg. Chem.* **1991**, *30*, 706-711. (b) Chuang, W.-J.; Van Wart, H. E. *J. Biol. Chem.* **1992**, *267*, 13293-13301. (c) Mansuy, D.; Lange, M.; Chottard, J. C. *J. Am. Chem. Soc.* **1979**, *101*, 6437-6439.

(6) Dolphin, D.; Felton, R. H. *Acc. Chem. Res.* **1974**, *7*, 26-32.

(7) Schultz, C. E.; Devaney, P. W.; Winkler, H. D. P. G.; Doan, N.; Chiang, R.; Rutter, R.; Hager, L. P. *FEBS Lett.* **1979**, *103*, 102.

(8) (a) Morishima, I.; Takamuki, Y.; Shiro, Y. *J. Am. Chem. Soc.* **1984**, *106*, 7666-7672. (b) La Mar, G. N.; Thanabal, V.; Johnson, R. D.; Smith, K. M.; Parish, D. W. *J. Biol. Chem.* **1989**, *264*, 5428.

(9) (a) Paeng, K.-J.; Kincaid, J. R. *J. Am. Chem. Soc.* **1988**, *110*, 7913-7915. (b) Hashimoto, S.; Mizutani, Y.; Tatsuno, Y.; Kitagawa, T. *J. Am. Chem. Soc.* **1991**, *113*, 6542-6549.

(10) Moss, T. H.; Ehrenberg, A.; Bearden, A. J. *Biochemistry* **1969**, *8*, 4159-4162.

(11) (a) Makino, R.; Ishimura, Y. In *Taisha*, **1982**, *19*, 27. (b) Ortiz de Montellano, P. R. In *Cytochrome P-450*; Ortiz de Montellano, P. R. Ed. Plenum Press, New York, **1986**, p217. (c) Watanabe, Y. In *Shokubai*, **1990**, *32*, 294. (d) Mueller, E.J.; Loida, P.L.; Sligar, S.G. In *Cytochrome P-450*; Ortiz de Montellano, P. R. Ed. Plenum Press, New York, **1995**, 2nd Edition, p83.

(12) For example: (a) Watanabe, Y.; Groves, J. T. In *The Enzymes* ; P. D. Boyer and D. S. Sigman, Ed.; Academic Press: New York,**1992**; Vol. 20; p 405-452. (b) Meunuier, B. *Chem. Rev.* **1992**, *92*, 1411-1456.

(13) Egawa, T.; Shimada, H.; Ishimura, Y. *Biochem. Biophys. Res. Commun.* **1994**, *201*, 1464-1469.

(14) Champion, P. M. *J. Am. Chem. Soc.* **1989**, *111*, 3433-3434.

(15) Yamaguchi, K.; Watanabe, Y.; Morishima, I. *J. Chem. Soc., Chem. Comunn.* **1992**, 1721-1723.

(16) Jayaraj, K.; Terner, J.; Gold, A.; Roberts, D. A.; Austin, R. N.; Mandon, D.; Weiss, R.; Bill, E.; Müther, M.; Trautwein, A. X. *Inorg. Chem.* **1996**, *35*, 1632-1640.

(17) Lindsey, J. S.; Wagner, R. W. *J. Org. Chem.* **1989**, *54*, 828-836.

(18) Fajer, J.; Borg, D.; Forman, A.; Dolphin, D.; Felton, R. H. *J. Am. Chem. Soc.* **1970**, *92*, 3451-3459.

(19) Gross, Z.; Kaustov, L. *Tetrahedron Lett.* **1995**, *36*, 3735-3736.

(20) Kobayashi, H.; Higuchi, T.; Kaizu, Y.; Osada, H.; Aoki, M. *Bull. Chem. Soc. Jpn.* **1975**, *48*, 3137.

(21) Reed, C. A.; Mashiko, T.; Bentley, S. P.; Kastner, M. E.; Scheidt, W. R.; Spartalian, K.; Lang, G. *J. Am. Chem. Soc.* **1979**, *101*, 2948-2958.

(22) Schmeisser, M.; Dahmen, K.; Satori, P. *Chem. Ber* **1967**, *100*, 1633.

(23) (a) Schwartz, N. N.; Blumbergs, J. H. *J. Org. Chem.* **1964**, *29*, (b) Silbert, L. S.; Siegel, E.; Swern, D. *J. Org. Chem.* **1962**, *27*, 1336.
(24) Fujii, H. *J. Am. Chem. Soc.* **1993**, *115*, 4641-4648.
(25) Gold, A.; Jayaraj, K.; Doppelt, P.; Weiss, R.; Chottard, G.; Bill, E.; Ding, X.; Trautwein, A. X. *J. Am. Chem. Soc.* **1988**, *110*, 5756-5761.
(26) (a) Traylor, T. G.; Popovitz-Biro, R. *J. Am. Chem. Soc.* **1988**, *110*, 239. (b) Traylor, P. S.; Dolphin, D.; Traylor, T. G. *J. Chem. Soc. Chem. Commun.* **1984**, 279-280. (c) Traylor, T. G.; Lee, W. A.; Stynes, D. V. *J. Am. Chem. Soc.* **1984**, *106*, 755-764. (d) Traylor, T. G.; Xu, F. *J. Am. Chem. Soc.* **1990**, *112*, 178-186. (e) Lee, W. A.; Bruice, T. C. *J. Am. Chem. Soc.* **1985**, *107*, 513-514. (f) Zipplies, M. F.; Lee, W. A.; Bruice, T. C. *J. Am. Chem Soc.* **1986**, *108*, 4433-4445. (f) Yuan, L.-C.; Bruice, T. C. *J. Am. Chem. Soc.* **1986**, *108*, 1643-1650. (g) Bruice, T. C.; Balasubramanian, P. N.; Lee, R. W.; Lindsay Smith, J. R. *J. Am. Chem. Soc.* **1988**, *110*, 7890-7892. (h) Panicucci, R.; Bruice, T. C. *J. Am. Chem. Soc.* **1990**, *112*, 6063-6071. (i) Gopinath, E.; Bruice, T. C. *J. Am. Chem. Soc.* **1991**, *113*, 4653-4665. (j) Groves, J. T.; Watanabe, Y. *J. Am. Chem. Soc.* **1986**, *108*, 7834-7836. (k) Labeque, R.; Marnett, L. J. *J. Am. Chem. Soc.* **1989**, *111*, 6621-6627. (l) Higuchi, T.; Uzu, S.; Hirobe, M. *J. Am. Chem. Soc.* **1990**, *112*, 7051-7053. (m) Yamaguchi, K.; Watanabe, Y.; Morishima, I. *Inorg. Chem.* **1992**, *31*, 156-157.
(27) Yamaguchi, K.; Watanabe, Y.; Morishima, I. *J. Am. Chem. Soc.* **1993**, *115*, 4058-4065.
(28) (a) Gold, A.; Jayaraj, K.; Doppelt, P.; Weiss, R.; Bill, E.; Ding, X.-Q.; Bominaar, E. L.; Trautwein, A. X.; Winkler, H. *New J. Chem.* **1989**, *13*, 169-172. (b) Balch, A. L.; Latos-Grazynski, L.; Renner, M. W. *J. Am. Chem. Soc.* **1985**, *107*, 2983-2985.
(29) Evans, D. F. *J. Chem. Soc.* **1959**, 2003-2005.
(30) (a) La Mar, G. N. In *NMR of Paramagnetic Molecules;* La Mar, G. N., Horrocks, W. D., Holm, R. H., Eds.; Academic Press: New York, **1973**, pp 85-126. (b) La Mar, G. N.; Walker, A. In *The Porphyrins*; Dolphin, D., Ed.; Academic Press: New York, **1978**; Vol. 4, pp 61-157.
(31) Deuterium source is only methanol-d_4 in this solution.
(32) Gross, Z.; Nimri, S. *Inorg. Chem.* **1994**, *33*, 1731-1732.
(33) (a) Groves, J. T.; Nemo, T. E.; Myers, R. S. *J. Am. Chem. Soc* . **1979**, *101*, 1032-1033. (b) Jørgensen, K. A. *J. Am. Chem. Soc.* **1987**, *109*, 698-705. (c) Groves, J. T.; Nemo, T. E. *J. Am. Chem. Soc.* **1983**, *105*, 5786-5791. (d) Groves, J. T.; Myers, R. S. *J. Am. Chem. Soc.* **1983**, *105*, 5791-5796. (e) Collman, J. P.; Kodadeck, T.; Raybuck, S. A.; Brauman, J. I.;

Papazian, I. M. *J. Am. Chem. Soc.* **1985**, *107*, 4343. (f) Dicken, C. M.; Woon, T. C.; Bruice, T. C. *J. Am. Chem. Soc.* **1986**, *108*, 1636-1634. (g) Groves, J. T.; Watanabe, Y. *J. Am. Chem. Soc.* **1986**, *108*, 507-508. (h) Artaud, I.; Devocelle, L.; Battioni, J.-P.; Girault, J.-P.; Mansuy, D. *J. Am. Chem. Soc.* **1987**, *109*, 3782-3783. (i) Mansuy, D.; Battioni, P.; Renaud, J.-P.; Guerin, P. *J. Chem. Soc. Chem. Commun.* **1985**, 155-156. (j) Mansuy, D.; Battioni, P.; Renaud, J.-P. *J. Chem. Soc. Chem. Commun.* **1984**, 1255-1257. (k) Fontecave, M.; Mansuy, D. *J. Chem. Soc. Chem. Commun.* **1984**, 879-881. (l) Traylor, T. G.; Miksztal, A. R. *J. Am. Chem. Soc.* **1989**, *111*, 7443-7448. (m) Lindsay Smith, J. R.; Sleath, P. R. *J. Chem. Soc. Perkin Trans II* **1982**, 1009-1015. (n) Naruta, Y.; Maruyana, K. *Tetrahedron Lett.* **1987**, *28*, 4553-4556. (o) He, G.-H.; Bruice, T. C. *J. Am. Chem. Soc.* **1991**, *113*, 2747-2753. (p) Leanord, D. R.; Lindsay Smith, J. R. *J. Chem. Soc. Perkin Trans. 2* **1991**, 25-30. (q) Ostovic, D.; Bruice, T. C. *Acc. Chem. Rev.* **1992**, *25*, 314-320. (r) Traylor, T. G.; Tsuchiya, S.; Byun, Y.-S.; Kim, C. *J. Am. Chem. Soc.* **1993**, *115*, 2775-2781. (s) Naruta, Y.; Tani, F.; Ishihara, N.; Maruyama, K. *J. Am. Chem. Soc.* **1991**, *113*, 6865-6872.
(34) Ozawa, S.; Watanabe, Y.; Morishima, I. *J. Am. Chem. Soc.* **1994**, *116*, 5832-5838.
(35) Machii, K.; Watanabe, Y.; Morishima, I. *J. Am. Chem. Soc.* **1995**, *117*, 6691-6697.

PART III.

MECHANISM OF HEME METABOLISM BY HEME OXYGENASE

CHAPTER 1.

New Oxidation Reaction of an Iron Porphyrin Complex Related to Heme Catabolism

Abstract

Heme oxygenase (HO) catalyzes the degradation of heme to biliverdin through α-*meso*-hydroxyheme. In order to examine more detail of the α-*meso*-hydroxylation mechanism, we have prepared a novel iron porphyrin complex, in which less hindered *p*-chlorophenyl groups were introduced to two *meso*-positions and the other two *meso*-positions were protected by mesityl groups; Fe^{III}BMB*p*CPP (**1c**) [BMB*p*CPP: 5,15-bis(mesityl)-10,20-bis(*p*-chlorophenyl)porphyrin]. The reaction of **1c**-trifluoroacetate and a small excess of *p*-nitroperbenzoic acid (*p*NPBA) was carried out in dichloromethane containing 4 equiv of trifluoroacetic acid at -70°C. The oxidation product (**2c**) showed two intense absorption in the near-IR region, and *g* values (6.18, 5.68, and 1.98) typical of an iron(III) rhombic high spin complex. These spectroscopic features readily lead us to identify **2c** as a ferric isoporphyrin complex. Further, IR and electrospray ionization (ESI) mass spectral measurements indicated **2c** bearing a *p*-nitrobenzoyloxy group at a *meso*-position.

Introduction

Heme degradation to biliverdin is carried out by heme oxygenase (HO) under O_2-NADPH-cytochrome P-450 reductase system.[1] Three molecules of O_2 are involved in the overall reaction. It is widely believed that the initial O_2 binding and activation at the heme iron are responsible for the formation of α-*meso*-hydroxyheme and the following two sequential utilization of O_2 affords biliverdin IXα through verdoheme with simultaneous elimination of CO derived from the α-*meso*-carbon.[2] While recent model studies support hypothetical mechanistic schemes for the second (α-*meso*-hydroxyheme → verdoheme) and third step (verdoheme → biliverdin IXα) of HO-catalyzed reactions,[3] little is known about the mechanism for the first step of heme degradation, i.e., the conversion of heme to α-*meso*-hydroxyheme (Scheme 1).[4,5] Three candidates for the active intermediate to give α-*meso*-hydroxyheme have been considered; (a) ferryl complexes equivalent to compound I or II, (b) a peroxo- or hydroperoxy-iron(III) complex, and (c) hydroxyl radical formed by homolytic O-O bond cleavage of the hydroperoxy-iron(III) complex.[5] Though hydrogen peroxide and ethyl hydroperoxide can be used to complete the biliverdin formation in the presence of molecular oxygen, peracetic acid and *m*-chloroperbenzoic acid (*m*CPBA) gave compound II instead of the heme degradation. On the basis of these observations, Ortiz de Montellano and

Scheme 1

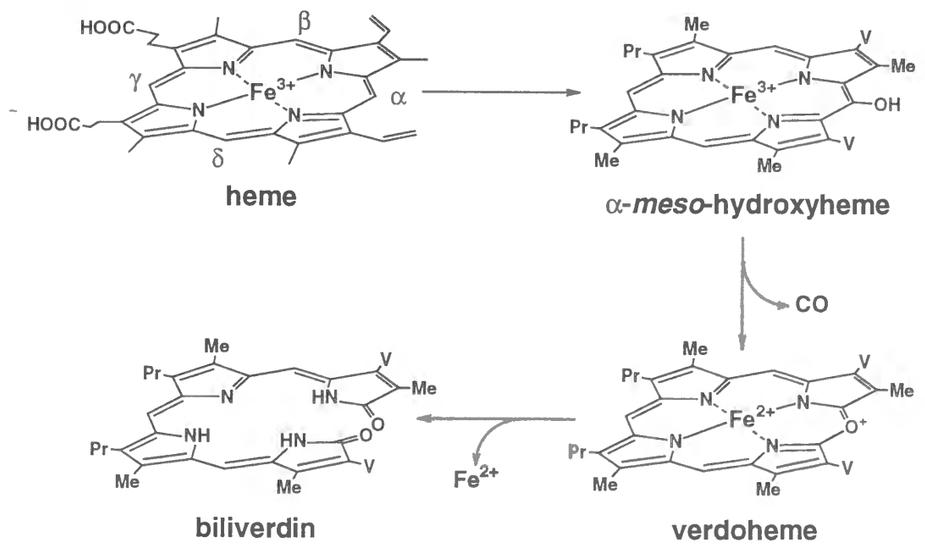

his coworkers suggested involvement of a hydroperoxy-iron(III) complex. Noguchi et al. also reported possible involvement of the complex during the α-*meso*-hydroxyheme formation.[6]

Through mechanistic studies on the formation of oxo-iron(IV) porphyrin π-cation radicals by employing Fe(TPP) derivatives and peracids, we have shown that the formation of acylperoxo-iron(III) complexes and the following heterolytic O-O bond cleavage afford oxo-iron(IV) porphyrin π-cation radicals.[7] The Fe(TPP) derivatives (**1**) used for these studies require bulky substituents at the *meso*-positions such as mesityl (**1c**) and 2,6-dichlorophenyl groups (**1d**) (Figure 1) to prevent heme degradation under the conditions. These results may imply that the introduction of one or two less hindered phenyl group(s) at *meso*-position(s) could allow us to examine details of heme degradation related to HO-catalyzed formation of α-*meso*-hydroxyheme. For this purpose, we have synthesized Fe^{III}(BMB*p*CPP) [**1a**, BMB*p*CPP: 5,15-bis(mesityl)-10,20-bis(*p*-chlorophenyl)porphyrin] and found new reactions related to the α-*meso*-hydroxyheme formation.

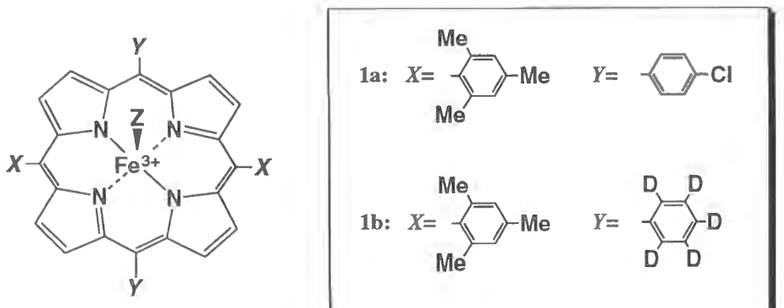

Figure 1. Iron porphyrin complexes: (a) **1a**, (b) **1b**, (c) **1c**

Experimental Section

Materials. Dichloromethane was refluxed over CaH_2 and distilled under argon just before the use. *p*-Nitroperbenzoic acid (*p*NPBA) was synthesised and purified as described earlier.[8,9] *m*-Chloroperbenzoic acid (*m*CPBA) was purchased from Wako Chemicals and purified by a method reported before.[8] Trifluoroacetic acid (TFA), tetra-*n*-butylammonium iodide

(TBAI), and methanol-d_4 were purchased from Wako Chemicals. TBAI was purified by recrystallization from dichloromethane/hexane and dried *in vacuo*.

Porphyrins. Porphyrins used in this study were synthesised according to the method reported by Lee and Lindsey with modification.[10] A solution of *meso*-(mesityl)dipyrromethane (895 mg, 3.42 mmol) and *p*-chlorobenzaldehyde (481 mg, 3.42 mmol) in dry $CHCl_3$ (250 ml) was purged with argon for 15 min, in which $BF_3 \bullet O(Et)_2$ (140 μl, 1.14×10^{-3} mmol) was added. The solution was stirred for 1h at room temperature, then, DDQ (574 mg, 2.53 mmol) was added. The mixture was stirred at room temperature for an additional 1h and the solvent was removed. Column chromatography (silica, 4 × 30 cm, CH_2Cl_2/*n*-hexane 1:1) afforded 5,15-bis(mesityl)-10,20-bis(*p*-chlorophenyl)porphyrin (H_2BMB*p*CPP) as a first eluent. 5,15-Bis(mesityl)-10,20-bis(phenyl-d_5)porphyrin (H_2BMB(P-d_5)P) was obtained by a similar procedure with *meso*-(mesityl)dipyrromethane and benzaldehyde-d_5 synthesised from benzene-d_6.

Iron Porphyrin Complexes. Chloroiron(III) complexes of BMB*p*CPP (**1a**-Cl) and BMB(P-d_5)P (**1b**-Cl) were prepared as described.[11] Iron(III) porphyrin complexes bearing a hydroxo ligand (**1a**-OH and **1b**-OH) were obtained by passing **1a**- and **1b**-Cl through a basic Al_2O_3 column (eluent EtOAc). **1a**- and **1a**-trifluoroacetate (Tfa) were generated by adding 5 equiv of TFA into dichloromethane solutions of **1a**- and **1b**-OH, *in situ*. UV-vis absorption (CH_2Cl_2) [λ_{max}, nm (ε, mM)]: **1a**-Cl, 687 (3.0), 575 (4.5), 509 (15.5), 418 (120.0), 377 (65.0); **1b**-Cl, 692 (3.0), 576 (3.6), 510 (15.2), 417 (121.5), 377 (66.8). ^{1}H-NMR ($CDCl_3$, 23°C): **1a**-Cl, δ 81.5, 80.4 (8H, β-pyrrole H), 15.7, 14.2, 13.5, 12.3 (8H, mesityl and *p*-chlorophenyl *m*-H); **1b**-Cl, δ 83.0, 82.1 (8H, β-pyrrole H), 16.1, 14.4 (4H, mesityl *m*-H). FAB-MS: m/z (relative intensity), **1a**-Cl: 820.2 (M^+ - Cl, 100), **1b**-Cl: 762.3 (M^+ - Cl, 100).

Physical Measurements. ^{1}H- and ^{2}H-NMR spectra were recorded at 500 MHz in pulsed Fourier transform mode on a Brucker DRX 500 spectrometer equipped with a SGI Indy workstation. Chemical shifts are reported relative to tetramethylsilane (TMS). UV-vis absorption spectra were obtained with a Perkin Elmer Lambda 19 spectrometer equipped with a DN 1704 variable-temperature liquid-nitrogen cryostat (Oxford Instruments). EPR spectra were recorded on a Brucker ESP-300

spectrometer equipped with an Oxford liquid helium cryostat. FT-IR spectra were obtained on a Shimadzu FTIR-8100 spectrometer equipped with a DN 1754 variable temperature liquid-nitrogen cryostat (Oxford Instruments) and a digital temperature controller-Model ITC4 (Oxford Instruments). ESI mass spectra were recorded with a Perkin Elmer SCIEX API 300.

Preparation of Iron(III) Isoporphyrin Complex (2a). In a typical run, a dichloromethane solution (containing 4 equiv of free TFA) of Fe^{III}BMB*p*CPP(Tfa) (**1a**-Tfa) [1.0×10^{-5} M, 4 ml] in an 1-cm UV cuvette was placed in a cryostat attached to an UV-vis absorption spectrometer. After equilibration at -70°C, 100 µl of dichloromethane containing 1.5 equiv of *p*NPBA was injected to yield **2a**.

NMR and EPR samples of **2a** [1.0×10^{-3} M] were prepared at -70°C according to the stoichiometry described above. A dichloromethane solution of **2a** [1.0×10^{-3} M] was evaporated at -70°C *in vacuo*, and the resulting solid was dissolved in acetonitrile [1.0×10^{-5} M] at -40°C. This solution was used for ESI-MS. In FT-IR spectral measurement, *m*-chloroperbenzoic acid (*m*CPBA, 1.0×10^{-3} M) was employed as the oxidant.

Results

Characterization of the Oxidation Product (2a). Oxidation of Fe^{III}BMB*p*CPP(trifluoroacetate) (**1a**-Tfa) by a small excess amount (1.5 equiv) of *p*-nitroperbenzoic acid (*p*NPBA) in dry dichloromethane at -70°C was monitored by UV-vis absorption spectroscopy (Figure 2). The addition of *p*NPBA to **1a**-Tfa caused solution colour change from dark brown to light brown. The spectrum of the final product (**2a**) shows a broad band in the Soret region and two intense bands in a near-IR region at 806 and 901 nm, typical of isoporphyrins.[12] The EPR spectra of **1a**-Tfa and **2a** measured in dichloromethane at 5K are shown in Figure 3 (a, b). **2a** shows a typical rhombic iron(III) high spin spectrum with g values at 6.18, 5.68, and 1.98, possibly due to decrease in plane symmetry. Figure 4 shows ^{1}H-NMRspectra of **1a**-Tfa (trace (a)) and **2a** (trace (b)) at -70°C. The β-pyrrole protons of **1a**-Tfa appear at a typical region of ferric high-spin porphyrincomplexes (100 ppm downfield from TMS) and show a doublet peak consistent with the C_{2v} symmetry of the porphyrin. The four

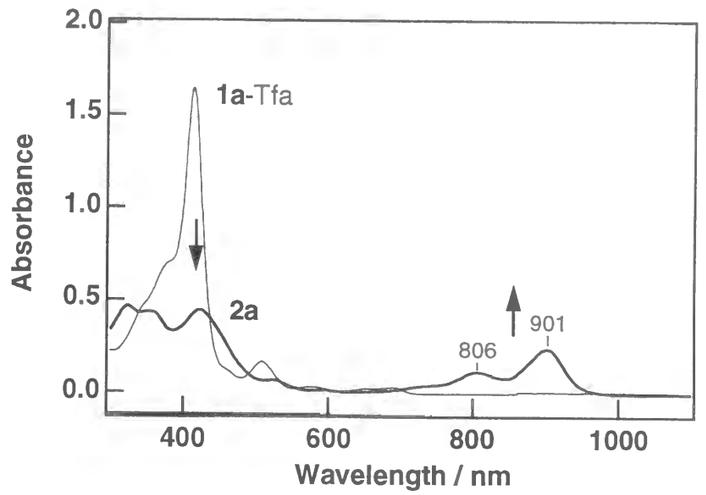

Figure 2. UV-vis spectra of **1a**-Tfa (——) [1.0×10^{-5} M] and **2a** (▬▬) prepared by the addition of 1.5 equiv of *p*NPBA in dichloromethane containing 4 equiv of TFA at -70°C.

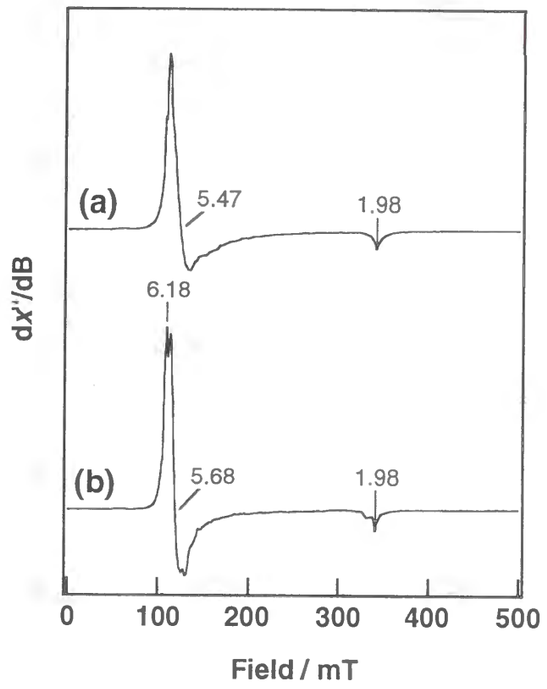

Figure 3. X-band EPR spectra of (a) **1a**-Tfa [1.0×10^{-3} M] and (b) **2a** as a frozen dichloromethane solution at 5K, 9.46 GHz, 0.5 mW microwave power.

broadened signals around 100~120 ppm with 1:1:1:1 ratio observed for **2a** are readily assigned to the β-pyrrole protons, and clearly suggest that the structure of **2a** is C_s symmetry expected for an isoporphyrin.

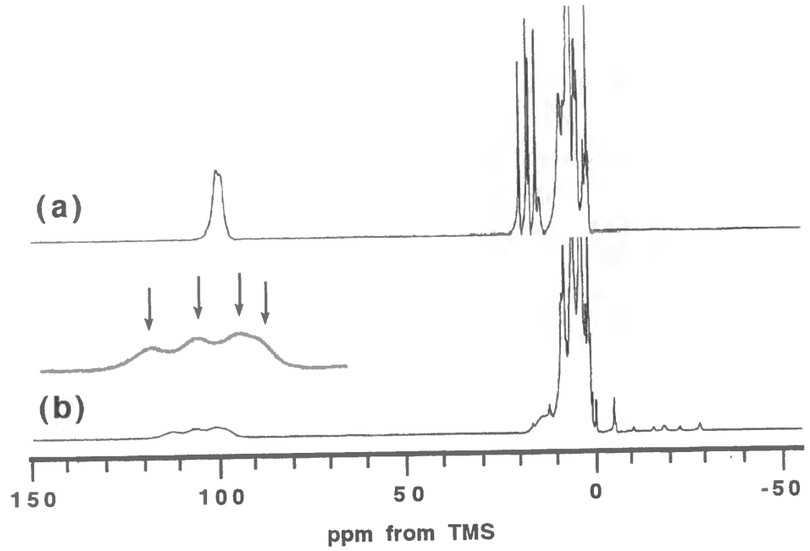

Figure 4. ^{1}H-NMR of (a) **1a**-Tfa [1.0×10^{-3} M], (b) **2a** in dichloromethane-d_2 containing 4 equiv of TFA at -70°C. In (a), the signals at 14.7, 16.5, 17.1, and 19.3 ppm are assigned to the *meta*-H, and the signals at 99.0 and 100.0 ppm to β-pyrrole H. In (b), the signals of the β-pyrrole H can be seen around ~100 ppm.

Figure 5 depicts ^{2}H-NMR spectra of Fe^{III}(BMB(P-d_5)P)(trifluoroacetate) (**1b**-Tfa) [BMB(P-d_5)P: 5,15-bis(mesityl)-10,20-bis(phenyl-d_5)porphyrin] and its oxidation product (**2b**). These spectra were recorded at -20°C for the correct signal assignment. The signals at 7.3, 11.4, and 13.7 and 14.8 in **1b**-Tfa are assigned to the *o*-, *p*-, and *m*-deuteriums, respectively, on the basis of the intensity and alternative shift of each signal. The *o*-deuterium resonances are not resolved into distinct set because of the broadening caused by closer proximity to the paramagnetic iron center. Therefore, an out-of-plane position of the iron results in split signals for *m*-deuteriums and partially resolved signals for *o*-deuteriums. While the ^{2}H-NMR spectrum of **1b**-Tfa shows one set of signals for *o*-, *m*-, and *p*-deuteriums due to the equivalency of two deuterated phenyl groups, that of **2b** gives more complicated signals due to inequivalent two phenyl

groups. The results imply that a less hindered *meso*-position having the phenyl-d_5 group is modified.

On the basis of these spectral measurements, we conclude **2a** to be the ferric isoporphyrin complex bearing a substituent (**X**) at a less hindered *meso*-position.

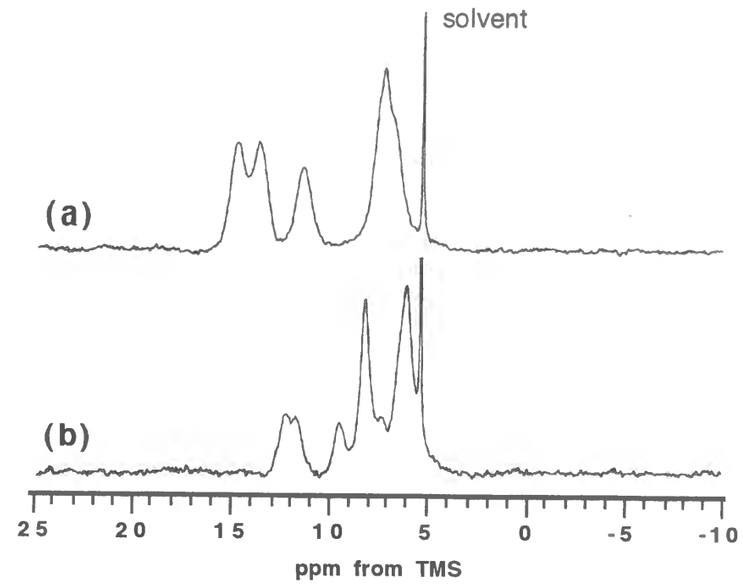

Figure 5. ^{2}H-NMR spectra of (a) **1b**-Tfa [1.0×10^{-3} M], and (b) **2b** in dichloromethane containing 4 equiv of TFA at -70°C. The signals of *o*-, *m*-, and *p*-deuteriums of **1b**-Tfa is observed at 7.3, 13.7 and 14.8, and 11.4 ppm, respectively.

Scheme 2

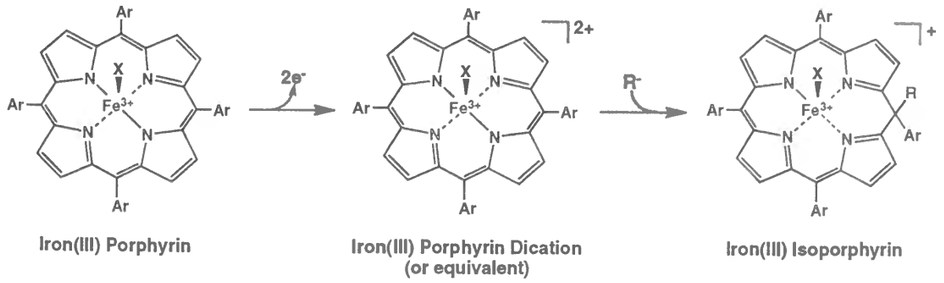

Formal Oxidation State of the ferric Isoporphyrin Complex (2a). Transformation of iron(III) porphyrin complexes to the corresponding

iron(III) isoporphyrin complexes is a two electron oxidation process (Scheme 2). If the substituent **X** is the oxidant itself as reported by Gold et al., **2a** is a four electron oxidized product of **1a**. To confirm the oxidation state of **2a**, we have examined the iodometric titration of **2a**. Figure 6 shows the UV-vis absorption spectra of **1a**-Tfa, **2a**, and a reduction product of **2a** by the addition of *tert*-butyl ammonium iodide (TBAI). The spectrum of the reduction product is expected for superposition of **1a**-Tfa and I_3^-. As shown in Figure 6 inset, the absorbance at 360 nm in difference spectrum of the reduction product and **1a**-Tfa (absorbance = 0.50) corresponds to that given by the reaction of 1.5 equiv of *p*NPBA with TBAI (0.51). The observation is suggestive of **2a** containing 2-electron oxidizing equivalent rather than 4-electron.

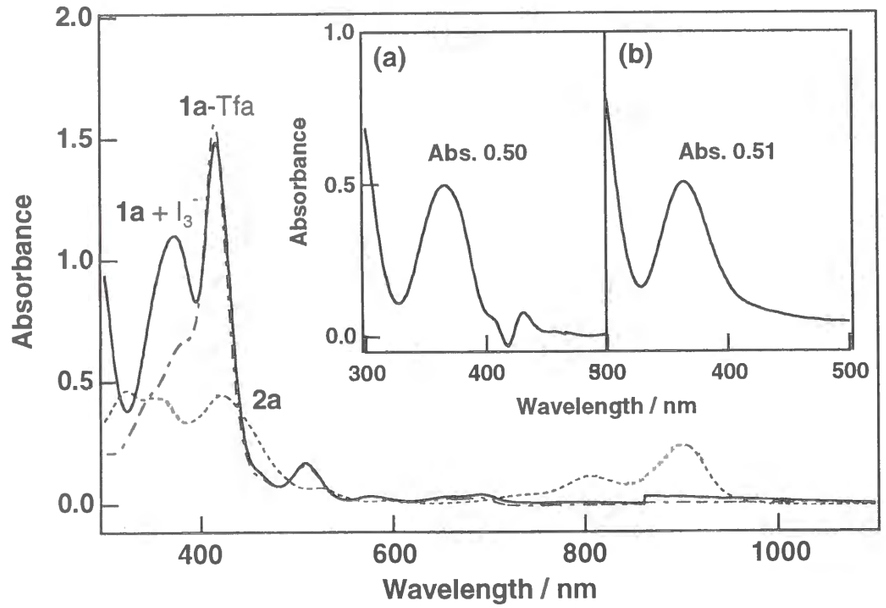

Figure 6. (a) UV-vis spectra of **1a**-Tfa (- • -) [1.0×10^{-3} M], **2a** (- - -), and **1a**-Tfa and I_3^- (—), which was obtained by the addition of TBAI to **2a**. (*inset*) (a) UV-vis spectrum of I_3^-, which was given by subtracting the spectrum of **1a**-Tfa from that of **1a**+I_3^-. (b) UV-vis spectra of I_3^-, which resulted from the reaction of 1.5 equiv of *p*NPBA with TBAI.

FT-IR Spectrum of 2a. Traces (a) and (b) of Figure 7 depict the IR spectra of **1a**-Tfa and the oxidation products (**2a'**) by using *m*CPBA, respectively. Since the two intense bands at 1786 and 1802 cm^{-1} in the

spectrum (a) is assignable to the C=O of free TFA in the solution by a separate measurement of only TFA in dichloromethane, a band at 1717 cm^{-1} is assigned to $\nu_{C=O}$ for ligated trifluoroacetate. As the reaction proceeds, a broad $\nu_{C=O}$ band in **2a'** appear around 1701 cm^{-1}. Weak bands at 1734 and 1788 cm^{-1} are from the small amounts of free *m*CPBA and trifluoroacetic acid remaining in the solution, respectively. Weak intensity of the 1788 cm^{-1} band also rules out possible involvement of Tfa as the substituent at a *meso*-position in **2a'**, since the $\nu_{C=O}$ band of alkyl trifluoroacetates are known to be observed around 1770-1790 cm^{-1} with moderate intensity.[13] Thus, we attribute a broad but very intense band at 1701 cm^{-1} to the overlapping of two C=O bands of Tfa as the axial ligand and *m*CBA as the *meso*-substituent in **2a'**. Ligation of Tfa to the iron in **2a'** is further confirmed by the ligand exchange/ESI mass experiments described below.

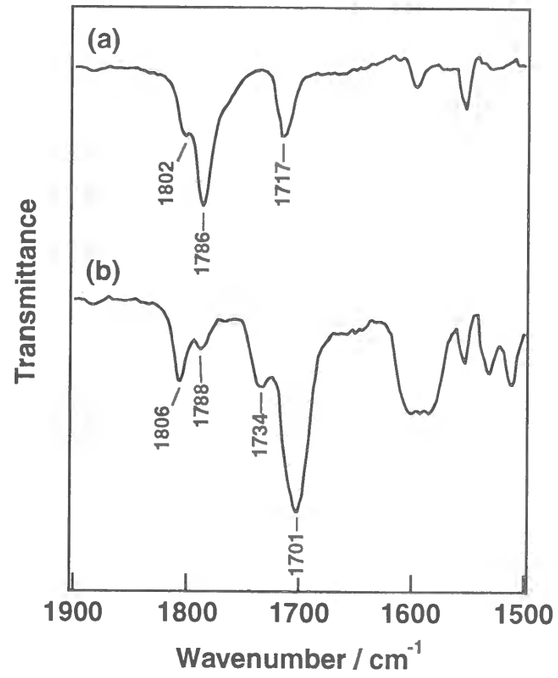

Figure 7. IR spectra of (a) **1a**-Tfa [1.0×10^{-3} M] and (b) **2a** prepared by using *m*CPBA (**2a**-^{16}O) in dichloromethane containing 4 equiv of TFA at -70°C. In (a), the $\nu_{C=O}$ of trifluoroacetate bound to the iron is seen at 1717 cm^{-1}. In (b), the band at 1701 cm^{-1} is assigned to the $\nu_{C=O}$ of *m*-chlorobenzoyloxy group at the *meso*-position, and 1734 cm^{-1} to $\nu_{C=O}$ of excess *m*CPBA. Two bands around 1790 cm^{-1} are derived from free TFA.

ESI-Mass Spectra of 2a. For the electrospray ionization (ESI) mass spectroscopic measurements, **2a** prepared in dichloromethane was dried *in vacuo* and then resolved in acetonitrile. That the parent ion peak of **2a** (Figure 8) appears at m/z 1099 establishes the presence of one *p*-nitrobenzoyloxy group and one trifluoroacetoxy group in **2a**. The inset in Figure 8 shows an expanded spectrum of the parent ion region (spectrum (a)), and the calculated spectrum for the elemental composition of $C_{59}H_{42}N_5O_6FeF_3{}^{35}Cl_2$. As suggested by IR spectra of **2**, *p*-nitrobenzoyloxy group is likely to be the *meso*-substituent rather than the axial ligand in **2a**.[14] Treatment of dichloromethane solution of **2a** with *tetra-n*-butylammonium chloride is expected to replace the axial ligand with chloride, and the result shows the appearance of the parent m/z peak at 1021 corresponding to the presence of one *p*-nitrobenzoyloxy group and one chloride.

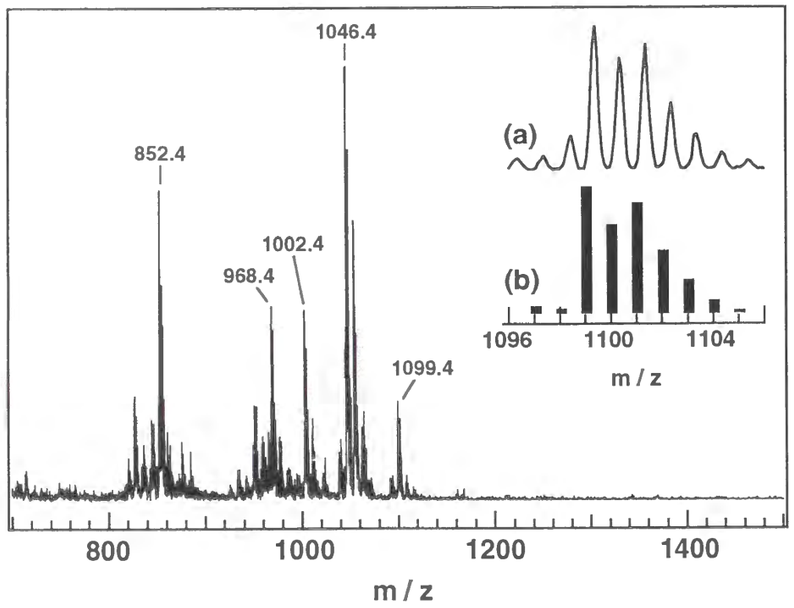

Figure 8. ESI mass spectrum of **2a** [5.0×10^{-5} M] in acetonitrile at r.t. (*inset*) (a) the expanded spectrum of **2a**, (b) the calculated spectrum for the elemental composition $C_{59}H_{42}N_5O_6FeF_3{}^{35}Cl_2$.

The observations of ligand exchange/ESI mass, iodometric titration, and FT-IR allow us to identify the *meso*-substituent being the *p*-nitrobenzoyloxy group derived from the peracid.

Discussion

Formation of oxo-iron(IV) porphyrin π-cation radicals (λ_{max}: 405 and 661 nm in dichloromethane for $O=Fe^{IV}(TMP^{+\bullet})$),[7] oxo-iron(V) porphyrins (λ_{max}: 418 and 546 nm in dichloromethane for $O=Fe^{V}$(TDCPP)),[15], iron(III) porphyrin *N*-oxides (λ_{max}: 441 and 547 nm in toluene for Fe^{III}TMP *N*-oxide),[16] and iron(III) porphyrin dications (λ_{max}: 412 nm in toluene for Fe^{III}TMP dication)[17] have been reported as two-electron oxidation products of iron(III) porphyrin complexes in which four *meso*-positions are protected by bulky substituents. These high valent iron porphyrin complexes have been examined in detail. In these cases, bulky *meso*-substituents such as mesityl and 2,6-dichlorophenyl groups are crucial to prevent heme degradation. In this study, we synthesized novel iron porphyrin complexes, in which less hindered aromatic groups are attached to two *meso*-positions, to understand more detail about the heme degradation mechanism related to heme oxygenase reactions.

The reaction of an iron(III) porphyrin complex bearing two less hindered substituents at 5- and 15-*meso*-position (**1a**) with peracid results in ring modification at a *meso*-position to yield an isoporphyrin complex (**2a**). Formation of the isoporphyrin complex is suggested by the electronic absorption and ^{1}H-NMR analysis. Like an isoporphyrin complex reported by Gold et al. (λ_{max}: 450, 805, and 881 nm in dichloromethane),[12a] the UV-vis absorption spectrum of **2a** shows two intense bands in a near-IR region and the indistinct Soret band with decreased intensity (λ_{max}: 421, 806, and 901 nm in dichloromethane). *Meso*-addition of a substituent is confirmed by the fact that the β-pyrrole protons of **2a** afford four-splitting signals indicative of C_s ring symmetry. If the substituent was introduced at a β-pyrrole carbon, all the β-pyrrole protons should become inequivalent.

^{2}H-NMR spectrum in Figure 5b shows no large paramagnetic shift of the *o*-, *m*-, and *p*-deuterium signals of the *meso*-phenyl-d_5 groups in **2b**, indicating that the porphyrin ring of **2b** (and also **2a**) should be neutral.[18] Gold et al. assigned two-splitting signals in the NMR spectrum of an iron(III) isoporphyrin complex to the *m*-protons of the *p*-methoxyphenyl

group at the *meso*-position where an alkyl peroxy group was introduced, and a singlet signal to *m*-protons of the other *p*-methoxyphenyl groups.[12a] Accordingly, we can readily assign the doublet signals at 11.8 and 12.2 ppm in Figure 5b to the *m*-deuteriums of the phenyl-d_5 group at the modified *meso*-position, and the singlet signal at 8.1 ppm corresponds to the *m*-deuteriums at the unmodified *meso*-positions. The signal at 5.9 ppm is also assignable to the *o*-deuteriums on the basis of the intensity and alternative shift of each signal. The singlet signal of the *m*-deuteriums at the unmodified *meso*-position and the relatively sharp signal of the *o*-deuteriums suggest a ligation of two identical ligands in **2b** (and also **2a**).

The EPR spectrum of **2a** is typical of iron(III) high spin complexes. A large downfield shift of the β-pyrrole proton signals of **2a** is consistent with this assignment.

To confirm the substituent at a less hindered *meso*-position being benzoate derived from perbenzoic acid, we examined ESI mass and FT-IR spectroscopy and iodometric titration. First of all, ESI-MS provided direct evidence of *p*-nitrobenzoyloxyl and trifluoroacetoxy group being in **2a**. The observation of parent ion peak at 1099 for a mono-cation form of **2a** suggest 6th ligand is Tfa, since only 1.5 equiv moles of *p*NPBA was used to complete the **2a** formation in the presence of excess amount of trifluoroacetic acid. According to the ^{2}H-NMR measurements of **2b**, two ligands in **2b** are suggested to be the same. These considerations suggest Tfa to be the ligands. The ligation of trifluoroacetate to the iron in **2b** was further confirmed by the ligand exchange experiment with Cl^-. Therefore, the *p*-nitrobenzoyloxy group is assigned to the substituent at the *meso*-position. Possible decomposition of perbenzoyloxy group attached to the *meso*-position during the mass measurement is readily eliminated by the iodometric titration of **2a**. The reduction of isoporphyrin to the corresponding porphyrin should give one equivalent mole of I_3^- which is consistent with the present observation. If the perbenzoyloxy group is the substituent at the *meso*-position on the isoporphyrin ring, additional one equivalent mole of I_3^- must be obtained. Although the use of 1.5 equiv moles of *p*-nitroperbenzoic acid was required to complete the **2a** formation, that one equiv mole of *p*-nitroperbenzoic acid is able to form more than 80% of **2a** is further support for stoichiometric formation of **2a** from **1a** by one equiv mole of *p*-nitroperbenzoic acid. The same conclusion was also obtained by FT-IR measurement of **2a**.

In summary, we have shown the formation of isoporphyrin in the reaction of peracid and less sterically hindered iron porphyrin. If the same

reaction proceeded in the HO-catalyzed reaction *via* hydroperoxy-iron(III) intermediate, deprotonation from isoporphyrin can form α-*meso*-hydroxyheme. As reported by Wilks et al, peracids such *m*CPBA and peracetic acid produced compound II of HO instead of heme degradation, while hydrogen peroxide and ethyl hydroperoxide can be used to complete heme degradation in the presence of O_2.[5] Oxidant dependence of HO catalyzed reactions could be caused by either specific hydrogen bond with iron bound hydroperoxide (and ethyl peroxide) or steric hindrance of the distal site of HO,[19] since such effects are expected to alter the structure of the oxidant-iron(III) heme adduct. In fact, recent resonance Raman studies indicates that the molecular oxygen bound to a ferrous iron of HO is highly bent toward α-*meso*-carbon.[20] Thus, such structure dependency has been mimicked by changing substituents at the *meso*-position of Fe(TPP) complexes.

References

(1) (a) Maines, M. D. *FEBS Lett.* **1988**, *2*, 2557-2568. (b) Kikuchi, G.; Yoshida, T. *Mol. Cell. Biochem.* **1983**, *53/54*, 163-183. (c) Lemberg, R. *Biochem. J.* **1935**, *29*, 1322-1335. (d) O'Carra, P. *Porphyrins and Metaloporphyrins*; Elsevier: Amsterdam, 1975. (e) Tenhunen, R.; Marver, H. S.; Schmid, R. *Proc. Natl. Acad. Sci. U.S.A.* **1969**, *61*, 748-755.

(2) Tenhunen, R.; Marver, H. S.; Schmid, R. *J. Biol. Chem.* **1969**, *244*, 6388-6394.

(3) (a) Chang, C. K.; Aviles, G.; Bag, N. *J. Am. Chem. Soc.* **1994**, *116*, 12127-12128. (b) Morishima, I.; Fujii, H.; Shiro, Y.; Sano, S. *Inorg. Chem.* **1995**, *34*, 1528-1535. (c) Balch, A. L.; Mazzanti, M.; Olmstead, M. M. *J. Chem. Soc., Chem. Commun.* **1994**, 269-270. (d) Balch, A. L.; Mazzanti, M. M.; St. Claire, T. N.; Olmstead, M. M. *Inorg. Chem.* **1995**, *34*, 2194-2200. (e) Choe, Y. S.; Ortiz de Montellano, P. R. *J. Biol. Chem.* **1991**, *266*, 8523-8530. (f) Sano, S.; Sugiura, Y.; Maeda, Y.; Ogawa, S.; Morishima, I. *J. Am. Chem. Soc.* **1981**, *103*, 2888-2890. (g) Sano, S.; Morishima, I.; Shiro, Y.; Maeda, Y. *Proc. Natl. Acad. Sci. U.S.A.* **1986**, *83*, 531-535.

(4) Wilks, A.; Ortiz de Montellano, P. R. *J. Biol. Chem.* **1993**, *268*, 22357-22362.

(5) Wilks, A.; Torpey, J.; Ortiz de Montellano, P. R. *J. Biol. Chem.* **1994**, *269*, 29553-29556.
(6) Noguchi, M.; Yoshida, T.; Kikuchi, G. *J. Biochem.* (Tokyo) **1983**, *93*, 1027-1036.
(7) (a) Groves, J. T.; Watanabe, Y. *J. Am. Chem. Soc.* **1986**, *108*, 7834-7836. (b) Groves, J. T.; Watanabe, Y. *Inorg. Chem.* **1987**, *26*, 785-786. (c) Yamaguchi, K.; Watanabe, Y.; Morishima, I. *J. Am. Chem. Soc.* **1993**, *115*, 4058-4065. (d) Machii, K.; Watanabe, Y.; Morishima, I. *J. Am. Chem. Soc.* **1995**, *117*, 6691-6697.
(8) (a) Schwartz, N. N.; Blumbergs, J. H. *J. Org. Chem.* **1964**, *29*, 1976-1979. (b) Silbert, L. S.; Siegel, E.; Swern, D. *J. Org. Chem.* **1962**, *27*, 1336.
(9) Schmeisser, M.; Dahmen, K.; Satori, P. *Chem. Ber* **1967**, *100*, 1633.
(10) Lee, C.; Lidsey, J. S. *Tetrahedron* **1994**, *50*, 11427-11440.
(11) Kobayashi, H.; Higuchi, T.; Kaizu, Y.; Osada, H.; Aoki, M. *Bull. Chem. Soc. Jpn.* **1975**, *48*, 3137.
(12) (a) Gold, A.; Ivey, W.; Toney, G. E.; Sangaiah, R. *Inorg. Chem.* **1984**, *23*, 2932-2935. (b) Dolphin, D.; Felton, R. H.; Borg, D. C.; Fajar, J. *J. Am. Chem. Soc.* **1970**, *92*, 743-745. (c) Takeda, Y.; Takahara, S.; Kobayashi, Y.; Misawa, H.; Sakuragi, H.; Tokumaru, K. *Chem. Lett* **1990**, 2103-2106. (d) Xie, H.; Smith, K. M. *Tetrahedron Lett.* **1992**, *33*, 1197-1200.
(13) Dolphin, D.; Wick, A., *Tabulation of Infrared Spectral Data*. John Wiley and Sons, New York, 1977.
(14) We confirmed the formation of **1a**-Tfa by the addition of TFA to **1a**-*p*-nitrobenzoate by UV-vis absorption measurement. This result clearly suggests that Tfa can preferentially coordinate to the iron(III) in the presence of both TFA and *p*NBA.
(15) Yamaguchi, K.; Watanabe, Y.; Morishima, I. *J. Chem. Soc., Chem. Commun.* **1992**, 1721-1723.
(16) (a)Watanabe, Y.; Takehira, K.; Shimizu, M.; Hayakawa, T.; Orita, H.; Kaise, M. *Transformation of Fe(III)TMP N-oxide to a two electron oxidized equivalent of Fe(III)TMP complex*; Simándi, L.I., Ed.; Elsevier Science Publishers B.V.: Amsterdam, 1991; Vol. 66, pp 213-220. (b) Tsurumaki, H.; Watanabe, Y.; Morishima, I. *J. Am. Chem. Soc.* **1993**, *115*, 11784-11788.
(17) (a) Fajar, J.; Borg, D. C.; Forman, A.; Dolphin, D.; Felton, R. H. *J. Am. Chem. Soc.* **1970**, *92*, 3451-3459. (b)Tsurumaki, H.; Watanabe, Y.; Morishima, I. *J. Am. Chem. Soc.* **1993**, *115*, 11784-11788.

(18) (a) Goff, H. M.; Phillippi, M. A. *J. Am. Chem. Soc.* **1983**, *105*, 7567-7571. (b)Gans, P.; Buisson, G.; Duee, E.; Marchon, J. C.; Erler, B. S.; Scholz, W. F.; Reed, C., A *J. Am. Chem. Soc.* **1986**, *108*, 1223-1234.
(19) (a) Wilks, A.; Ortiz de Motellano, P. R.; Sun, J.; Loehr, T. M. *J. Biol. Chem.* **1996**, *35*, 930-936. (b) Hernández, G.; Wilks, A.; Paolesse, R.; Smith, K. M.; Ortiz de Montellano, P. R.; La Mar, G. N. *Biochemistry* **1994**, *33*, 6631-6641. (c) Brown, S. B.; Chabot, A. A.; Enderby, E. A.; North, A. C. T. *Nature* **1981**, *289*, 93-95.
(20) Takahashi, S.; Ishikawa, K.; Takeuchi, N.; Ikeda-Saito, M.; Yoshida, T.; Rousseau, D. L. *J. Am. Chem. Soc.* **1995**, *117*, 6002-6006.

CHAPTER 2.

Mechanistic Studies of a Novel Suicidal *meso*-Oxidation of an Iron Porphyrin Complex as a Model of Heme Metabolism.

Abstract

For the mechanistic studies on the formation of α-*meso*-hydroxyheme catalyzed by Heme Oxygenase (HO), we have prepared a novel iron porphyrin complex, in which less hindered *p*-chlorophenyl groups are introduced to the 5- and 15-*meso*-positions and the other two *meso*-positions are protected by mesityl groups; Fe^{III}BMB*p*CPP (**1a**) [BMB*p*CPP: 5,15-bis(mesityl)-10,20-bis(*p*-chlorophenyl)porphyrin]. The reaction of **1a**-trifluoroacetate (Tfa) and a small excess of *p*-nitroperbenzoic acid (*p*NPBA) has been carried out in dichloromethane containing 4 equiv of trifluoroacetic acid at -70°C to yield a ferric isoporphyrin complex bearing a *p*-nitrobenzoyloxy group at a *meso*-position (**2a**). On the basis of the kinetic profile of the reaction between **1a**-Tfa and *p*NPBA, the reaction has been concluded to proceed *via* the formation of a *p*-nitroperbenzoate-iron(III) complex followed by an O-O bond cleavage, and more importantly, an intermediate (**3a**) prior to **2a** formation has been observed. Substituent effect of perbenzoic acid on the rate of the O-O bond cleavage shows that electron-withdrawing substituents accelerate the reaction, indicative of heterolysis of the O-O bond. When the reaction of **1a** and ^{18}O labeled *m*CPBA (Ar-C(=^{16}O)-^{18}OH) is carried out, *m*-chlorobenzoate is attached to a *meso*-position as Ar-C(=^{16}O)-^{18}O-. These results demonstrate that the iron(III) isoporphyrin complex (**2a**) is formed via a *p*NPBA-iron(III) porphyrin complex and the following intermediate (**3a**) by the heterolytic O-O bond cleavage coupled with a intramolecular migration of *p*-nitrobenzoyloxy group to the *meso*-position.

Introduction

Heme oxygenase (HO) catalyzes the regiospecific degradation of heme to biliverdin IXα by utilizing O_2, NADPH, and cytochrome P-450 reductase.[1] The heme metabolism proceeds *via* a multistep mechanism that involves at least two intermediates.[2] The first step of the reaction is thought to be the O_2-dependent oxidation of heme to α-*meso*-hydroxyheme. In this stage, the bound O_2 to the reduced heme iron is activated *via* another one-electron reduction as observed in the catalytic cycle of cytochrome P-450. The intermediary of α-*meso*-hydroxyheme is demonstrated by the finding of synthetic α-*meso*-hydroxyheme being converted to biliverdin IXα by HO and many model studies also support the mechanism.[3] Recently, Liu et al. reported UV-vis absorption spectral observation of α-*meso*-hydroxyheme in the anaerobic reaction of a heme-HO complex with 1 equiv of H_2O_2.[4] α-*Meso*-hydroxyheme is subsequently oxidized to yield carbon monoxide and enzyme-bound verdoheme.[4,5] The final step of the catalytic process produces biliverdin IXα by consumption of two electrons and O_2.

While recent studies including model systems suggest mechanisms for the catalytic cycle,[6] the mechanism for the first step of heme degradation to yield α-*meso*-hydroxyheme is still obscure.[7,8] On the basis of similarities between cytochrome P-450 and HO in the O_2 activation on the heme iron, several reaction intermediates responsible for the *meso*-hydroxylation are expected as follows; (a) an oxo-ferryl complexes equivalent to compound I, (b) a peroxo- or hydroperoxy-iron(III) complex, and (c) hydroxyl radical formed by homolytic O-O bond cleavage of the hydroperoxy-iron(III) complex. Though a high-valent oxo-iron complex, compound I is an attractive candidate,[9] Wilks et al. reported that the reaction of HO-heme and peracid only gave an oxo ferryl species which did not convert to any metabolites including α-*meso*-hydroxyheme.[7] Furthermore, replacement of the oxidant from peracid to H_2O_2 under aerobic condition afforded verdoheme, suggesting the hydroperoxide bound to heme to be the reactive intermediate.[7,10] Bonnet et al. also suggested the formation of the hydroperoxy-iron(III) complex, and raised a possibility of hydroxyl radical as the reactive species formed by homolytic O-O bond cleavage of the hydroperoxy-iron(III) complexes.[11] Considering that the *meso*-hydroxylation by the bound oxygen is also the key step for the regiospecificity, the first step is the best described as the unique function of HO.

Most of the difficulties in studying mechanistic aspects of the heme degradation catalyzed by HO are caused by high reactivity of α-*meso*-hydroxyheme. Synthetic iron(III) *meso*-hydroxyporphyrin complexes are labile to give rapidly the corresponding verdohemes under aerobic conditions.[6g] On the other hand, Gold et al. observed a suicidal *meso*-oxygenation of FeTPP derivatives by their reactions with alkyl hydroperoxide under an aerobic condition to afford iron(III) isoporphyrin complexes bearing the alkyl peroxy group at a *meso*-position (eq. 1).[12]

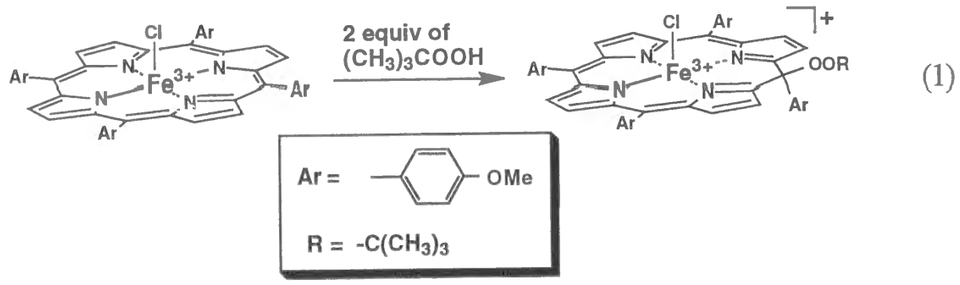

(1)

Formation of the isoporphyrin complex is related to the initial step of the heme oxygenase reaction, since deprotonation of α-*meso*-hydroxy isoporphyrin results in the formation of α-*meso*-hydroxyheme as shown in Scheme 1. In fact, isoporphyrin complexes are prepared by oxidative *meso*-addition of alkyl group to horseradish peroxidase,[13] and more

Scheme 1

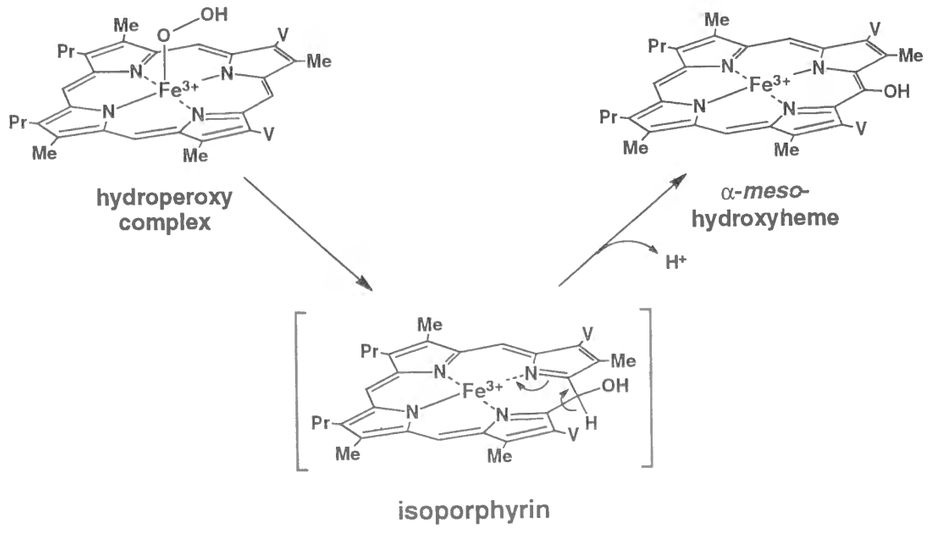

importantly, deprotonation from the *meso*-alkylated isoporphyrin complexes gives *meso*-alkyl heme.[13,14] However, the isoporphyrin complex reported by Gold et al. contains a *peroxy group (-O-OR)* by a direct attack of the second oxidant to the oxidized porphyrin ring by the fist oxidant, thus, two moles of alkylperoxide are consumed while the stoichiometry for the formation of α-*meso-hydroxy*heme requires one mole of the oxidant.[12] Very recently, we have prepared iron(III) isoporphyrin complexes having an *oxy group (-OR)* at a *meso*-position by the reaction of

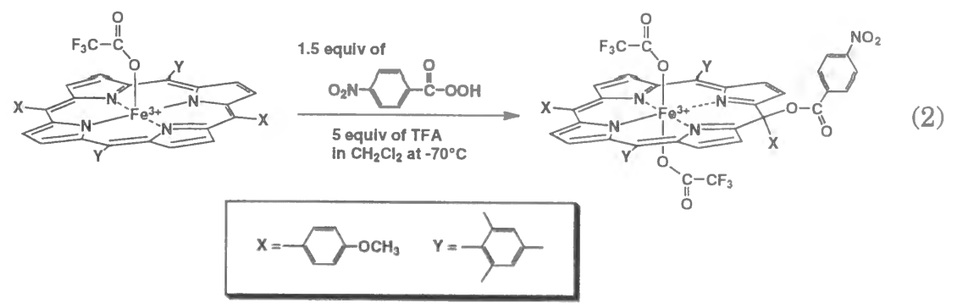

(2)

reaction of a novel iron(III) porphyrin complex with one equiv mole of peracid (eq. 2).[15] This system is rather close to the initial step of HO-catalyzed heme degradation. In this paper, we describe more details about the isoporphyrin formation as a model system for HO.

Results

Kinetic Studies of the Formation of 2a. Oxidation of Fe^{III}BMB*p*CPP(trifluoroacetate) (**1a**-Tfa) by a small excess amount (1.5 equiv) of *p*-nitroperbenzoic acid (*p*NPBA) in dry dichloromethane at -70°C was monitored by UV-vis absorption spectroscopy (Figure 1). The addition of *p*NPBA to **1a**-Tfa caused solution colour change from dark brown to light brown *via* transient dark green which allowed us to imagine the formation of a porphyrin radical as an intermediate (**3a**).[16]

As shown in Figure 1, the UV-vis absorption spectrum recorded two minutes after the addition of *p*NPBA obviously demonstrates existence of an intermediate (**3a**) which shows a broad and less intense Soret band in the visible region. For the elucidation of **3a** formation, we have monitored time dependent absorbance changes at 412 nm since it is an isosbestic point of **2a** and **3a** (Figure 1 (inset)). The reaction profile is not as simple as one expected for a second order reaction in [**1a**-Tfa] and [*p*NPBA], i.e., a

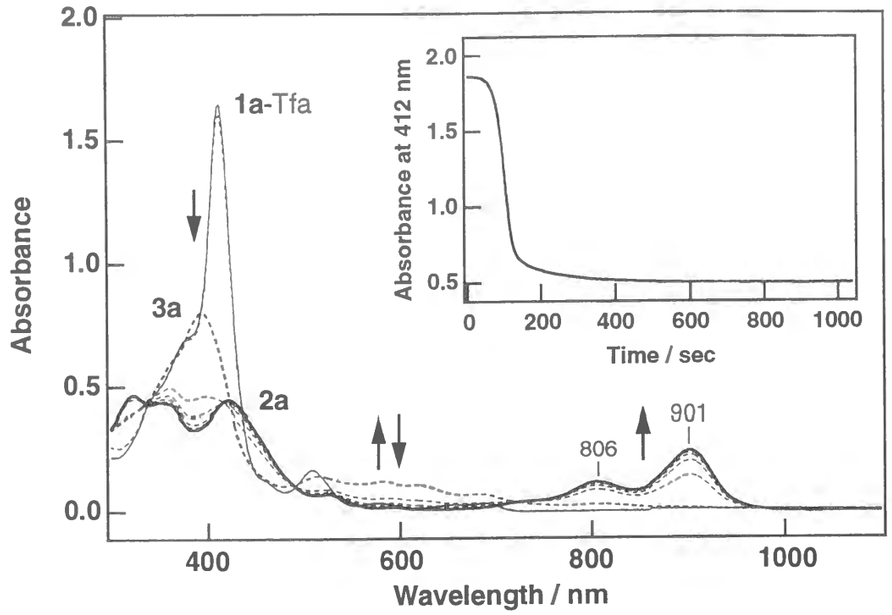

Figure 1. UV-vis spectral changes upon the addition of 1.5 equiv of *p*NPBA in dichloromethane containing 4 equiv of TFA at -70°C from **1a**-Tfa (——) [1.0×10^{-5} M] to **2a** (▬▬). The transitional spectra were shown with a broken band (- - - - -). The first spectrum was recorded immediately after the addition and the later spectra at 2-minute intervals. (*inset*) Time-dependent change of absorbance at 412 nm upon the addition of 1.5 equiv of *p*NPBA to the solution of **1a**-Tfa.

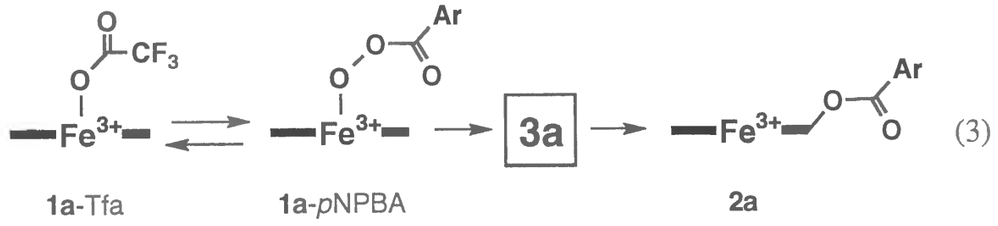

(3)

significant induction period was followed by very fast disappearance of **1a**-Tfa to afford **3a**. Very similar kinetic profiles have been observed in the reaction of Fe^{III}(TMP)(Cl) [TMP: 5,10, 15, 20-tetrakis(mesityl)porphyrin] and *m*CPBA to yield O=Fe^{IV}(TMP$^{+\bullet}$). As demonstrated by Groves and Watanabe,[17] the presence of the induction period is due to the pre-equilibrium between Fe^{III}(TMP)(Cl) and Fe^{III}(TMP)(*m*CPBA) which are spectroscopically indistinguishable. Therefore, the mechanism that

explains the observation can be expressed as eq. 3. Several mono-substituted perbenzoic acids have been employed to elucidate the nature of the O-O bond cleavage step. Figure 2 illustrates absorbance changes at 412 nm after the addition of substituted peroxybenzoic acids. Apparently, the formation of **3a** is accelerated by the electron-withdrawing substituents and exactly the same substituent effect has been observed for the formation of O=Fe^{IV}(TMP$^{+\bullet}$).[17] The difference between FeTMP and FeBMB*p*CPP is that the two *meso*-positions are less hindered in the latter complex. Thus, the product of the heterolytic O-O bond cleavage in **1a**-*p*NPBA is highly dependent on the structure of porphyrin.

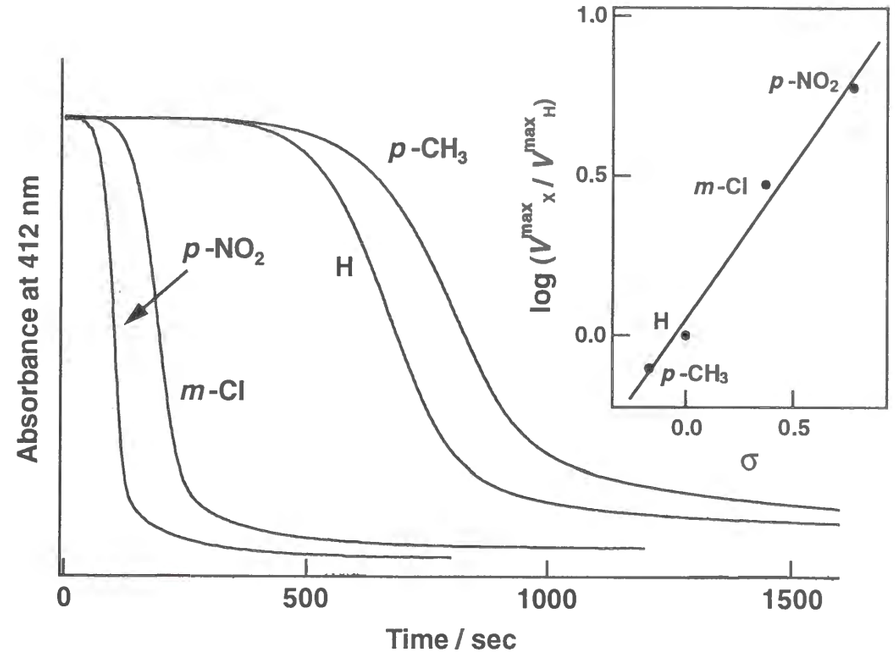

Figure 2 Time-dependent absorption changes at 412 upon the addition of various substituted perbenzoic acids to **1a**-Tfa at -70°C. (*inset*) Hammett plots of V_{max}.

Isotope Effect of the Oxidant on the Structure of 2a. To gain mechanistic insights into the *meso*-introduction of the benzoyloxy group afforded by the heterolysis of the O-O bond in the peracid-iron(III) complex, isotope labeling experiments have been carried out. Traces (a),

(b), and (c) of Figure 3 depict the IR spectra of **1a**-Tfa and the oxidation products (**2a**-^{16}O and **2a**-^{18}O) by using *m*CPBA and ^{18}O labeled *m*CPBA (Ar-C(=^{16}O)^{18}O-^{18}OH),[18] respectively. A broad band at 1701 cm^{-1} in Figure 3b has been assigned to the C=O bands of *m*CBA as the *meso*-substituent in **2a**-^{16}O. The same oxidation by ^{18}O-labeled *m*CPBA (Ar-C(=^{16}O)-^{18}O-^{18}OH) afforded the identical IR spectrum (Figure 3c), indicating that the peroxy oxygen adjacent to the C=O group in **1a**-*m*CPBA attacks the *meso*-position (see discussion).

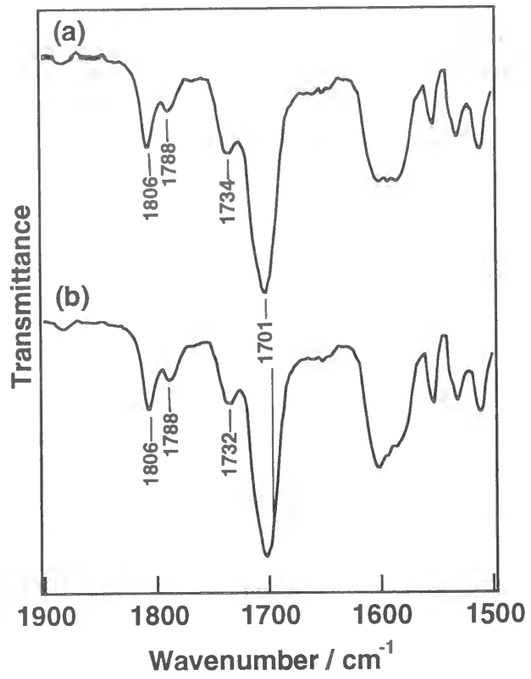

Figure 3. IR spectra of (a) **2a** [1.0×10^{-3} M] prepared by using *m*CPBA (**2a**-^{16}O) and (b) **2a** obtained by the addition of *m*CPBA-(^{18}O)$_2$ (**2a**-^{18}O) in dichloromethane containing 4 equiv of TFA at -70°C. In (a), the band at 1701 cm^{-1} is assigned to the $\nu_{C=O}$ of *m*-chlorobenzoyloxy group at the *meso*-position, and 1734 cm^{-1} to the $\nu_{C=O}$ of excess *m*CPBA-(^{18}O)$_2$. In (b), the band at 1701 cm^{-1} is assigned to the $\nu_{C=O}$ of *m*-chlorobenzoyloxy group at the *meso*-position, and 1732 cm^{-1} to the $\nu_{C=O}$ of excess *m*CPBA-(^{18}O)$_2$.

Structure of 3a. According to the reaction of peracid and **1a**-Tfa, the solution color changes from brown to light brown *via* dark green. Dark

green color and gentle absorption in the visible region of **3a** might suggest the formation of a porphyrin π-cation radical complex, e.g. O=Fe^{IV}Por$^{+\bullet}$(**4**) as in the case observed for the heterolytic O-O bond cleavage in the reaction of sterically hindered iron porphyrins such as Fe^{III}TMP with peracids.[9] To examine whether O=Fe^{IV}(BMB*p*CPP$^{+\bullet}$) (**4a**) is **3a** or not, we have successfully prepared **4a** by the reaction of **1a**-Tfa [1 mM] with 2 equiv of pentafluoroiodosylbenzene in dichloromethane containing 100 equiv of methanol-d_4[19] in the absence of TFA at -70°C (Figure 10). The UV-vis absorption spectrum of **4a**[20] shows λ_{max} at 656 nm, typical of oxo-iron(IV) porphyrin π-cation radicals (O=Fe^{IV}(TDCPP$^{+\bullet}$) [TDCPP: 5,10,15,20-tetrakis(2,6-dichlorophenyl)porphyrin]) as shown in Figure 4 (inset), and is clearly different from those of **3a** shown in Figure 2. In addition, that the introduction of 1 equiv of *p*-nitrobenzoic acid and 4 equiv of TFA to the solution of **4a** does not cause the complete conversion to an isoporphyrin complex[21] (ca. 30 % yield) readily eliminates the involvement of **4a** during the formation of **2a**.

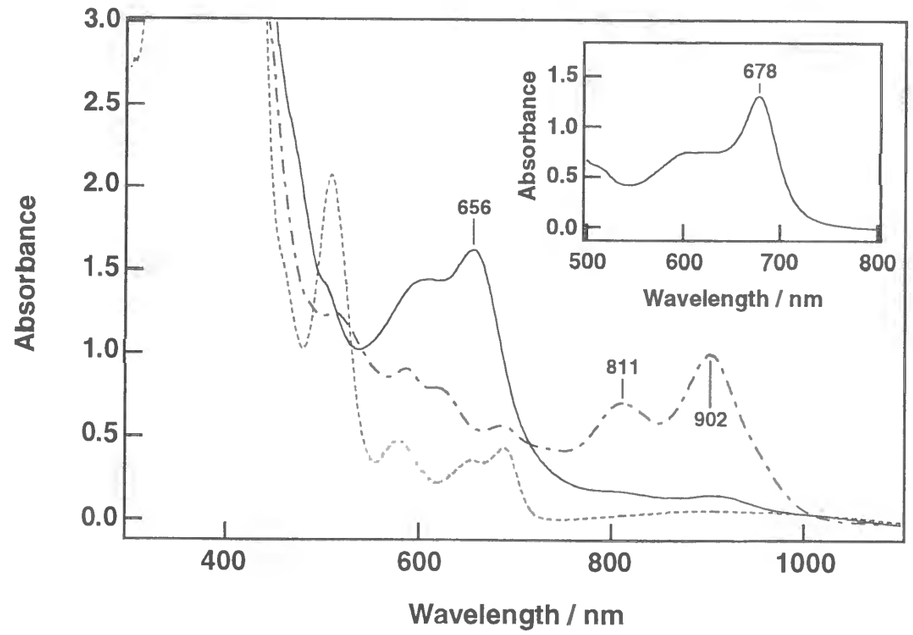

Figure 4. UV-vis spectra of **1a**-Tfa (- - -) [1×10^{-3} M], **4a** (——) prepared by the reaction with 2 equiv of C_6F_5IO in dichloromethane containing 100 equiv of methanol-d_4, and the product (- • -) obtained by the addition of 1 equiv of *p*NBA and 4 equiv of TFA to **4a** at -70 °C. (inset) The spectrum of O=Fe^{IV}(TDCPP$^{+\bullet}$) [TDCPP: 5,10,15,20-tetrakis(2,6-dichlorophenyl)-porphyrin].

For the EPR spectral measurement of **3a**, the sample was prepared by freezing a reaction solution immediately after the introduction of peracid (Figure 5b). Dark green color of the sample solution indicates the generation of **3a**. Less intense signals at g = ~6 and ~2 than those for **1a**-Tfa and **2a** in Figure 5a and 5c, respectively, are attributed to **1a**-Tfa remaining and partial formation of **2a**. Thus, **3a** is EPR silent, at least under our conditions.

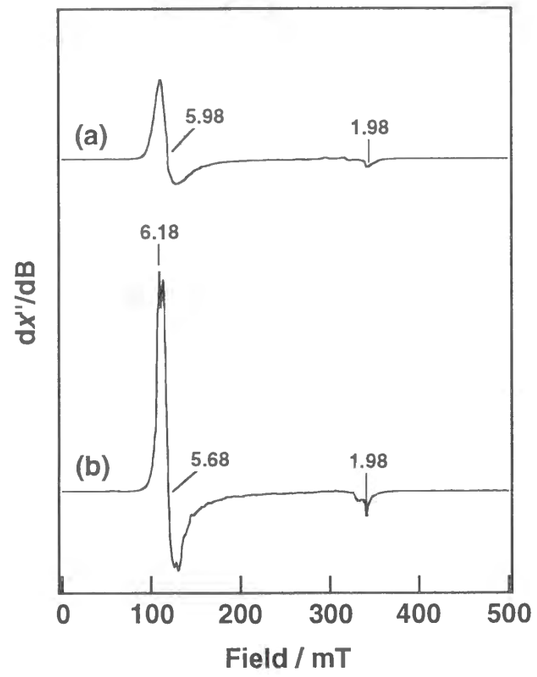

Figure 5. X-band EPR spectra of (a) the sample [1.0×10^{-3} M] prepared by freezing immediately after observation of dark green colour solution due to formation of the intermediate (**3a**), and (b) **2a** as a frozen dichloromethane solution at 5K, 9.46 GHz, 0.5 mW microwave power.

Discussion

Various metalloisoporphyrins have been synthesized from TPP derivatives by chemical[22a-d] or electrochemical[22e-g] oxidations. The latter cases involve two-electron oxidation of the porphyrin ring to yield the porphyrin dication, and the following addition of a nucleophile, for example methanol, lead to the isoporphyrin formation (Scheme 2).

Scheme 2

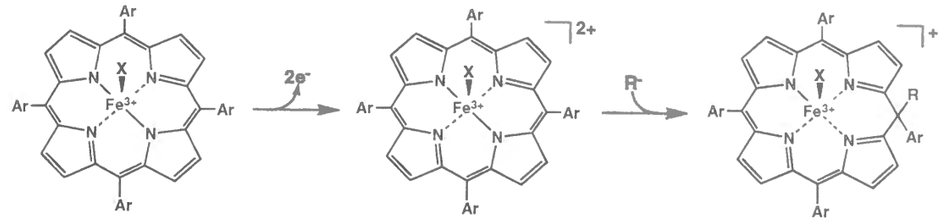

According to the result of Gold et al., a ferric isoporphyrin high spin complex bearing *tert*-butyl hydroperoxide at a *meso*-position was prepared by chemical oxidation of Fe^{III}TAP(Cl) [TAP: 5,10,15,20-tetrakis(4-anisyl)porphyrin] with 2 equiv moles of *tert*-butyl hydroperoxide in dichloromethane at room temperature. The iron(III) isoporphyrin formation is similar to the first step of heme degradation by heme oxygenase (HO) to afford an α-*meso*-hydroxyheme. For example, recent mechanistic studies of the HO catalyzed α-*meso*-hydroxyheme formation suggest the involvement of an iron(III)-isoporphyrin and the following deprotonation as shown in Scheme 1.[7] Certainly, the phenyl group sharing the same *meso*-carbon with *tert*-butyl hydroperoxide prevents the transformation of the isoporphyrin to the corresponding porphyrin in the model system.

Eq.2 also represents the major difference between the results by Gold and the HO reaction; the conversion of heme to α-*meso*-hydroxyheme by HO is completed by *one mole* of hydroperoxide bound to the heme, while *two moles* of peroxide are required in the model reaction. On the other hand, an iron(III) isoporphyrin complex **2a** formed in our reaction conditions is formally equivalent to the *meso*-hydroxyheme. Thus, we have examined the mechanism of **2a** formation as a model reaction of α-*meso*-hydroxyheme formation.

The kinetic profile at 412 nm, an isosbestic point between **2a** and **3a**, shows the presence of an induction period for the formation of **3a** (Figure 2 inset). At the same time, a linear correlation between the electron-withdrawing ability of the substituent on the phenyl group of perbenzoic acid and the reaction rates (V_{max}) was obtained (Figure 2). As discussed in **Results**, similar sigmoidal kinetic behavior and substituent effect in the reaction of Fe^{III}(TMP)(Cl) with *m*CPBA to afford O=$Fe^{IV}TMP^{+\bullet}$ have been

observed under similar conditions.[18] As shown below (eq. 4), electron-withdrawing substituents on the phenyl group of perbenzoic acid stabilize the localization of negative charge on the carboxy oxygen to assist the heterolytic O-O bond cleavage.[23] On the basis of these observations, it seems quite clear that the heterolytic O-O bond cleavage of a peracid-iron(III) complex results in the **3a** formation.

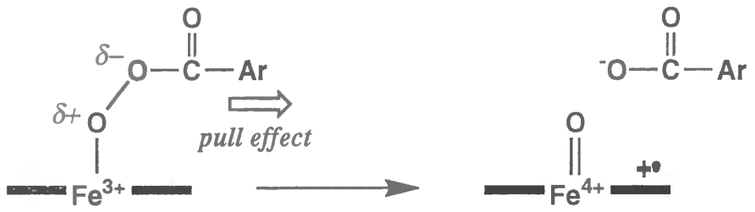

(4)

IR spectra of **2a**-^{16}O and **2a**-^{18}O prepared by *m*CPBA and ^{18}O labeled *m*CPBA (Ar-C(=^{16}O)-^{18}O-^{18}OH), respectively, show the $\nu_{C=O}$ bands of *m*-chlorobenzoate bound to the *meso*-position at the same wavenumber (Figure 3). As shown in Scheme 3, there are three possible pathways to introduce benzoate to the *meso*-position. In path (a), two carboxylate oxygens become equivalent before attacking the *meso*-position. Path (b) shows a concerted nucleophilic addition of the oxygen of the C=O concomitant with the O-O bond scission. Path (c) also displays a similar mechanism to path (b), but the oxygen responsible for the *meso*-addition is different. **2a**-^{18}O formed by path (a) is expected to give two bands corresponding to the C=^{16}O and C=^{18}O due to the scrambling of two carboxylate oxygens. If **2a**-^{18}O is formed through the path (b), tautomerization of the ArC(=^{16}O)^{18}O- group to the ArC(=^{18}O)^{16}O- group takes place and the C=O band is expected to shift to lower wavenumber. On the contrary, path (c) affords the isoporphyrin complex **2a**-^{18}O with the C=^{16}O group. Apparently, appearance of the band in **2a**-^{16}O and **2a**-^{18}O at the same wavenumber suggests that the reaction proceeds through path (c). The results could suggest that the peroxide oxygen bound to the carbonyl carbon in the peracid-iron(III) adduct is close enough to interact with a less hindered *meso*-carbon before the O-O bond cleavage. Takahashi et al. observed highly bent structure of the coordinated oxygens of the oxygen-bound heme-HO complex to result in van der waals contact of the terminal oxygen atom with the α-*meso*-carbon of the porphyrin ring.[24]

Scheme 3

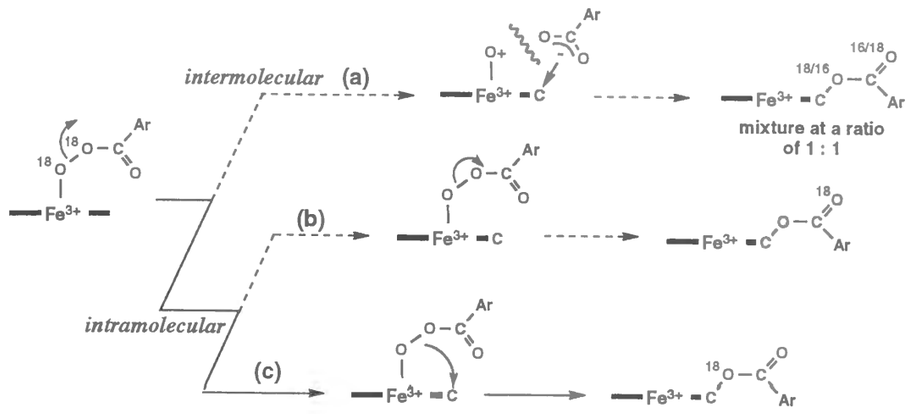

Since the heterolysis of an acylperoxo-Fe^{III}(TMP), whose *meso*-positions are fully protected by bulky mesityl groups, leads to the O=Fe^{IV}(TMP)$^{+\bullet}$ formation, possible generation of O=Fe^{IV}(BMB*p*CPP)$^{+\bullet}$ (**4a**) is the most attractive candidate for **3a**. Gentle absorption in the visible region and dark green color of **3a** is indicative of a ring oxidation. However, the successful preparation of **4a** by the reaction of **1a**-Tfa with C_6F_5IO readily eliminates such assignment because the UV-vis absorption spectrum of **4a** is different from that of **2a** (Figure 4). In addition, the introduction of one equiv mole of *p*-nitrobenzoic acid and four equiv mole of TFA to **4a** afforded a small amount of isoporphyrin. EPR spectrum of **3a** prepared by rapid freezing of a solution of **3a** essentially showed no signal, while **4a** gave the spectrum with g = 4.28, 3.64, and 1.97. Moreover, UV-vis absorption and EPR Spectra of an iron(III) porphyrin dication[25] and oxo-iron(V) porphyrins[26] are quite different from those of **2a**.

If we assume that **3a** is yielded by the heterolytic O-O bond cleavage of the acylperoxo-Fe^{III}BMB*p*CPP and the subsequent *meso*-addition of the carboxylate, a high valent intermediate could be initially formed (Scheme 4). Several resonance forms are available for the intermediate and reorganization of double bonds with concomitant electron transfer from the ring to the oxo-iron unit finally yields the isoporphyrin. Ozawa et al. observed the similar aromatization of the ring due to an intramolecular electron transfer, i.e. the transformation of an oxo-iron(IV) chlorin π-cation radical to an iron(III) porphyrin complex.[27] Unfortunately, we are

not able to specify the intermediate **3a** at this moment due to the short lifetime.

Scheme 4

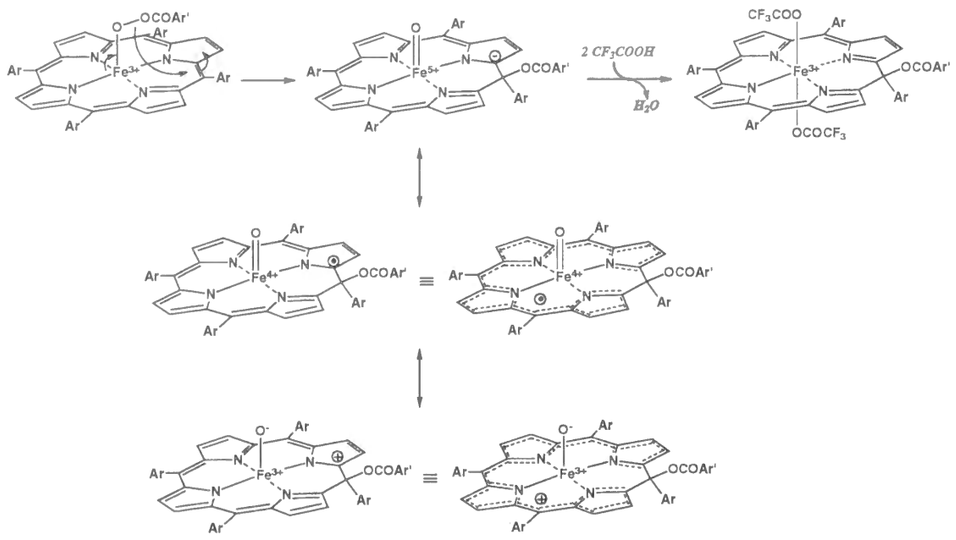

Biological Implications

A novel iron(III) isoporphyrin complex is formed by the reaction of peracid and **1a**. The intramolecular nucleophilic addition of benzoate formed by the heterolytic O-O bond cleavage of an acylperoxo-iron(III) complex gives the iron(III) isoporphyrin complex. Wilks et al. reported that H_2O_2 also converts HO bound heme to verdoheme *via* α-*meso*-hydroxyheme in the presence of O_2.[7] In addition, α-*meso*-hydroxyheme formation by anaerobic addition of H_2O_2 (1 equiv) to a heme-HO complex has been recently reported.[4] These observations suggest involvement of a hydroperoxy-iron(III) heme, which is equivalent to an acylperoxo-iron(III) porphyrin complex. The active site of HO binds heme to make a heme-HO complex with greater exposure of heme to solvent than myoglobin and other heme proteins.[28] A polar heme environment enhances the heterolytic scission of the O-O bond.[29] According to our model reaction, the heterolysis of the O-O bond of a peracid-iron(III) complex gives the isoporphyrin *via a nucleophilic addition* of carboxylate to a *meso*-carbon. On the contrary, Wilks et al. have proposed *a*

nucleophilic attack of the α-*meso*-carbon to the terminal oxygen of hydroperoxide bound to heme, i.e., the nature of the O-O bond cleavage is *inverse heterolysis* as shown below (eq. 5).[7] If this is the case, there must be a protic amino acid residue or water around the distal site to neutralize an oxy anion bound to heme, otherwise it seems quite unlikely to proceed this type of the O-O cleavage. Especially, there are no clear examples demonstrating *the inverse heterolysis* of the O-O bond bound to ferric porphyrins.[30]

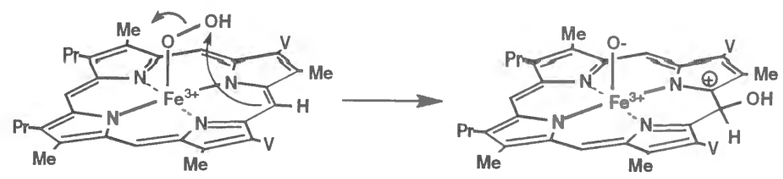

(5)

In conclusion, we have shown mechanism of the formation of the ferric isoporphyrin complex equivalent to *meso*-hydroxy heme *via* an intermediate. Kinetic studies are suggestive of the nucleophilic addition of carboxylate released by the heterolytic O-O bond cleavage in the acylperoxo-iron(III) complex affords isoporphyrin.

References

(1) (a) Tenhunen, R.; Marver, H. S.; Schmid, R. J. *Proc. Natl. Acad. Sci. U.S.A.* **1968**, *61*, 748. (b) Tenhunen, R.; Marver, H. S.; Schmid, R. *J. Biol. Chem.* **1969**, *244*, 6388-6394.

(2) (a)O'Carra, P. *Porphyrins and Metaloporphyrins*; Smith, K. M.; Elsevier: Amsterdam, 1975, pp 123-153. (b) Kikuchi, G.; Yoshida, T. *Mol. Cell. Biochem.* **1983**, *53/54*, 163-183. (c) Maines, M. D. *FEBS Lett.* **1988**, *2*, 2557-2568.

(3) (a)Yoshida, T.; Kikuchi, G.; Sano, S. *J. Biochem. (Tokyo)* **1981**, *90*, 125-131. (b)Yoshinaga, T.; Sudo, Y.; Samo, S. *Biophys. J.* **1990**, *270*, 659-664.

(4) Liu, Y.; Moënne-Loccoz, P.; Loehr, T. M.; Ortiz de Motellano, P. R. *J. Biol. Chem.* **1997**, *272*, 6909-6917.

(5) Mansfield Matera, K.; Takahashi, S.; Fujii, H.; Zhou, H.; Ishikawa, K.; Yoshimura, T.; Rousseau, D. L.; Yoshida, T.; Ikedasaito, M. *J Biol Chem* **1996**, *271*, 6618-6624.

(6) (a) Chang, C. K.; Aviles, G.; Bag, N. *J. Am. Chem. Soc.* **1994**, *116*, 12127-12128. (b) Morishima, I.; Fujii, H.; Shiro, Y.; Sano, S. *Inorg. Chem.*

1995, *34*, 1528-1535. (c) Balch, A. L.; Mazzanti, M.; Olmstead, M. M. *J. Chem. Soc., Chem. Commun.* **1994**, 269-270. (d) Balch, A. L.; Mazzanti, M. M.; St. Claire, T. N.; Olmstead, M. M. *Inorg. Chem.* **1995**, *34*, 2194-2200. (e) Choe, Y. S.; Ortiz de Montellano, P. R. *J. Biol. Chem.* **1991**, *266*, 8523-8530. (f) Sano, S.; Sugiura, Y.; Maeda, Y.; Ogawa, S.; Morishima, I. *J. Am. Chem. Soc.* **1981**, *103*, 2888-2890. (g) Sano, S.; Morishima, I.; Shiro, Y.; Maeda, Y. *Proc. Natl. Acad. Sci. U.S.A.* **1986**, *83*, 531-535.

(7) Wilks, A.; Ortiz de Montellano, P. R. *J. Biol. Chem.* **1993**, *268*, 22357-22362.

(8) Wilks, A.; Torpey, J.; Ortiz de Montellano, P. R. *J. Biol. Chem.* **1994**, *269*, 29553-29556.

(9) Groves, J. T.; Haushalter, R. C.; Nakamura, M.; Nemo, T. E.; Evans, B. J. *J. Am. Chem. Soc.* **1981**, *103*, 2884-2886.

(10) Noguchi, M.; Yoshida, T.; Kikuchi, G. *J. BioChem. (Tokyo)* **1983**, *93*, 1027-1036.

(11) Bonnett, R.; Dimsdale, M. J. *J. Chem. Soc. Perkin. Trans. 1* **1972**, 2540-2548.

(12) Gold, A.; Ivey, W.; Toney, G. E.; Sangaiah, R. *Inorg. Chem.* **1984**, *23*, 2932-2935.

(13) (a) Ator, M. A.; David, S. K.; Ortiz de Montellano, P. R. *J. Biol. Chem.* **1989**, *264*, 9250-9257. (b)Ator, M. A.; David, S. K.; Ortiz de Montellano, P. R. *J. Biol. Chem.* **1987**, *262*, 14954-14960.

(14) Choe, Y. S.; Ortiz de Montellano, P. R. *J. Biol. Chem.* **1991**, *266*, 8523-8530.

(15) Murakami, T; Watanabe, Y.; Morishima, I. *Chem. Lett*, in press.

(16) (a) Goff, H. M.; Phillippi, M. A. *J. Am. Chem. Soc.* **1983**, *105*, 7567-7571. (b)Gans, P.; Buisson, G.; Duee, E.; Marchon, J. C.; Erler, B. S.; Scholz, W. F.; Reed, C., A *J. Am. Chem. Soc.* **1986**, *108*, 1223-1234.

(17) Groves, J. T.; Watanabe, Y. *J. Am. Chem. Soc.* **1988**, *110*, 8443-8452.

(18) Wagner, W. R.; Rastetter, W. H. *J. Org. Chem.* **1983**, *48*, 402-404.

(19) Methanol is added to dissolve C_6F_5IO in dichloromethane.

(20) The formation of **4a** is also confirmed by ^{1}H-NMR and ESR measurements at -70°C and 5 K, respectively (β-pyrrole H: -12.4 and -11.1 ppm, g = 4.28, 3.64, and 1.97; see reference, Fujii, H. *J. Am. Chem. Soc.* **1993**, *115*, 4641-4648.).

(21) Judging from the absorption maxima in the near-IR region, the isoporphyrin complex obtained by the addition of the acids to **4a** seems to be different from **2a**.

(22) (a) Dolphin, D.; Felton, R. H.; Borg, D. C.; Fajar, J. *J. Am. Chem. Soc.* **1970**, *92*, 743-745. (b)Fajar, J.; Borg, D. C.; Forman, A.; Dolphin, D.; Felton, R. H. *J. Am. Chem. Soc.* **1970**, *92*, 3451-3459. (c)Fawcett, W. R.; Fedurco, M.; Smith, K. M.; Xie, H. *J. Electroanal. Chem.* **1993**, *354*, 281-287. (d) Lee, W. A.; Bruice, T. C. *Inorg. Chem.* **1986**, *25*, 131-135. (e)Hinman, A. S.; Pavelich, B. J.; Kondo, A. E.; Pons, S. *J. Electroanal. Chem.* **1987**, *234*, 145-162. (f) Oliver Su, Y.; Kim, D.; Spiro, T. G. *J. Electroanal. Chem.* **1988**, *246*, 363-371. (g) Takeda, Y.; Takahara, S.; Kobayashi, Y.; Misawa, H.; Sakuragi, H.; Tokumaru, K. *Chem. Lett* **1990**, 2103-2106.

(23) Yamaguchi, K.; Watanabe, Y.; Morishima, I. *Inorg. Chem.* **1992**, *31*, 156-157.

(24) Takahashi, S.; Ishikawa, K.; Takeuchi, N.; Ikeda-Saito, M.; Yoshida, T.; Rousseau, D. L. *J. Am. Chem. Soc.* **1995**, *117*, 6002-6006.

(25) (a)Watanabe, Y.; Takehira, K.; Shimizu, M.; Hayakawa, T.; Orita, H.; Kaise, M. *Transformation of Fe(III)TMP N-oxide to a two electron oxidized equivalent of Fe(III)TMP complex*; Simándi, L.I., Ed.; Elsevier Science Publishers B.V.: Amsterdam, 1991; Vol. 66, pp 213-220. (b) Tsurumaki, H.; Watanabe, Y.; Morishima, I. *J. Am. Chem. Soc.* **1993**, *115*, 11784-11788.

(26) Yamaguchi, K.; Watanabe, Y.; Morishima, I. *J. Chem. Soc., Chem. Commun.* **1992**, 1721-1723.

(27) Ozawa, S.; Watanabe, Y.; Morishima, I. *J. Am. Chem. Soc.* **1994**, *116*, 5832-5838.

(28) (a) Takahashi, S.; Wang, J.; Rousseau, D. L.; Ishikawa, K.; Yoshida, T.; Takeuchi, N.; Ikeda-Saito, M. *Biochemistry* **1994**, *33*, 5531-5538. (b) Hernández, G.; Wilks, A.; Paolesse, R.; Smith, K. M.; Ortiz de Montellano, P. R.; La Mar, G. N. *Biochemistry* **1994**, *33*, 6631-6641.

(29) (a) Groves, J. T.; Watanabe, Y. *J. Am. Chem. Soc.* **1986**, *108*, 7834-7836. (b) Groves, J. T.; Watanabe, Y. *J. Am. Chem. Soc.* **1986**, *108*, 7836-7837. (c) Watanabe, Y.; Yamaguchi, K.; Morishima, I.; Takehira, K.; Shimizu, M.; Hayakawa, T.; Orita, H. *Inorg. Chem* **1991**, *30*, 2581-2582. (d) Groves, J. T.; Watanabe, Y. *Inorg. Chem.* **1986**, *25*, 4808-4810.

(30) Valentine, J. S.; Quinn, A. E. *Inorg. Chem.* **1976**, *15*, 1997. (b) Sisemore, M. F.; Burstyn, J. N.; Valentine, J. S. *Angew. Chem. Int. Ed. Engl.* **1996**, *35*, 206-208. (c) Sisemore, M. F.; Selke, M.; Burstyn, J. N.; Valentine, J. S. *Inorg. Chem.* **1997**, *36*, 979-984.

PART IV.

STRUCTURES AND FUNCTIONS OF SITE-DIRECTED MUTANTS OF MYOGLOBIN

CHAPTER 1.

Effects of the Arrangement of A Distal Catalytic Residue on Regioselectivity and Reactivity in the Coupled Oxidation of Sperm Whale Myoglobin Mutants

Abstract

Sperm whale myoglobin (Mb) mutants have been constructed by the double substitution of amino acid residues in the distal site to relocate the distal His-64 to the positions of Leu-29, Phe-43, and Ile-107. The coupled oxidation of the resulting Mb mutants, L29H/H64L, F43H/H64L, and I107H/H64L Mbs, as well as H64L Mb was carried out to mimic the heme oxygenase-catalyzed reaction and examine whether or not the regiospecific and efficient heme degradation are controlled by changing the location of the distal His. HPLC analysis of biliverdin formed by the coupled oxidation of heme showed that L29H/H64L Mb almost exclusively gave biliverdin IXγ along with a small amount of the α-isomer. On the other hand, the F43H/H64L was found to give the β-isomer as the major product with small amounts of the α- and γ-isomer. I107H/H64L Mb maintained α-selectivity as observed for wild-type Mb while a small amount of the γ-isomer was also observed. Simple elimination of the distal His in Mb (H64L) affords the α-isomer, indicating the location of the distal His in these Mb double mutants are effective on the regioselectivity. While resonance Raman studies and relatively slow autooxidation rates of the oxy complexes of the mutants suggest electrostatic interaction of the distal His with the iron-bound oxygen, these interactions are not effective enough to regulate the restricted regioselectivity in the heme degradation of the Mbs except for L29H/H64L Mb. In the case of L29H/H64L Mb, an unusual polar distal site is possibly liable for the nearly perfect regioselectivity. On the other hand, relocation of the distal His-64 to the three positions also caused rapid degradation of heme in the coupled oxidation.

Introduction

Heme oxygenase (HO) is a central monooxygenase of the heme catabolism[1] and forms a 1 : 1 stoichiometric complex with protoheme IX, which is a prosthetic active center and at the same time the substrate of the enzyme.[2] The enzyme utilizes electrons and molecular oxygen for catalyzing the heme degradation to yield biliverdin and carbon monoxide through three sequential oxygenase reactions; heme is degraded with a regiospecific opening of the tetrapyrrole macrocycle at the α-*meso*-position to biliverdin *via* α-*meso*-hydroxyheme and verdoheme as the first and second metabolites, respectively (Scheme 1). The formation of the first metabolite involves O_2 binding and activation at the heme iron followed by hydroxylation of the α-*meso*-carbon probably *via* the formation of a ferric hydroperoxide complex (Fe^{3+}-OOH).[3] The *meso*-hydroxylation by the bound oxygen is the key step for the regiospecificity.

Scheme 1

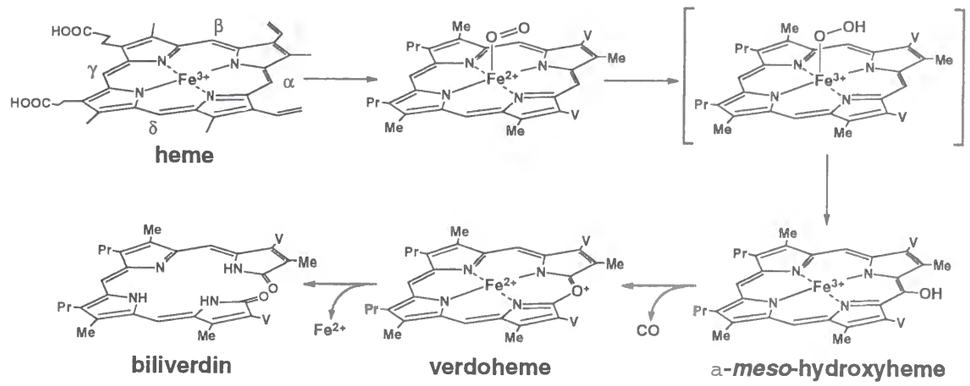

Recently, Torpey et al. examined regioselectivity of the oxidized products of methylmesoheme and formylmesoheme by HO, and suggested that the regiochemistry of the reaction could be primarily controlled by electronic rather than steric effect.[4] On the other hand, recent resonance Raman studies suggested that the O_2-bound heme-HO complex had a highly bent structure of the coordinated oxygens whose terminal oxygen atom was in van der waals contact with the α-*meso*-carbon of the porphyrin ring.[5] Furthermore, ESR studies of the O_2-bound cobalt heme-HO complex provides evidence for hydrogen bonding of a distal residue to the bound oxygen on the basis of an isotope-sensitive signal in both ^1H_2O

and ^2H_2O [6] Therefore, a specific orientation of the bound oxygen toward the α-*meso*-carbon induced by the hydrogen bonding may also be a factor for the regioselectivity.

Myoglobin (Mb) shares a neutral His ligand with the heme-HO complex,[7] and shows HO-type heme degradation site-specifically at the α-*meso*-position even though the activity is much lower than HO.[8] The specific oxidation of the α-*meso*-position can be expected on the basis of its crystal structure of oxyMb. The molecular oxygen bound to the heme in the oxyMb is highly restricted by the distal His (His-64) toward the α-*meso*-position. This idea leads us to construct the distal site of Mb by relocation or elimination of the distal His to regulate the regiospecificity of the heme oxygenase reaction.

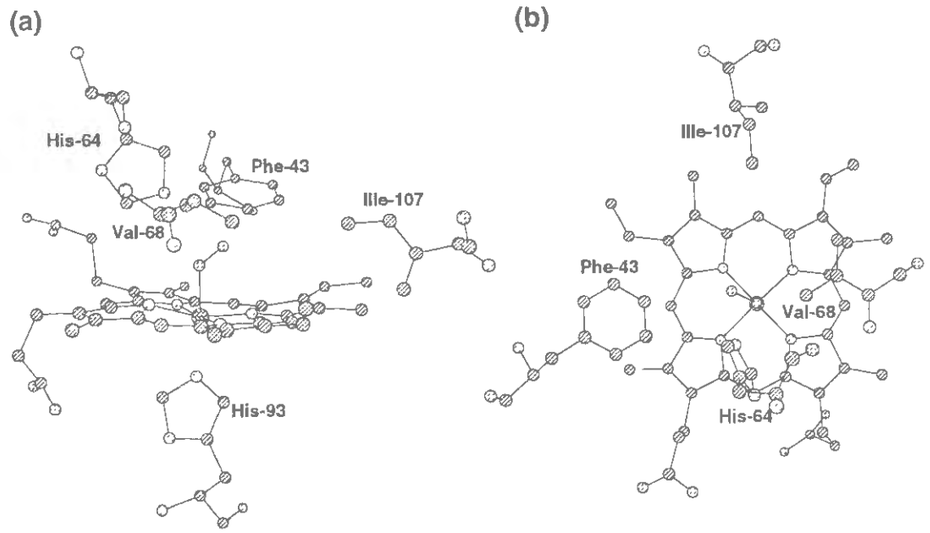

Figure 1. Heme environmental structure of myoglobin. Heme and some selected residues are shown. (a) Side view. (b) Top view.

As shown in Scheme 1, both HO and peroxidase reactions utilize a common key intermediate, Fe^{3+}-OOH.[3] Very recently, we have prepared Mb mutants, in which the distal His is relocated to the positions of Leu-29[9] and Phe-43[10] to mimic the distal site structures of CcP and beef liver catalase. Among them, F43H/H64L showed efficient O-O bond cleavage resulting in enhancement of the sulfoxidation rate by 190-fold. Heme

degradation of Mb and the other heme proteins by the aerobic addition of ascorbate, the so-called coupled oxidation, is known to mimic the HO-catalyzed reaction.[11] Thus, we have used these mutants to examine whether the HO activity is enhanced or not. At the same time, we have prepared an I107H/H64L mutant since His-107 is expected to be located nearby the α-*meso*-position while His-43 is located close to the β-*meso*-position respectively (Figure 1). Different location of the distal His could be effective on the regioselectivity of HO reaction. In fact, our preliminary results have indicated the importance of histidine location for the regioselectivity.[12] In this paper, we discuss more detail about the HO mimic reactions by the Mb mutants.

Experimental Section

Sodium dithionite, and sodium ascorbate were purchased from Wako Pure Chemical Industries, Ltd.

Site-Directed Mutagenesis, Preparation, and Purification. Site-directed mutagenesis of Leu-29, Phe-43, and Ile-107 in recombinant sperm whale myoglobin was carried out by using the polymerase chain reaction (PCR) according to methods previously reported.[13]

The His-64→Leu replacement was achieved by cassette mutagenesis. The cassette including desired His-64 substitution and a new silent *Hpa*I restriction site was inserted between the *Bgl*II and *Hpa*I sites. The expression and purification of the mutants were performed according to methods previously described.[13]

Spectroscopy. All spectroscopic measurements were performed in 50 mM sodium phosphate buffer (pH 7.0) unless otherwise stated. Electronic absorption spectra were recorded on a Perkin Elmer Lambda 19 spectrometer with the samples whose concentration was adjusted to ca. 5 μM. The coupled oxidation assays were performed in the buffer containing ascorbate (1 mM) at 37°C. Spectra were recorded (300-850 nm) for 5 h. Measurements of autooxidation rates of the oxy complexes of wild-type Mb and mutants were made at 37°C using ca. 5 μM protein in the buffer. The mutants were reduced with excess sodium dithionite, and loaded on a small Sephadex G-25 (Pharmacia) column equilibrated and eluted with CO-saturated 50 mM sodium phosphate buffer, pH 7.0. The

resultant CO-Mbs without any reductant were converted to the oxyMbs by irradiation of white lamp under O_2 atmosphere at 0°C. The oxy complex of wild-type Mb was directly prepared from the metMb by passing the reduced complex by sodium dithionite through a small G-25 column equilibrated and eluted with air-saturated buffer. Autooxidation rates were evaluated by observing the absorption spectra between 390 and 430 nm. The intensity of the Soret band maxima of the oxyMbs was used for the calculation. Spectral changes with clear isosbestic points were chosen for the data analysis.

Raman scattering was excited at 406.7 nm by a Kr^+ ion laser (Spectra Physics, Model 2016), and detected by a charge-coupled device (CCD) (Astromed spectral) attached to a single monochromator (Ritsu). The slit width was 6 cm^{-1} except for L29H/H64L Mb (12 cm^{-1}). Therefore, the Raman lines in trace C in Figure 7 was slightly broad, which might affect the frequency of the lines. RR spectra were measured at room temperature with a spinning quart cell. Raman shifts were calibrated to an accuracy of 1 cm^{-1} with potassium ferricyanide and indene.

Electrochemistry. For the reduction potential measurements of Fe^{3+}/Fe^{2+} couple all the samples were degassed by Ar gas and further by the glucose (5 mM), glucose oxidase, and catalase system.[14] The metMbs were then reduced to the ferrous states by the irradiation of a white lamp, in the presence of EDTA (1 mM). Methylene blue, thionine, and phenosafranine were used as mediators. The reduction potentials and the optical absorption spectra were measured at the same time at 25°C by Metrohm 744 pH meter equipped with Metrohm AG 9100 Herisau electrode, and by a Perkin Elmer Lambda 19 spectrometer, respectively. Sample concentration was ca. 5 μM.

The midpoint potential (E_0) of Mb was obtained from the plot of the monitored electrode potential (E_h) against the percentage of reduced Mb estimated from the absorbance change at the Soret band of the oxidized Mb by using the following Nernst equation:

$$E_h = E_0 + (RT/\nu F) \log\{[\text{oxidized Mb}]/[\text{reduced Mb}]\}$$

where ν and F denote number of electrons involved in the redox reaction and Faraday constant, respectively. The midpoint potentials were corrected by utilizing methylene blue (-11 mV) as a standard.

Biliverdin Extraction and HPLC Analysis. To a 250 μl solution of the ferric complexes of wild-type, mutant Mbs or human Hb (40 μM) was added sodium ascorbate (2 mg) and the resulting solution was incubated at 37°C for 3 h. Extraction of biliverdin regioisomers was performed as previously reported.[15] The products dissolved in methanol were loaded on a high-pressure liquid chromatograph (Waters 600) equipped with Waters 741 data module and TOSOH CO-8020 column oven. A reverse-phase HPLC column (Whatman Partisil 5 ODS-3) was employed at 40°C at a flow rate of 0.7 ml/min with 75:25 (v/v) methanol-25 mM ammonium phosphate buffer (pH 3.5) and detected at 380 nm.

A mixture of four biliverdin regioisomers was prepared from protoheme IX according to the method reported.[4b]

Results

HPLC Analysis of the Coupled Oxidation Products. The regiospecificity of the coupled oxidation of Mb mutants was examined by incubating the samples with ascorbate in aerobic condition at 37°C for 3 h. Since Fe^{3+}-biliverdin is known to be formed instead of a free form of biliverdin[16] in the coupled oxidation with ascorbate, we have converted Fe^{3+}-biliverdin•Mb complexes to biliverdins by the treatment with acetic acid and HCl. A HPLC system separates four biliverdin regioisomers derived from heme.

Figure 2a shows a HPLC chart for the products of the coupled oxidation of hemin. Peaks at the retention time of 8.4, 9.8, 10.4, and 13.6 min correspond to four biliverdin isomers because each peak shows absorption maxima around 380 and 650 nm typical of biliverdin. An isomer having retention time of 8.4 min is identified as the α-isomer by comparison with authentic biliverdin IXα and the product of wild-type Mb (Figure 2b) which affords biliverdin IXα exclusively. Figure 2c shows two oxidation products from human Hb (8.4 and 9.8 min). That human Hb is known to give the α- and β-isomer in the coupled oxidation allows us to identify the peak at 10.2 min to be biliverdin IXβ.[17] We also assigned the peak at 13.6 min to the γ-isomer on the basis of the results reported before.[17] Therefore, the elution sequence of the isomers of biliverdin is assigned to the α- (8.4 min), β- (9.8 min), δ- (10.4 min), and γ-isomer (13.6 min).

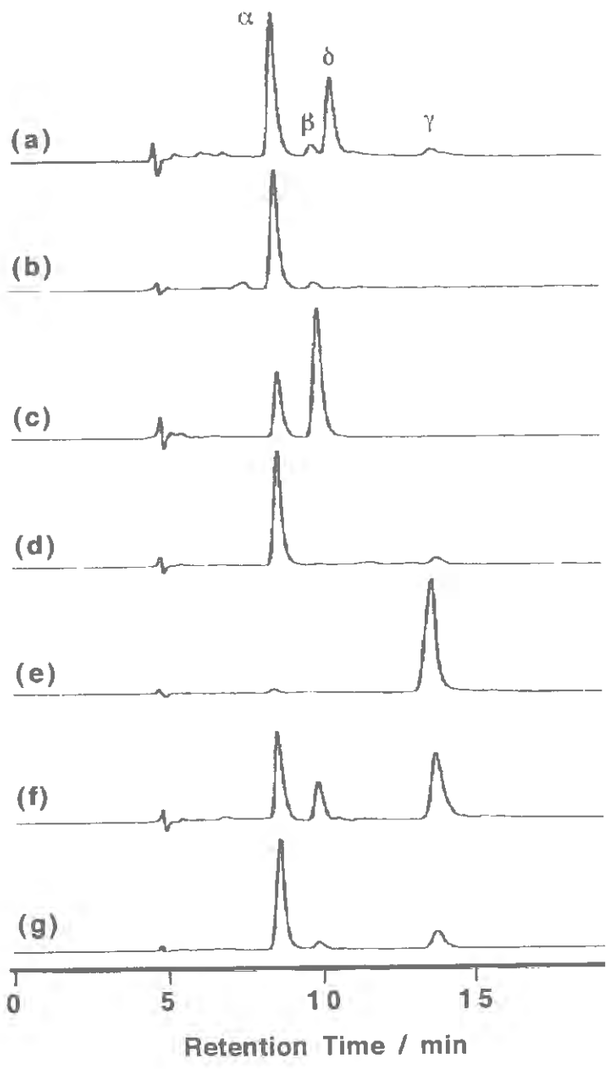

Figure 2. HPLC analysis of product isolated from the coupled oxidation of Mbs with ascorbate at 37°C for 3 h: (a) four biliverdin isomers, and products extracted from (b) wild-type Mb, (c) Hbα, (d) H64L, (e) L29H/H64L, (f) F43H/H64L, and (g) I107H/H64L Mbs.

Based on these results, the coupled oxidation products from Mb mutants are identified as follows: the major α-isomer with a small amount of the γ-isomer for H64L Mb (Figure 2d), the major γ-isomer with the α-isomer for L29H/H64L Mb (Figure 2e), the α-, β-, and γ-isomer for F43H/H64L Mb (Figure 2f), the major α-isomer with the minor γ-isomer and a very small amount of the β-isomer for I107H/H64L Mb (Figure 2g). These data are summarized in Table 1.

Table 1. Ratio of four biliverdin isomers produced by the coupled oxidation of Mbs.[a]

Mb	α	:	β	:	γ	:	δ	(%)
wild-type	95	:	5	:	0	:	0	
L29H/H64L	3	:	0	:	97	:	0	
F43H/H64L	40	:	16	:	44	:	0	
I107H/H64L	72	:	6	:	22	:	0	
H64L	94	:	0	:	6	:	0	

[a] Ratio of the peak area.

Monitoring of the Coupled Oxidation by Electronic Absorption Spectroscopy. Figure 3 shows the electronic absorption spectral changes upon the aerobic addition of ascorbate to Mbs at 1-hr intervals. As reported for horse wild-type Mb,[18] electronic absorption spectral changes upon the addition of ascorbate to sperm whale wild-type Mb showed a slow conversion of metMb to oxyMb with subsequent slow degradation to an Fe^{3+}-biliverdin•Mb complex. On the basis of the spectral changes shown in Figure 3a, the rate constants for the oxyMb formation and its decay are 3.0×10^{-2} and 5.1×10^{-3} min^{-1}, respectively. Addition of ascorbate to L29H/H64L Mb resulted in rapid disappearance of the Soret band to afford Fe^{3+}-biliverdin in five hours (Figure 3b). Absorbance decay at 408 nm was fitted by two single-exponential processes, and the rate constants calculated were 4.3×10^{-2} and 7.5×10^{-3} min^{-1}. As shown in Figure 3c and 3d, the coupled oxidation of F43H/H64L and I107H/H64L Mbs showed a different reaction profile from wild-type and L29H/H64L Mbs. Spectra of F43H/H64L and I107H/H64L Mbs exhibited a red-shifted and relatively sharp Soret band in an hour, suggesting the formation of the CO-Mbs. The absorption maxima of the Soret bands after five hours in Figure 3c

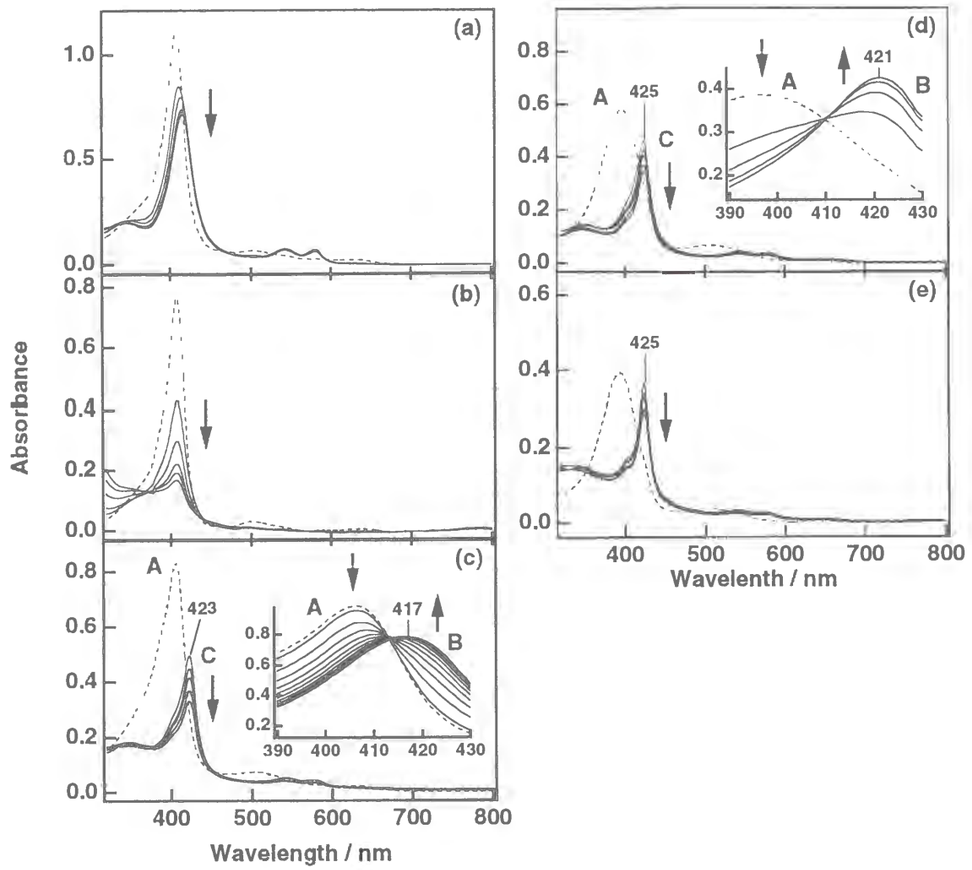

Figure 3. Electronic absorption spectral changes (320-800 nm) of the metMbs during coupled oxidation containing 1 mM ascorbate at 37°C: (a) wild-type Mb, (b) L29H/H64L, (c) F43H/H64L, (d) I107H/H64L, and (e) H64L Mbs. The spectra were recorded at 1-h intervals. (inset) initial spectral changes at 1-min intervals.

and 3d were identical with those of the corresponding CO-Mbs, respectively. Insets in Figure 3c and 3d depict the initial spectral changes at 1-min intervals after the addition of ascorbate to F43H/H64L and I107H/H64L Mbs, respectively. These absorption maxima of the Soret bands correspond to those of the oxyMbs (Table 2). Transient formation of the oxy intermediates was further confirmed by the observation that the intermediates during the reactions were transformed to the CO-Mbs by bubbling CO. Thus the spectral changes for F43H/H64L and I107H/H64L

Table 2. Formation Rates (k_{O_2}) of Oxy-ferrous Heme of Mbs in the Initial Stage of the Coupled Oxidation, and Autooxidation rates (k_{ox})

Mb	first order rate [min^{-1}]	
	k_{O_2} [a]	k_{ox}
wild-type	3.2×10^{-2}	3.0×10^{-3}
F43H/H64L	3.4×10^{-1}	7.4×10^{-2}
I107H/H64L	9.3×10^{-1}	7.6×10^{-2}

[a] Rates were determined based on absorbance change at the Soret band of the ferric heme of Mbs until 30, 11, and 4 min after the addition of ascorbate at 37°C to wild-type Mb, F43H/H64L mutant, and I107H/H64L mutant, respectively.

Mbs indicate that CO formed by the coupled oxidation of the heme was trapped by the oxy intermediates remained in the solution (Scheme 2). According to these observations, the total spectral changes in Figure 3c and 3d were described as follows: F43H/H64L and I107H/H64L metMbs (spectra A) were converted to the oxyMbs (Spectra B) very rapidly, and then the oxyMbs subsequently gave a mixture of the oxy and CO-Mbs (spectra C). After these changes, sharpening and disappearing of the Soret band in the spectra C were observed due to further degradation of the oxyMbs. In separate runs, F43H/H64L and I107H/H64L CO-Mbs were also degraded under the conditions, suggesting slow dissociation of CO from the CO-Mbs. Compared to wild-type and L29H/H64L Mbs, the coupled

Scheme 2

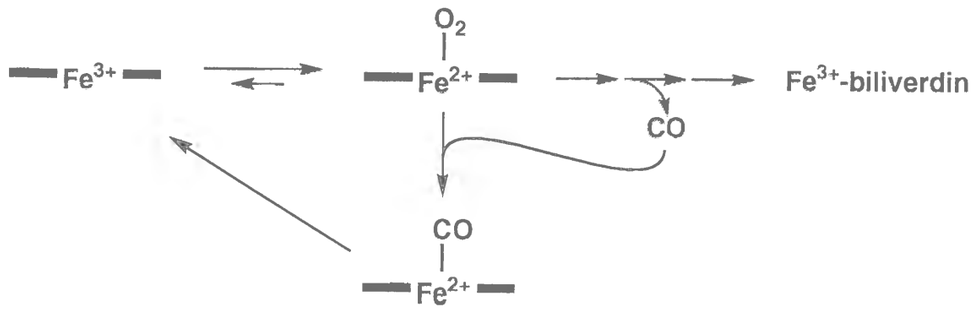

oxidation of F43H/H64L and I107H/H64L Mbs afforded a greater amount of the CO-Mbs as the result of the product (CO) inhibition. H64L Mb was degraded without distinct accumulation of the oxy form but still gave the CO-Mb. Since Fe^{3+}-biliverdin does not have absorption in the visible region,[19] the formation of biliverdin was confirmed as a free form. For

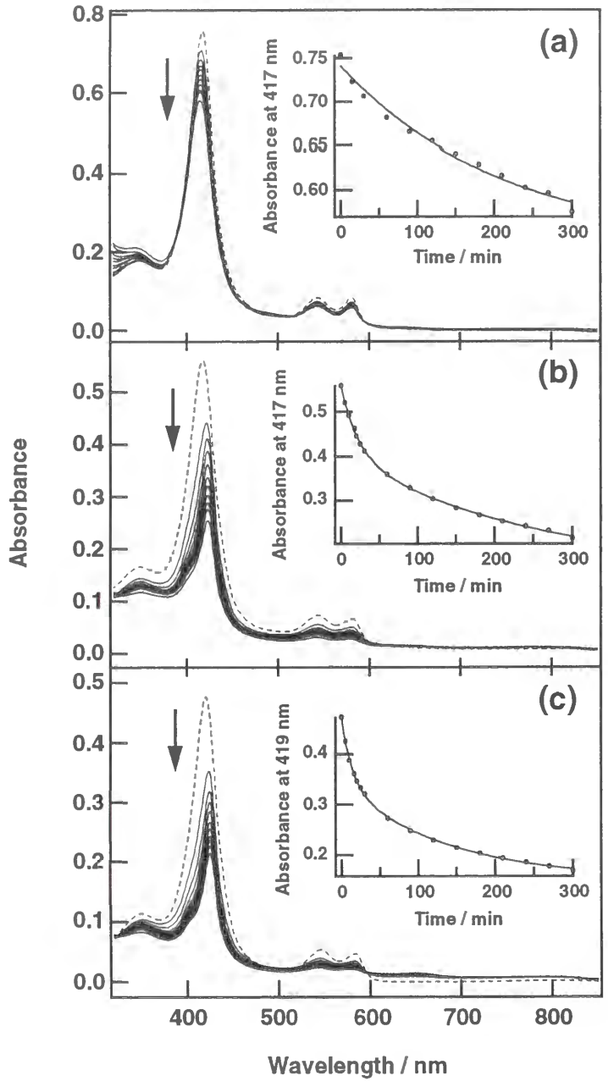

Figure 4. Electronic absorption spectral changes (320-850 nm) of the oxyMbs during coupled oxidation containinf 1 mM ascorbate: (a) wild-type Mb, (b) F43H/H64L, and (c) I107H/H64L Mbs. The spectra were recorded at 30-min intervals. (inset) absorbance change at the isosbestic point between the oxy and CO-Mbs.

I107H/H64L Mb, accumulation of CO-bound verdoheme, which is a CO-inhibited form of the intermediate in heme degradation (Scheme 1), was revealed by the observation of increased absorbance at ~ 650 nm.[20] Low yield of Fe^{3+}-biliverdin compared to the consumption of the starting complex may be attributable to further oxidative destruction of the Fe^{3+}-biliverdin and/or another degradation pathway not yielding biliverdin.[21]

The formation rates of the oxy complexes of F43H/H64L and I107H/H64L Mbs are determined by fitting for the initial stage. The results were summarized in Table 2. The oxy complex formation of F43H/H64L and I107H/H64L Mbs is much faster than that of wild-type Mb, resulting in the accumulation of the oxyMbs followed by the unusual CO-inhibition. Therefore, the rate for the biliverdin formation can not be correctly evaluated by the rate constants determined from absorbance change at 408 nm as reported before.[18] These difficulties prevent us from calculating the accurate rate constants to determine whether the hydroxyheme formation is accelerated or not by His-43 and His-107.

To examine the heme degradation from the oxy complexes of wild-type Mb and the mutants, the rate constants were calculated based on the absorbance change at an isosbestic point between the oxy and CO-Mbs (Figure 4). Thus, we have monitored the time dependent absorbance changes at 417 nm for wild-type and F43H/H64L Mbs, and 419 nm for the I107H/H64L mutants (Figure 4 inset). Preparation of the oxy complex of L29H/H64L Mb was precluded by rapid autooxidation of the complex. For the oxy complexes of F43H/H64L and I107H/H64L Mbs, the formation of Fe^{3+}-biliverdin was found to be fitted by two single-exponential functions as applied before,[18] while the kinetics of the reaction of the oxy complex of wild-type Mb was fitted as a single-exponential process. By the comparison of the rate constants listed in Table 3, it is clear that the bound oxygens of F43H/H64L and I107H/H64L Mbs are efficiently activated, and used for the heme degradation.

Table 3. Coupled Oxidation Rates of OxyMbs in 50 mM Sodium Phosphate Buffer, pH 7.0 at 37°C

Mb	first order rate [min^{-1}]	
wild-type	3.2×10^{-3}	
F43H/H64L	4.5×10^{-2}	3.8×10^{-3}
I107H/H64L	7.0×10^{-2}	7.0×10^{-3}

Nature of the OxyMb Mutants. The oxy complexes of F43H/H64L and I107H/H64L Mbs were stable enough to run a spectroscopic analysis at pH 7.0 at ambient temperature. As shown in Figure 5, I107H/H64L oxyMb shows a red-shifted Soret band at 421 nm as compared to that of wild-type oxyMb (418 nm), while the spectrum of the oxy complex of F43H/H64L Mb (417 nm) is nearly identical to that of wild-type oxyMb. The absorption spectrum of the O_2-bound heme-HO complex was reported to show the Soret band at 412 nm.[22]

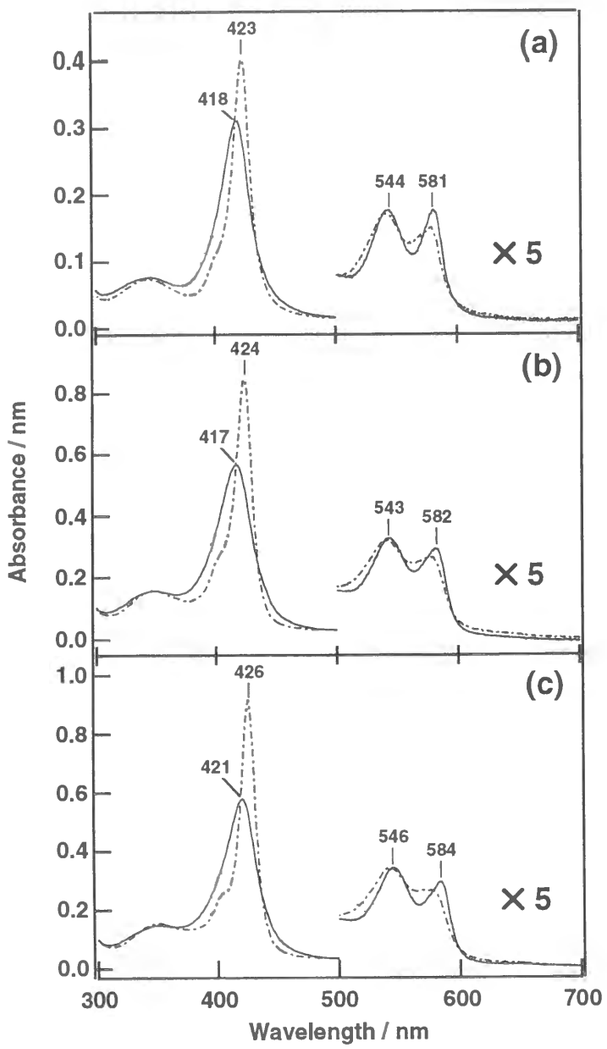

Figure 5. Electronic absorption spectra of the oxyMbs (——) and CO-Mbs (– – –).

The oxyMbs for the kinetic measurements were prepared by the method described in the Materials and Methods. The rates of autooxidation were determined based on the change in absorbance of the Soret band of the oxyMbs at 37 °C. All spectra showed the conversion of the oxyMbs to the metMbs with clear isosbestic points. First order autooxidation rates for wild-type and mutant Mbs are shown in Table 2. The oxy complexes of F43H/H64L and I107H/H64L Mbs were autooxidized over 20-fold faster than that of wild-type Mb while the autooxidation rate for H64L Mb is known to be higher than that of wild-type Mb by ~ 200-fold.[23]

Reduction Potential Measurement of Fe^{3+}/Fe^{2+} Couple. Reduction potential of the Fe^{3+}/Fe^{2+} couple was examined for wild-type Mb and the mutants. The reduction potentials of F43H/H64L, I107H/H64L, and H64L Mbs were determined to be 88, 60, and 83 mV, respectively, which were higher than the corresponding value of wild-type Mb (52 mV) under the conditions. On the contrary, L29H/H64L Mb exhibited a lower value of -22 mV. These values are listed in Table 4. The low value for L29H/H64L Mb might reflect a relatively polar active site of the mutant.[24]

Table 4. Reduction Potentials of Fe^{3+}/Fe^{2+} couple at 25°C

Mb	E_0 [mV]
wild-type	52
L29H/H64L	-22
F43H/H64L	88
I107H/H64L	60
H64L	83

Heme Environmental Structure of the Mb mutants. Heme-bound peroxide can accommodate two different types of hydrogen bonding as illustrated in Figure 6. Figure 6a is a case for wild-type Mb while the hydrogen bonding shown in Figure 6b is expected for peroxidases and catalases. As reported before,[10] the latter type of the hydrogen bonding is also expected for F43H/H64L Mb. The major difference of these two

hydrogen bonding is that the former does not stabilize the charge separation in the O-O bond while the latter enhances the deposition of the negative charge on the terminal oxygen of the O-O bond (*pull effect*).[25] On the other hand, the distal His in L29H/H64L and I107H/H64L Mbs is expected to be too far from the peroxide bound to the heme to form hydrogen bonding. Thus, these two mutants are useful for the examination of polar residue effects on the HO reaction by comparing with that of H64L Mb, in which the distal site is hydrophobic and no amino acid residue is able to interact directly with the bound peroxide.

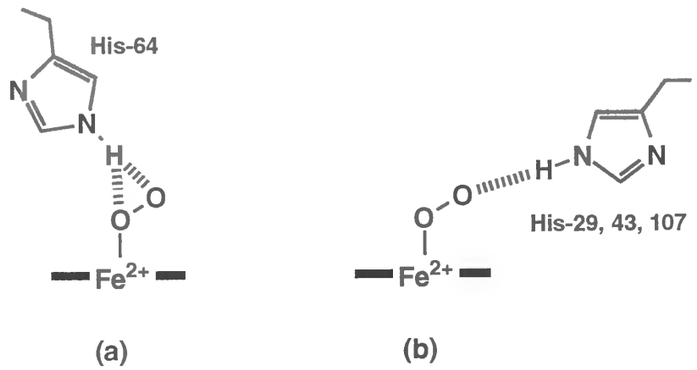

Figure 6. Two types of hydrogen bonding of a distal histidine to bound oxygen: (a) wild-type Mb and (b) the mutants in this study.

Since the stretching vibrations of the FeCO unit are sensitive to the environment of a heme distal pocket, resonance Raman studies were performed for the Mb mutants. Figure 7 depicts low- and high-frequency regions of resonance Raman spectra of the CO-Mbs. As reported previously, the line of the Fe-CO stretching, Fe-C-O bending, and C-O stretching modes for wild-type Mb were observed at 508, 575, and 1941 cm^{-1}, respectively (Figure 7a). For the CO-Mb mutants, three isotope sensitive lines were identified by employing $^{13}C^{18}O$ and $^{12}C^{16}O$ derivatives. In the case of L29H/H64L (Figure 7b) and F43H/H64L Mbs (Figure 7c), two lines of the C-O stretching mode appeared at 1932 and 1961, and ~1945 and 1962 cm^{-1}, respectively. In all the Mb mutants, the positions of the Fe-CO stretching modes are significantly lower than that observed for wild-type Mb, and the Fe-C-O bending modes are at almost the same frequency except for L29H/H64L Mb. The C-O stretching modes for all mutants exhibited upshift compared with that of wild-type Mb. The introduction of

His around the distal site of the H64L Mb, which affords L29H/H64L, F43H/H64L, and I107H/H64L, gave rise to downshift of the C-O stretching mode by 7, 6, and 8 cm^{-1}, respectively, indicative of at least electrostatic interaction between histidyl imidazole and the bound CO.[26] These values are similar to that of the CO-bound heme-HO complex (1958 cm^{-1}).[7a]

It is known that the line width for the Fe-CO and C-O stretching modes is quite broad in the CO-bound heme-HO complex compared to the CO complex of wild-type Mb. These broad lines have been attributed to a

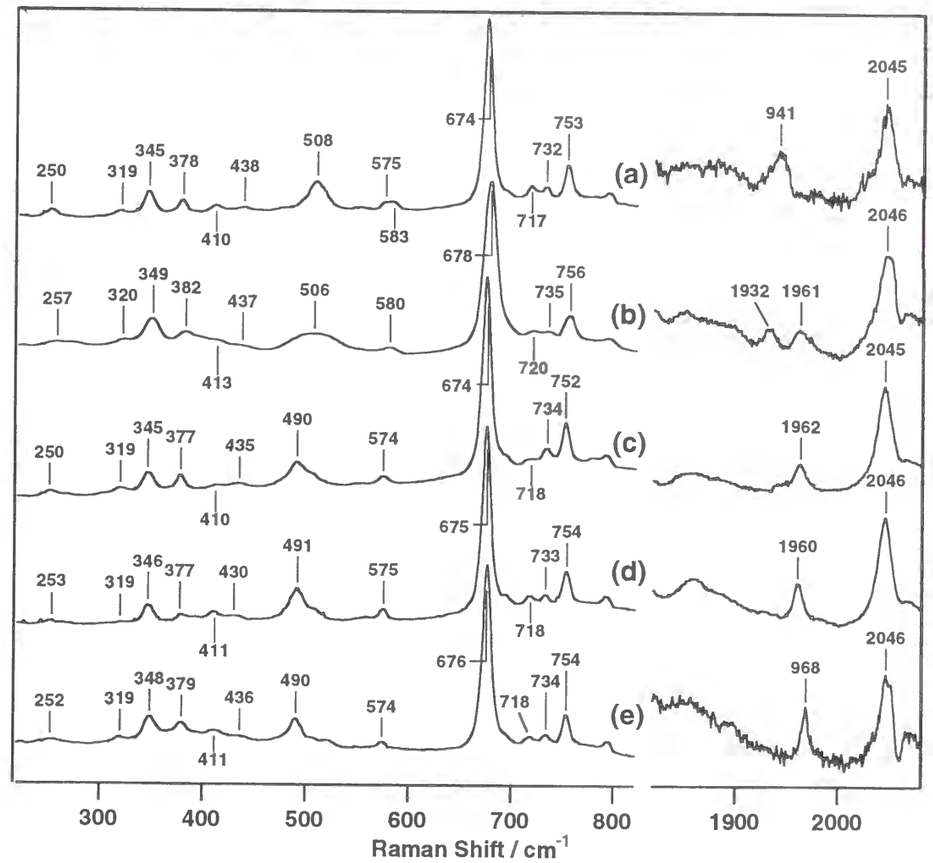

Figure 7. Resonance Raman spectra of the Fe-CO stretching mode and the C-O stretching mode regions of the CO-Mbs: (a) wild-type Mb, (b) F43H/H64L, (c) L29H/H64L, (d) I107H/H64L, and (e) H64L Mbs. The excitation wavelength was 406.7 nm with a power of about 1 mW. The slightly broad lines in the spectrum of L29H/H64L Mb is due to the larger slit width by 2-fold (see METHODS section). Such a larger slit width may also affect the Raman shifts for L29H/H64L Mb.

heterogeneous environment for the bound CO.[7a] While line-broadening was induced by introduction of His around the distal site of the H64L Mb as shown in Figure 7b-d, relocation of the distal His was insufficient to construct more heterogeneous environment than that of wild-type Mb since the line widths of the ν_{Fe-CO} and ν_{C-O} Raman line of F43H/H64L, and I107H/H64L Mbs are similar to those of wild-type Mb. On the contrary, those lines for L29H/H64L are relatively broad.

Table 5. Comparison of the Low- and High-Frequency Modes of CO-Mbs

	Fe-CO stretch	Fe-C-O bent	C-O stretch
wild-type Mb	508	575	1941
L29H/H64L Mb	507	580	1932 1961
F43H/H64L Mb	490	574	~1945 1960
I107H/H64L Mb	491	575	1960
H64L Mb	490	574	1966
heme-HO complex[a]	503	576	1958

[a] Takahashi et al. (1994)

Discussion

The hydrogen bonding of the neutral imidazole side chain of His-64 with the iron bound molecular oxygen plays the most crucial role in the inhibition of wild-type Mb heme iron from autooxidation. This interaction prevents the dissociation of the bound oxygen, and protonation and replacement of the bound oxygen with solvent water leading to autooxidation.[27] At the same time, the oxygen bound to the iron is forced to bent toward the α-*meso*-position. The regiospecific opening of the tetrapyrrole macrocycle at the α-*meso*-position in wild-type Mb, thus, can be partly attributed to the distal His-64 to regulate the direction of a putative hydroperoxide bound to the heme (see Scheme 1). Replacement of His-64 with apolar and less bulky residues including Leu results in 100~800-fold increase in the rate of the autooxidation due to the loss of this hydrogen bonding interaction.[23] In addition, elimination of the distal His-

64 may allow the bound hydroperoxide to rotate around the heme. The observation that the coupled oxidation products of H64L Mb afforded a small amount of the γ-isomer, which was absent in the case of wild-type Mb, is in good agreement with the consideration. The calculation shows the highest energy for the orientation of the oxygen bound to the heme iron of Mb toward the γ-*meso*-position because of a steric effect of the distal His residue,[28] thus, replacement of His-64 to a smaller residue allows the bound oxygen to be directed toward the γ-*meso*-position. However, the major α-selectivity of H64L Mb indicates that the hydroperoxide bound to the iron in the H64L Mb still stays mostly above the α-*meso*-position even without His-64.

H64L Mb is a good starting hemoprotein to elucidate specific effects of a catalytic residue introduced to the distal site by comparison of the properties of mutated H64L Mb with those of H64L Mb. First of all, we have examined whether the regiospecificity is affected by the distal His located far enough to avoid the steric interaction with the hydroperoxide bound to the heme (Figure 6b). For this purpose, a His residue has been introduced to three different positions in H64L Mb to construct L29H/H64L, F43H/H64L, and I107H/H64L Mbs.

The $\nu_{C=O}$ Raman lines of L29H/H64L, F43H/H64L, and I107H/H64L Mbs were lower than that of H64L Mb by 7, 6, and 8 cm^{-1}, respectively, while still higher than that of wild-type Mb (Table 5). The result suggests that the distal His of the mutants exerts an electrostatic effect on the bound CO because positively charged or protic amino acid residues near the proximal ligand atom usually promote the formation of resonance structures with lower C-O and higher Fe-C bond order.[26]

Very recently, we have examined the peroxygenase activity of the L29H/H64L and F43H/H64L mutants.[9,10] The distance between the heme iron and the N_ε atom of His-29 is determined to be 6.6 Å on the basis of its crystal structure while that in the F43H/H64L is estimated to be about 5.4 Å using the program Discover.[29] The latter is the distance observed for cytochrome *c* peroxidase and beef liver catalase and suitable to have the hydrogen bonding shown in Figure 6b. Therefore, F43H/H64L Mb shows not only efficient O-O bond cleavage but also high oxygenation ability.[10] In the case of I107H/H64L, the distance between the heme iron and the N_ε atom of His-107 is calculated to be 7.4 Å. Therefore, the His in L29H/H64L and I107H/H64L Mbs are not able to form a peroxidase-type hydrogen bonding with the hydroperoxide bound to the heme iron, however, the His at the positions of 29 and 107 effectively perturbs the distal site atmosphere

of H64L Mb as observed by resonance Raman measurements for the CO-Mbs. In addition, lower autooxidation rate of I107H/H64L Mb than that of H64L Mb also suggests electrostatic interaction between the distal His and the bound ligand.

Regioselectivity. We have for the first time observed the change of the regiospecificity of the coupled oxidation process of Mb by relocating the distal His in the distal site.[12] This is well illustrated by the finding that the L29H/H64L mutant is almost regiospecifically oxidized to biliverdin IXγ. However, the other mutants provided a complicated regioselectivity. I107H/H64L Mb showed the α-selectivity in the coupled oxidation with a small amount of the γ-isomer even though the His-107 is located near the α-*meso*-position. In the case of F43H/H64L Mb, the β-isomer was obtained along with the α- and γ-isomer. As shown in Figure 1, the β, γ, and δ-*meso*-positions of heme of wild-type Mb are covered with the side chains of Phe-43, His-64, and Val-68, respectively. As described above, the increased amount of the γ-isomer for H64L Mb can be explained in terms of elimination of His-64 which sterically blocks the γ-*meso*-position. On the other hand, introduction of the His to H64L Mb tends to further enhance the γ-isomer formation. Although the mechanism is not clear at this moment, these observations could imply that the distal His except for His-64 enhances orientation of the hydroperoxide toward the γ-position by an indirect effect, e.g. a biased polarity in the distal site. This consideration is compatible with the fact that the X-ray crystal structure of L29H/H64L Mb, which exclusively affords the γ-isomer, shows almost the same hindrance around the α-*meso*-position to wild-type Mb which leaves the α-*meso*-position still accessible. The induced polarity of heme environment by introduction of a distal His could explain the observation that L29H/H64L Mb yielded the γ-isomer more than F43H/H64L and I107H/H64L Mb, because L29H/H64L Mb bears an unusually polar heme environment in our mutants.

When we focus on the formation of the significant amount of the β-isomer from F43H/H64L Mb in which the distal His is located near the β-*meso*-position, an additional factor must be considered for the regioselectivity: altered orientation of the hydroperoxide from the α- and γ-*meso* positions to the β-*meso* position could be caused by the hydrogen bonding with His-43 to attack the β-*meso*-position. However, comparable formation of the β-isomer to the α- and γ-isomer indicates that the hydrogen bonding is not the sole factor for the regioselectivity.

The basis for the regiospecificity of HO is not known, but the regiochemistry of the coupled oxidation of the heme of wild-type Mb and Hb has led to the proposal that the reaction regiospecificity is controlled by steric orientation of the bound oxygen. That no Mb mutants in this study oxidize the δ-*meso*-position where is largely covered with Val-68 while the other *meso*-positions were oxidized also suggests a steric effect being a significant factor of the regioselectivity in heme degradation. On the contrary to this, it has been reported that an electronic effect of the porphyrin ligand rather than steric effect in the HO regulates the regioselectivity.[4] ^{1}H-NMR of HO[30] showed a similar spectrum to that of a synthetic iron porphyrin with an electron-donating substituent at α-*meso*-position,[31] also suggesting the electronic control. As discussed above, the regioselectivity of the coupled oxidation of L29H/H64L Mb, in which the distal His is located at the position far from the heme iron, is almost perfectly regulated by the position of the distal His. Moreover, that the coupled oxidation of F43H/H64L Mb afforded significant amount of the β-isomer suggests the hydrogen-bonding is also a potent factor for regioselectivity because the distance of ~ 5.4 Å between the heme iron and the N_ε atom of His-43 is suitable to form the hydrogen bonding. Thus, we suggest that the location of a distal catalytic residue may be also an important factor to define the regioselectivity of HO as well as other factors proposed.

Reactivity. Coupled oxidation of the mutants employed in this study showed various reaction profiles. While the addition of excess ascorbate to wild-type Mb results in a slow conversion of metMb to oxyMb with subsequent slow decay to the Mb-biliverdin complex, heme of L29H/H64L Mb is efficiently degraded without any intermediate. The reactions of F43H/H64L and I107H/H64L Mbs show rapid conversion of the metMbs to the oxyMbs followed by the heme degradation with concomitant formation of the CO-Mbs. Rapid formation of the oxyMbs is due to the higher reduction potentials of Fe^{3+}/Fe^{2+} couple compared with that of wild-type Mb. In the initial stage of the coupled oxidation of H64L Mb, distinct accumulation of the oxy form was not observed due to rapid autooxidation.

While kinetics of the coupled oxidation of the ferric complex of wild-type Mb could be analyzed by fitting to a sum of two single-exponential processes with the rate constants of 3.0×10^{-2} and 5.1×10^{-3} min^{-1} based on absorbance change at 408 nm, the heme degradation from the oxy complex of wild-type Mb is described as a single-exponential process (k= 3.2×10^{-3}

min^{-1}). Therefore, the rate constants obtained from the coupled oxidation of oxyMb correspond to the α-*meso*-hydroxyheme formation followed by rapid degradation leading to the Fe^{3+}-biliverdin•Mb complex. The kinetics of the coupled oxidation of the oxy complexes of F43H/H64L and I107H/H64L Mbs could be described as a sum of two single-exponential processes with 4.5×10^{-2} and 3.8×10^{-3}, and 7.0×10^{-2} and 7.0×10^{-3} min^{-1}, respectively. According to the discussion by Hildebrand et al,[18] these two kinetically detectable processes may correspond to the formation of verdoheme from heme *via meso*-hydroxyheme and the following conversion to biliverdin. A greater reactivity of the oxy forms of F43H/H64L and I107H/H64L Mbs to Mb-biliverdins than wild-type Mb could be caused by the elimination of very tight hydrogen bonding of the distal His-64 with the oxygen bound to the heme.

In the coupled oxidation of the metMbs, L29H/H64L Mb was degraded most rapidly without forming any observable intermediates. Certainly, the elimination of His-64 should be one of the reasons. A recent study of the coupled oxidation of heme by using an active site variant of Mb (V67A/V68S) resulted in enhancement of the coupled oxidation rates with 1.1×10^{-1} and 5.3×10^{-3} min^{-1} while wild-type horse Mb gives 1.6×10^{-2} and 1.7×10^{-3} min^{-1}.[18] The V67A/V68S Mb showed a considerably lower reduction potential of Fe^{3+}/Fe^{2+} couple (-23 mV) than that of 61 mV determined for wild-type Mb,[18] suggesting that the active site of the mutant is more polar than that of the wild-type Mb.[25] Such an environment is known to enhance autooxidation and discourage CO binding to the heme iron, and similar considerations rationalize the higher autooxidation rate of L29H/H64L Mb and no CO-inhibition during the coupled oxidation of L29H/H64L Mb. In fact, the reduction potential of the L29H/H64L mutant is quite low compared to the other mutants (Table 4). A polar active site is also suggested for HO because its active site is exposed to solvent more than that of Mb.[30] More importantly, HO shows low reduction potential of -76 mV.[32] Therefore, we suggest that a polar active site could also play a crucial role in the heme degradation, possibly in the heterolytic O-O bond cleavage on the heme iron due to the localization in π* orbital of the O-O bond.

Conclusion

We have shown that the introduction of the distal His to H64L Mb affects the regiospecificity in the Fe^{3+}-biliverdin formation, even though His-29 and His-107 are too far to make direct interaction with hydroperoxide bound to the heme through the hydrogen bonding. The results are indicative of the roles of the His in the mutants to allow rotation of the hydroperoxide bound to the heme iron and to enhance the γ-selectivity. More importantly, these effects can almost completely regulate the regioselectivity for L29H/H64L Mb, while the regioselectivity for the other mutants are partly controlled. In addition, we have proposed the hydrogen bonding between the His-43 and the hydroperoxide being responsible for the β-selectivity.

References

(1) (a) Tenhunen, R.; Marver, H. S.; Schmid, R. J. *Proc. Natl. Acad. Sci. U.S.A.* **1968**, *61*, 748. (b) Tenhunen, R.; Marver, H. S.; Schmid, R. *J. Biol. Chem.* **1969**, *244*, 6388-6394.

(2) Yoshida, T.; Kikuchi, G. *J. Biol. Chem.* **1978**, *253*, 4224-4229.

(3) Wilks, A.; Torpey, J.; Ortiz de Montellano, P. R. *J. Biol. Chem.* **1994**, *269*, 29553-29556. Noguchi, M.; Yoshida, T.; Kikuchi, G. *J. BioChem. (Tokyo)* **1983**, *93*, 1027-1036.

(4) (a) Torpey, J.; Lee, A. D.; Smith, K. M.; Ortiz de Montellano, P. R. *J. Am. Chem. Soc.* **1996**, *118*, 9172-9173. (b) Torpey, J.; Ortiz de Montellano, P. R. *J. Biol. Chem.* **1996**, *271*, 26067-26073. (c) Torpey, J.; Ortiz de Montellano, P. R. *J. Biol. Chem.* **1997**, *272*, 22008-22014.

(5) Takahashi, S.; Ishikawa, K.; Takeuchi, N.; Ikeda-Saito, M.; Yoshida, T.; Rousseau, D. L. *J. Am. Chem. Soc.* **1995**, *117*, 6002-6006.

(6) private communication with H. Fujii et al.

(7) (a) Takahashi, S.; Wang, J.; Rousseau, D. L.; Ishikawa, K.; Yoshida, T.; Takeuchi, N.; Ikeda-Saito, M. *Biochemistry* **1994**, *33*, 5531-5538. (b) Sun, J.; Wilks, A.; Ortiz de Montellano, P. R.; Loehr, T. M. *Biochemistry* **1993**, *32*, 14151-14157.

(8) O'Carra, P.; Colleran, E. *FEBS Lett.* **1969**, *5*, 295-298.

(9) Ozaki, S.; Matsui, T.; Watanabe, Y. *J. Am. Chem. Soc.* **1996**, *118*, 9784-9785.

(10) Ozaki, S.; Matsui, T.; Watanabe, Y. *J. Am. Chem. Soc.* **1997**, *119*, 6666-6667.

(11) Lemberg, R. *Rev. Pure. Appl. Chem.* **1956**, *6*, 1-23.
(12) Murakami, T.; Morishima, I.; Matsui, T.; Ozaki, S.; Watanabe, Y. *Chem. Commun.* in press.
(13) Springer, B. A.; Egeberg, K. D.; Sliger, S. G.; Rohlfs, R. J.; Mathews, A. J.; Olson, J. S. *J. Biol. Chem.* **1989**, *264*, 3057-3060.
(14) Makino, R.; Uno, T.; Sakaguchi; Ishimura, Y. *Oxygenase and Oxygen Metabolism*; Makino, R.; Uno, T.; Sakaguchi; Ishimura, Y., Ed.; Academic Press: New York, 1982, pp 467-477.
(15) Brown, S. B.; Docherty, J. C. *Biochem. J.* **1978**, *173*, 985-987.
(16) Yoshida, T.; Ishikawa, K.; Sato, M. *Eur. J. Biochem.* **1991**, *199*, 729-733.
(17) Hirota, K.; Yamamoto, S.; Itano, H. A. *Biochem. J.* **1985**, *229*, 477-483.
(18) Hildebrand, D. P.; Tang, H.-l.; Luo, Y.; Hunter, C. L.; Smith, M.; Brayer, G. D.; Mauk, A. G. *J. Am. Chem. Soc.* **1996**, *118*, 12909-12915.
(19) Yoshida, T.; Kikuchi, G. *J. Biol. Chem.* **1978**, *253*, 4230-4236.
(20) (a) Yoshida, T.; Noguchi, M. *J. BioChem.* **1980**, *88*, 557-563. (b) Yoshida, T.; Noguchi, M.; Kikuchi, G. *J. Biol. Chem.* **1982**, *257*, 9345-9348.
(21) Schaefer, W. H.; Harris, T. M.; Guengerich, F. P. *Biochemistry* **1985**, *24*, 3254-3263.
(22) Yoshida, T.; Noguchi, M.; Kikuchi, G. *J. Biol. Chem.* **1980**, *255*, 4418-4420.
(23) Quillin, M. L.; Arduini, R. M.; Olson, J. S.; Phillips Jr, G. N. *J. Mol. Biol.* **1993**, *234*, 140-155.
(24) Varadarajan, R.; Zewert, T. E.; Gray, H. B.; Boxer, S. G. *Science* **1989**, *243*, 69-72.
(25) Dawson, J. H. *Science* **1988**, *240*, 433-439.
(26) Li, T.; Quillin, M. L.; Phillips Jr, G. N.; Olson, J. S. *Biochemistry* **1994**, *33*, 1433-1446.
(27) Brantley, J., R. E.; Smerdon, S. J.; Wilkinson, A. J.; Singleton, E. W.; Olson, J. S. *J. Biol. Chem.* **1993**, *268*, 6995-7010.
(28) Brown, S. B.; Chabot, A. A.; Enderby, E. A.; North, A. C. T. *Nature* **1981**, *289*, 93-95.
(29) Discover was obtained from Molecular Simulations Inc.
(30) Hernández, G.; Wilks, A.; Paolesse, R.; Smith, K. M.; Ortiz de Montellano, P. R.; La Mar, G. N. *Biochemistry* **1994**, *33*, 6631-6641.
(31) Tan, H.; Simonis, U.; Shokhirev, N. V.; Walker, F. A. *J. Am. Chem. Soc.* **1994**, *116*, 5784-5790.

(32) Omata, Y.; Noguchi, M. *A Spectroscopic Study on the Intermediates of Heme Degradation by Heme Oxygenase*; Ishimura, Y.; Shimada, H.; Suematsu, M., Ed.; Springer: Keio University, 1998, pp 322-327.

CHAPTER 2.

Alteration of Sperm Whale Myoglobin Distal Site Mimicking Heme Oxygenase

Abstract

Sperm whale myoglobin (Mb) mutants have been constructed by the double substitution of amino acid residues in the distal site to introduce an ionizable amino acid, Asp or His, near the α-*meso*-position with the concomitant substitution of His-64 with Leu (I107D/H64L and I107H/H64L) to mimic the distal site structure of the heme-heme oxygenase (HO) complex. The Asp and His residues show opposite effects on the electronic absorption spectra of various oxidation and ligation states, and more importantly those spectra of I107D/H64L Mb are very similar to spectra of heme-HO. The reduction potential of I107D/H64L metMb is lower (-35 mV) than wild-type metMb (52 mV) but very similar to heme-HO (-76mV). The NMR spectrum of I107D/H64L MbCN shows a similar contact shift pattern for the heme methyl proton resonances to that for wild-type MbCN, while the chemical shifts of the 2-vinyl resonances of I107D/H64L MbCN are perturbed by lowering the solution pH as observed for heme-HO, suggesting protonation of a carboxylate side chain could be responsible for the chemical shifts of 2-vinyl and 3-CH_3 of heme-HO. On the other hand, I107D/H64L Mb shows poor reactivity of the coupled oxidation, which is rationalized by the slow reduction of I107D/H64L metMb and possibly an uncoupling of the reaction to release H_2O_2 from the heme iron instead of the *meso*-hydroxylation.

Introduction

Heme oxygenase (HO) catalyzes NADPH/cytochrome P-450 reductase dependent metabolism of heme to biliverdin by utilizing molecular oxygen.[1] The catalytic cycle of HO begins with the binding of heme to form a heme-enzyme complex (heme-HO).[2] The first electron from the reductase reduces the ferric heme to a ferrous state followed by O_2 uptake to form a metastable O_2-bound form.[3] The second electron donation to the O_2-bound form initiates oxygenase reactions to afford biliverdin *through* a sequence that involves α-*meso*-hydroxylation of the heme, aerobic fragmentation of the α-*meso*-hydroxyheme to verdoheme, and oxidative cleavage of verdoheme to biliverdin. Thus, the heme serves as the prosthetic group and substrate.[4]

Recent Raman and ESR studies on heme-HO[5] have provided evidence for neutral proximal histidine and suggested that the O_2 activation process could be modulated by distal residues.[5b] Myoglobin (Mb), which shares neutral axial His with heme-HO, has been employed to mimic the heme degradation catalyzed by HO,[6] and it was suggested that the location of distal His is significantly effective on the regioselectivity of the coupled oxidation.[7]

The three dimensional structure of heme-HO has not been resolved yet, however, several amino acid residues around the distal site of heme-HO have been suggested by various spectroscopic analyses. A water molecule is bound to the ferric heme at neutral pH, and shows the acid/base transition at pK_a of 7.6,[5a] which is considered to be linked to the ionization of a distal amino acid residue that forms a hydrogen bond with the heme-bound water.[8] Further, unusual pattern of spin densities on the heme periphery of CN-bound heme-HO has been reported.[9] The pattern of hemin contact shifts suggests that the spin density is larger at the positions of 3 (methyl) and 2 (vinyl) near the α-*meso*-carbon of heme-HO and the results were explained by selective electron spin donation of a carboxylate side chain (either Asp or Glu) to the α-*meso* and/or γ-*meso*-carbon. Furthermore, this type of perturbation was suggested to control the reactivity and regioselectivity of the enzyme reaction.[9]

According to the similarity of Mb to heme-HO, active site mutants of Mb may provide structural information of heme-HO. As illustrated in Figure 1, the heme iron of Mb is surrounded by Ile-107, Phe-43, His-64, and Val-68 near the α, β, γ, and δ-*meso*-positions, respectively. Therefore, a substitution of Ile-107 of Mb could perturb the electric field around the α-*meso*-carbon. In this paper, we focus on effects of a carboxylate side chain

of Asp near the α-*meso*-position on the active site structure of Mb and the reactivity in the heme degradation to mimic HO.

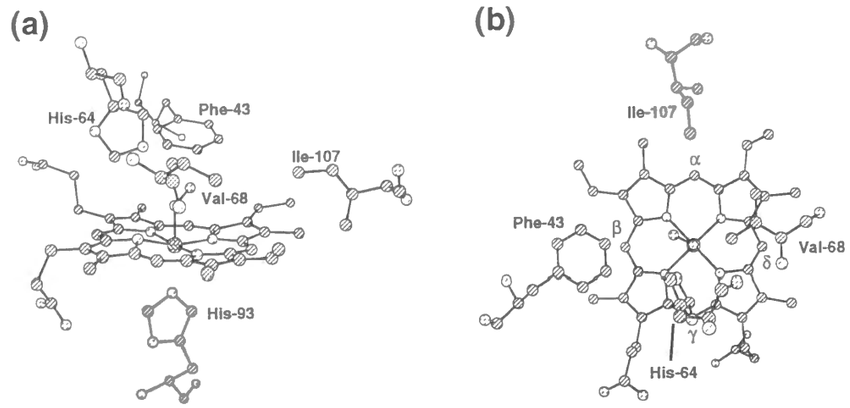

Figure 1. Heme environmental structure of myoglobin. Heme and some selected residues are shown. (a) Side view. (b) Top view.

Experimental Section

Sodium cyanide, sodium dithionite, and sodium ascorbate were purchased from Wako Pure Chemical Industries, Ltd.

Site-Directed Mutagenesis, Preparation, and Purification. Site-directed mutagenesis of Phe-43, Leu-29, and Ile-107 in recombinant sperm whale myoglobin was carried out by using the polymerase chain reaction (PCR) according to methods previously reported.[10]

The His-64→Leu replacement was achieved by cassette mutagenesis. The cassette including the desired His-64 substitution and a new silent *Hpa*I restriction site was inserted between the *Bgl*II and *Hpa*I sites. The expression and purification of the mutants were performed according to methods described.[10]

Spectroscopy. All spectroscopic measurements were performed in 50 mM sodium phosphate buffer (pH 7.0) unless otherwise stated. Electronic absorption spectra were recorded on a Perkin Elmer Lambda 19 spectrometer and the concentration of samples was adjusted at 5 μM. The MbCNs were prepared by the addition of 3 equiv of NaCN to the metMbs. Wild-type oxyMb was prepared by the sodium dithionite reduction of the

ferric complex and passing the reduced complex through a small G-25 column eluted with air-saturated buffer. Autooxidation rates were evaluated by observing the absorption spectra from 430 to 390 nm. The intensity of the Soret band maxima of the oxyMbs was used for the calculation. Coupled oxidation assay was performed in a buffer solution containing ascorbate (1 mM) at 37°C. Spectra were recorded (300-850 nm) for 5 h. Autooxidation rates of wild-type and mutant oxyMbs were measured at 37°C using ca. 5 μM protein. The mutants were reduced with excess sodium dithionite, and loaded on a small Sephadex G-25 (Pharmacia) column and eluted with CO-saturated 50 mM sodium phosphate buffer, pH 7.0. The resultant CO-Mbs without any reductant were converted to the oxyMbs by irradiation of white lamp under O_2 atmosphere at 0°C.

Hyperfine-shifted ^{1}H-NMR spectra were recorded at 23°C on a Brucker DRX 500 spectrometer equipped with a SGI Indy workstation. Chemical shifts were referenced to TMS, and the concentration of the samples was ca. 0.5 mM in 0.2 M NaCl (90 : 10 mixture of ^1H_2O and ^2H_2O). The MbCNs were prepared by adding 3 equiv of NaCN and after centrifuging supernatant was adjusted to desired pH by 0.1 M HCl and/or NaOH. pH of the solutions was measured before and after each run, using Beckman Model 3550 pH meter equipped with HORIBA 6029-10T electrode. The pH readings were uncorrected for the isotope effect, and hence referred to as 'pH'.

Raman scattering was excited at 406.7 nm by a Kr^+ ion laser (Spectra Physics, Model 2016), and detected by a charge-coupled device (CCD) (Astromed spectral) attached to a single monochromator (Ritsu). The slit width was 6 cm^{-1} except for I107D/H64L Mb (12 cm^{-1}). Therefore, the Raman lines in trace B in Figure 7 was slightly broad, which might affect the frequency of the lines. RR spectra were measured at room temperature with a spinning quart cell. Raman shifts were calibrated to an accuracy of 1 cm^{-1} with potassium ferricyanide and indene.

Electrochemistry. The reduction potential of Fe^{3+}/Fe^{2+} couple was measured for samples degassed by Ar gas and further treated by the glucose (5 mM), glucose oxidase, and catalase system.[11] The metMbs were then reduced to the ferrous states by the irradiation of a white lamp, in the presence of EDTA (1 mM). Methylene blue, thionine, and phenosafranine were used as mediators.

Results and Discussion

Electronic Absorption Spectroscopy. Figure 2 shows electronic absorption spectra of oxyMbs and CO-Mbs prepared by CO-bubbling of the oxyMbs at room temperature. The wavelength at the absorption maxima for various oxidation and ligation states of Mbs are compiled in Table 1. Inspection of Table 1 shows that the Asp and His residues at position 107 in Mb affect the spectra in different manner except for the spectra of the

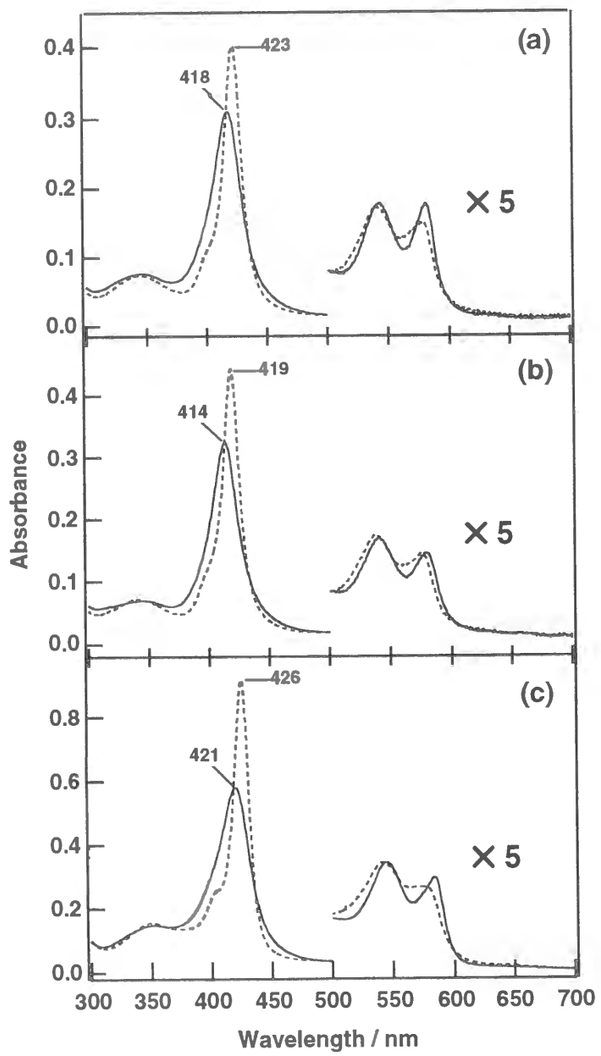

Figure 2. Electronic absorption spectra of oxy-ferrous Mbs (——) and CO-ferrous Mbs (- - - - -).

Table 1. Wavelength of Absorption Maxima in UV-vis Spectra of Some Derivatives for Mbs and heme-HO complex at pH 7.0

	Proteins	Soret	visible
Fe^{III}	wild-type Mb	409	502 634
	I107D/H64L	406	499 622
	I107H/H64L	396	507
	heme-HO	406	499 629
$Fe^{III}CN$	wild-type Mb	423	544
	I107D/H64L	419	538
	I107H/H64L	424	542
	heme-HO	418	536
$Fe^{II}O_2$	wild-type Mb	418	546 584
	I107D/H64L	414	542 580
	I107H/H64L	421	546 584
	heme-HO	412	540 575
$Fe^{II}CO$	wild-type Mb	423	541 579
	I107D/H64L	419	539 576
	I107H/H64L	426	543 576
	heme-HO	421	539 569

met forms. The Soret bands of the cyanomet, oxy, and CO-complexes of I107D/H64L Mb are blue-shifted relative to those of wild-type Mb, while those of I107H/H64L Mb are red-shifted. The blue-shifted Soret band of I107H/H64L metMb is due to a five-coordinate state. It should be noted that I107D/H64L Mb shows almost identical spectroscopic features of heme-HO.

The autooxidation of wild-type, I107D/H64L, and I107H/H64L Mbs has been examined at 25°C under air. The rate constants are calculated on the basis of absorbance change of the Soret bands of the oxyMbs (Table 2). I107D/H64L oxyMb is autooxidized faster only by ~ 4-fold than wild-type oxyMb, even though there is no proton donor to make hydrogen bonding in the distal site to stabilize the oxy form. Introduction of negative charge at 43- or 67-position is known to increase dramatically the rate of autooxidation while positive charge near the heme iron, i.e. position 43 or 67, inhibits the autooxidation.[12] Though I107H/H64L oxyMb is more stable than H64L oxyMb (1.7×10^{-1} min^{-1}),[14] our observations are inconsistent with the previous results.[12] We are not able to rationalize the instability of I107H/H64L oxyMb, however, a carboxylate near the α-*meso*-position apparently stabilizes the oxy form compared with the stability of H64L oxyMb. More importantly, the stability of I107D/H64L oxyMb is similar to that of O_2-bound heme-HO.[3]

Table 2. Autooxidation rates at 37°C and reduction potentials of Fe^{2+}/Fe^{3+} couple at 25°C

Proteins	first order rate [min^{-1}]	E_0 [mV]
wild-type	3.0×10^{-3}	52
I107D/H64L	1.1×10^{-2}	-35
I107H/H64L	7.4×10^{-2}	60
heme-HO	3.2×10^{-2}	-76[a]

[a] Omata & Noguchi, 1998.

Reduction Potential of Fe^{3+}/Fe^{2+} Couple. I107D/H64L Mb shows the reduction potential at -35 mV, while that of I107H/H64L Mb (60 mV) is similar to wild-type Mb (Table 2). The reduction potential of heme-HO complex has been determined to be -76 mV.[14] Important factors that affect the reduction potential of heme proteins include (i) nature of axial ligand(s) and the porphyrin ring,[15] (ii) electrostatic interaction of the heme iron with charged groups,[16] and (iii) conformational changes associated with reduction. The first factor does not explain the low

reduction potential of heme-HO because heme-HO and Mb share a neutral proximal histidine ligand[5] and protoheme IX. On the other hand, the second factor is likely conceivable for the low reduction potential of heme-HO, because it is observed that substitution of Ile-107 in the distal site of Mb by potentially charged and polar residues, Asp, leads to lowering the reduction potential to -35 mV. Hildebrand et al. also observed such a low reduction potential of -23 mV (pH 7.0, 25°C) for a Val67Ala/Val68Ser mutant of horse heart Mb.[17] In addition, lower reduction potential is also expected for polar heme environment. Recent NMR studies of heme-HO complex suggest the presence of a carboxylate near the α-*meso*-position as well as a polar distal atmosphere.[9] The introduction of Asp to the distal site of Mb successfully changed its reduction potential similar to that of heme HO.

Resonance Raman spectroscopy. Resonance Raman spectra of CO-Mbs have been measured because the stretching vibration of the FeCO unit is known to be a sensitive probe of the distal pocket structure (Figure 3).[18] Three isotope sensitive lines are assigned to Fe-CO stretching, Fe-C-O bending, and C-O stretching modes by using $^{13}C^{18}O$ and $^{12}C^{16}O$ derivatives (Table 3). The ν_{CO} line of I107D/H64L CO-Mb is observed at 1941 cm^{-1}, while that of I107H/H64L CO-Mb appears at 1960 cm^{-1}. Takahashi et al. reported the upshifted ν_{CO} line (1958 cm^{-1}) for the CO-inhibited heme-HO relative to that for wild-type CO-Mb (1945 cm^{-1}).[5b] Thus, the introduction of Asp at position 107 in Mb failed to mimic the FeCO structure of heme HO while electronic spectra of those proteins are very similar.

Positively charged amino acid residues near the proximal ligand atom usually promote the formation of resonance structures with lower C-O and higher Fe-C bond order. On the contrary to this, removal of proton donors or the addition of partial negative charge in the distal pocket has been recognized to have the opposite effect on the C-O and Fe-C bond order.[19] For example, the upshift of the ν_{CO} line for H64L Mb (1965 cm^{-1})[19] and for V68D Mb (1951 and 1972 cm^{-1})[20] were reported. However, Decatur et al. observed, that the CO complex of V68E Mb showed a down-shifted ν_{CO} line at 1937 cm^{-1}, while the other properties sensitive to local electrostatic interaction of V68E Mb such as blue-shifted absorption maxima of LMCT band of the aquometMb (620 nm) and Q_1 band of the CO-Mb (576 nm), and low reduction potential (-136.8 mV) were essentially the same as those of V68D Mb (622 nm, 574 nm, and -132.1 mV, respectively).[20]

They attributed the opposite effect of Asp and Glu at the position of 68 in Mb on the ν_{CO} to different orientation of dipole induced by the carboxylate, i.e. the negative end toward or away from the heme iron in V68D or V68E Mb, respectively. Since I107D/H64L Mb also exhibited the blue-shifted absorption maxima of LMCT band of the aquometMb (622 cm^{-1}) and Q_1 band of the CO-Mb (576 cm^{-1}), and the low reduction potential (-35 mV), the down shift of the ν_{CO} line for I107D/H64L CO-Mb could be explained by similar consideration. Therefore, if either Asp or Glu is in the distal site of heme-HO complex, the upshifted ν_{CO} line for the CO-inhibited heme-HO complex would be due to the negative end being directed to the heme iron.

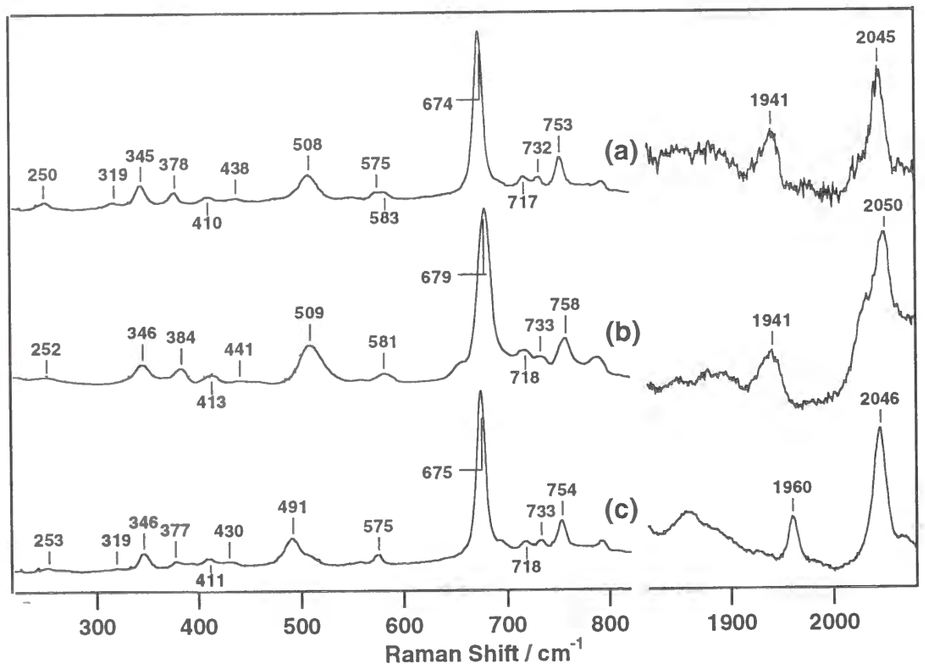

Figure 3. Resonance Raman spectra of the Fe-CO stretching mode and the C-O stretching mode regions of the CO-ferrous Mbs: (a) wild-type, (b) I107D/H64L, (c) I107H/H64L Mbs. The excitation wavelength was 406.7 nm with a power of about 1 mW.

While the CO-inhibited heme-HO complex shows an extremely broad ν_{CO} line,[5b] modest line-broadening of ν_{CO} line of I107D/H64L CO-Mb is similar to that for wild-type Mb (Figure 3c). Line-broadening of the ν_{CO}

line for Mb mutants suggests that the distal pocket cavity is made more accessible to solvent.[18] Exposure of the distal site has been also suggested for heme-HO by the 2D NMR spectra showing relatively few and weak cross peaks[9] when compared to other low-spin ferric heme proteins, such as MbCN[21] and CN-bound heme peroxidase.[22]

Table 3. Comparison of the Low- and High-Frequency Modes of CO-Ferrous Mbs

	Fe-CO stretch	Fe-C-O bent	C-O stretch
wild-type[a]	508	575	1941
I107D/H64L	509	581	1941
I107H/H64L[a]	491	575	1960
heme-HO complex[b]	503	576	1958

[a] Murakami et al. (1997) [b] Takahashi et al. (1994)

^{1}H-NMR Spectroscopy. Figure 4 shows ^{1}H-NMR spectra of wild-type, I107D/H64L, and I107H/H64L MbCNs in 90% ^1H_2O/10% ^2H_2O at pH 6.1, 23°C. The resonances in Figure 4b and 4c are designated to D_i and H_i, respectively, where "i" is the peak labels in Figure 4. Based on separate measurements in ^2H_2O, the resonances D_2, and H_2 and H_6 in Figure 4b and 4c, respectively, are assigned to exchangeable protons, which would be the proximal histidine N_1H and peptide NH.[23] The three resonances assignable to the heme methyl groups are observed between 10-30 ppm for I107D/H64L (D_1, D_3, and D_6) and I107H/H64L MbCNs (H_1, H_3, and H_8). Figure 5 shows pH effect on the chemical shifts of the hyperfine-shifted resonance of the MbCNs. The peak labels in Figure 5 correspond to those in Figure 4. As pH is lowered, the resonance D_1 is largely upshifted, and the resonance D_3 shows a slight up-downshift while the resonance D_6 shows a downshift (Figure 5b). As shown in Figure 5a, the pH-dependent chemical shifts of the 5, 1, and 8-CH_3 resonances of wild-type MbCN (peak label 1, 3, and 7, respectively) essentially shows the same profile as the D_1, D_3, and D_6 resonances of I107D/H64L MbCN, respectively. These allow us to assign the resonances D_1, D_3, and D_6 in Figure 5b to the 5, 1, and 8-CH_3, respectively. We could suggest at the same time that the negative charge

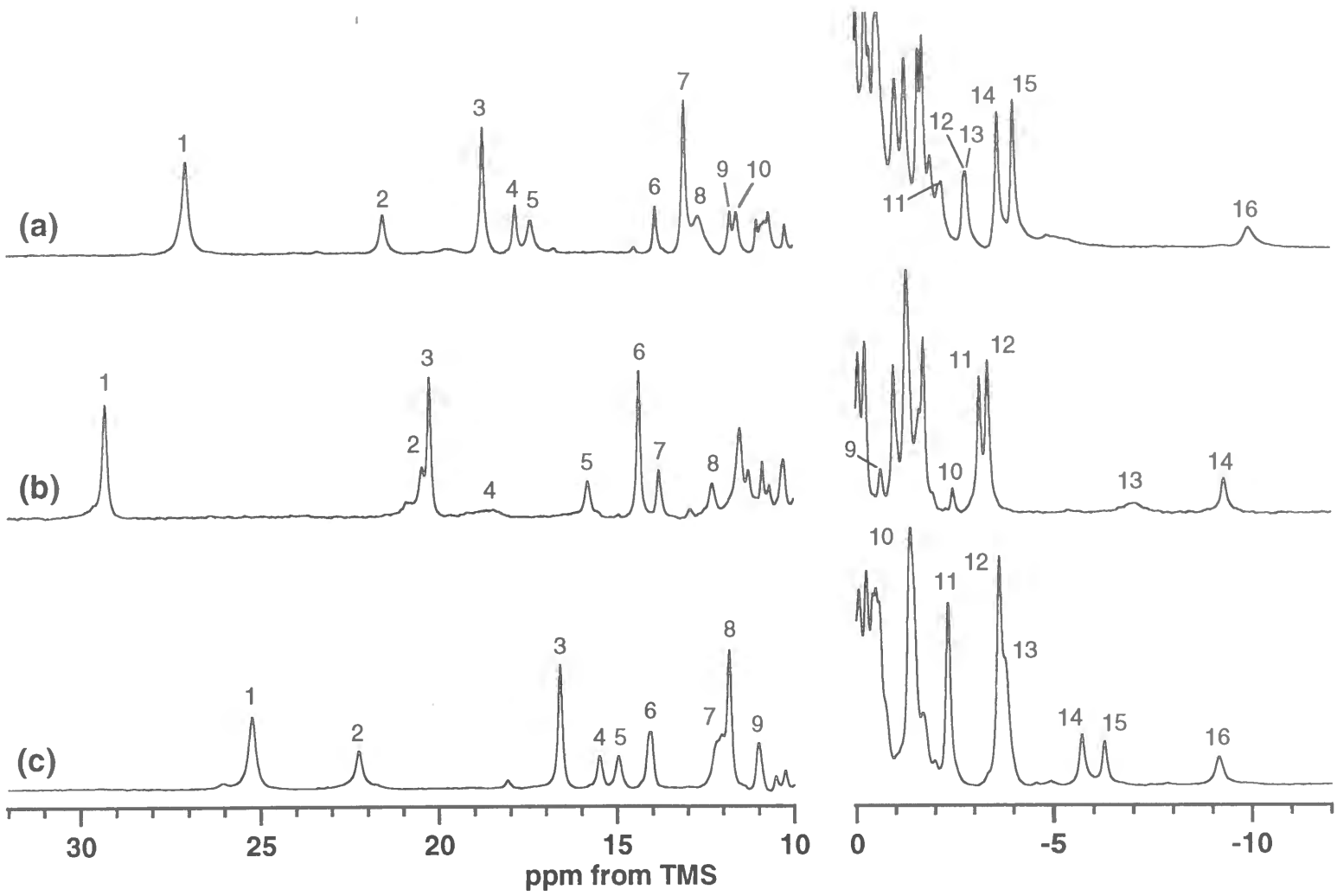

Figure 4. 500-MHz ^{1}H-NMR spectra of (a) wild-type, (b) I107D/H64L and (c) I107H/H64L MbCNs (0.5 mM) in 90%$^{1}H_2O$/10%$^{2}H2_2O$ (pH 6.1) at 23 °C.

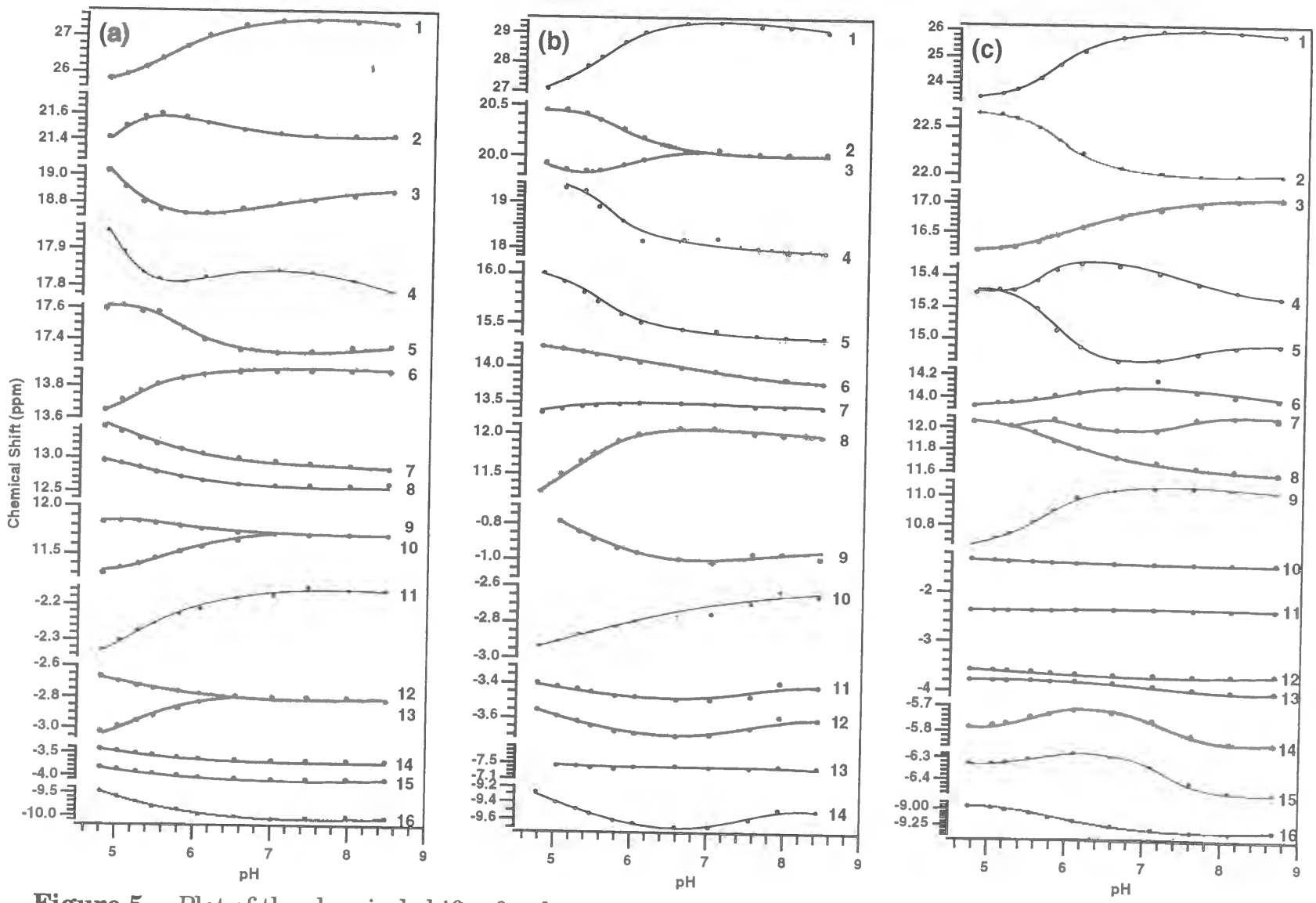

Figure 5. Plot of the chemical shifts for the resolved low-field resonances of (a) wild-type, I107D/H64L, and (b) I107H/H64L MbCNs, as a function of solution pH. While the pH profiles are completely reversible, pH instabilities at acidic pH results in significant uncertainties in pH values.

near the α-*meso*-position did not cause a drastic change of the pattern of the unpaired spin distribution on the heme periphery in the highest bonding orbital. Based on these assignments, the resonances H_1, H_3, and H_8 of I107D/H64L MbCN could be assigned to the 5, 1, and 8-CH_3, respectively, while the relatively large pH dependence of the signal H_3 is not rationalized at this moment.

The pK_a values for the methyl protons of I107D/H64L MbCN are smaller than those of I107H/H64L MbCN (Table 4). This result may be related to protonation of the side chain of the Asp and His residue, while the π-π interaction between the imidazole of the His-97 and the heme is mainly responsible for pH dependence of the chemical shifts of the sperm whale MbCN under pH 6.5.[24]

Table 4. pK_a Values for the Traces in Figure 5

wild-type			I107D/H64L		I107H/H64L	
peak label	assignment	pK_a	*i* (for D_i)	pK_a	*i* (for H_i)	pK_a
1	5-CH_3	5.6	1	5.4	1	5.8
2	His93 $N_\delta H$	ND	2	5.9	2	5.8
3	1-CH_3	ND	3	ND	3	6.1
4	2-H_α	ND	4	5.4	4	5.8 / 7.5
5	Phe43 $C_\zeta H$	5.8	5	5.4	5	5.7 / 7.7
6	His93 $N_p H$	4.8	6	5.7	6	5.8
7	8-CH_3	5.3	7	ND	7	ND
8	Phe43 $C_\varepsilon Hs$	5.4	8	5.0	8	5.9
9	His64 $C_\delta H$	ND	9	5.2	9	5.6
10	His93 $C_\beta H$	5.6	10	5.4	10	ND
11	2-H_β (*cis*)	5.3	11	5.2	11	ND
12	——	4.9	12	5.1	12	5.7
13	2-H_β (*trans*)	5.4	13	ND	13	7.1
14	Ile99 $C_\gamma H_3$	ND	14	5.0	14	5.6 / 7.3
15	Ile99 $C_\delta H_3$	ND			15	5.8 / 7.3
16	Ile99 $C_\gamma H$	5.2			16	5.8

ND, not determined.

A significant pH effect on the chemical shift is also observed for the signal D_5 (Δ 0.6 ppm) and D_{10} (Δ 0.3 ppm) in the down and up field, respectively, under pH 6.5 in Figure 5a, and for the resonances H_5, and H_{14} and H_{15} (Δ 0.1 ppm) in the down and up field, respectively, over pH 6.5 in Figure 5b. Furthermore, the traces D_5 and D_{10} show the same pK_a value of 5.4, and the traces H_5, H_{14}, and H_{15} exhibit a relatively large value (Table 4). The alternative and similar pH-dependent shifts of the resonances allow us to assign the resonances D_5 and H_5, and the resonances D_{10}, H_{14}, and H_{15} to the 2-H_α and 2-H_β, respectively.[25] The chemical shift of the 2-H_α resonance of wild-type MbCN (peak label 4) is independent of pH, and those of the 2-H_β resonances (peak label 11 and 13) are not perturbed over pH 6.5 and hardly perturbed under pH 6.5 (Δ 0.2 ppm).[25] Accordingly, we could conclude that the protonation of the Asp-107 and His-107 near the α-*meso*-position influences the chemical shift of the 2-vinyl signals, while the effects are not so strong as observed for the 2-vinyl signal of the CN-bound heme-HO complex.

Recently, Hernández et al. observed largely paramagnetically shifted signals of the 2-vinyl and 3-methyl groups of the CN-bound heme-HO complex, and more importantly, unique contact shift pattern is strongly pH dependent and is largely abolished at acidic pH.[9] Based on these features, they postulated direct electronic perturbation of hemin by the protein matrix having an anionic side chain close to the α or γ-*meso*-carbon.[9] However, our observation that the NMR spectrum of I107D/H64L MbCN exhibits the same contact shift pattern for the methyl groups as wild-type MbCN indicates that the unique contact shift pattern for the CN-bound heme-HO complex results from another mechanism, for example, a dihedral angle between the heme N_{II}-Fe-N_{IV} axis and projection of the axial His imidazole plane onto the heme,[26] because *Dolabella*[27] and *Aplysia* MbCNs[28] exhibit a similar contact shift pattern of the methyl signals to that for heme-HO.[9] On the other hand, protonation of titrating groups, Asp and His, near the α-*meso*-position in the mutant MbCNs can affect the chemical shift of the 2-vinyl protons and pH-dependence is analyzed by a simple titration curve with a pK_a value corresponding to that of the side chain. Furthermore, pH-dependent chemical shift was not observed for *Aplysia* MbCN.[27] Therefore, the result for I107D/H64L Mb directly suggests that protonation of a carboxylate side chain near the α-*meso*-position is linked to the pH-dependent chemical shift of the 2-vinyl and 3-methyl groups of the CN-bound heme-HO complex under neutral

pH, but does not essentially alter the distribution of π unpaired spin density on the heme periphery.

Monitoring of the Coupled Oxidation by Electronic Absorption Spectroscopy. The coupled oxidation of heme to Fe^{3+}-biliverdin by the aerobic addition of ascorbate has been monitored (320-800 nm) for wild-type, I107D/H64L, and I107H/H64L metMbs (Figure 6). As reported before,[17] wild-type metMb is slowly converted to oxyMb followed by the degradation to a Fe^{3+}-biliverdin•Mb complex (Figure 6a). On the basis of the absorbance changes at 409 nm, the rate constants for the oxyMb formation and its decay are 3.0×10^{-2} and 5.1×10^{-3} min^{-1}, respectively. In the case of I107H/H64L Mb, the oxy complex is formed by the addition of ascorbate in a few minutes (data not shown) and then degrades with concomitant formation of I107H/H64L CO-Mb as a result of the product (CO) inhibition. I107H/H64L CO-Mb is also degraded under the conditions (Figure 6c), due to a slow release of CO from the CO-inhibited state at 37 °C. On the other hand, only a small decrease of the Soret band of I107D/H64L metMb was observed while the reaction profile shows a relatively large decrease of the Soret band in early stage followed by very slow decay (Figure 6b). Two weak absorption maxima, which is characteristic of the oxy form, are observed in the visible region. Absorbance decay at 406 nm is fitted by two single-exponential processes, and the rate constants are calculated to be 5.9×10^{-2} and 2.8×10^{-3} min^{-1}, which correspond to the rate constants for the oxyMb formation and its decay, respectively, since the anaerobic addition of ascorbate to I107D/H64L metMb affords the deoxyferrous Mb at the rate of 7.9×10^{-2} min^{-1}. That small accumulation of the oxy form though the rate constant for the decay of the oxy form is one order of magnitude smaller than the reduction of the met-form indicates the decomposition of the oxy form to regenerate the met-form to be faster than the reduction. Though the low reduction potential of I107D/H64L metMb could explain the slow reduction of the oxyMb, that the ferric heme-HO complex with lower reduction potential of -76 mV[14] is efficiently reduced and degraded in the coupled oxidation with ascorbate is very different from I107D/H64L Mb.[29]

To understand more details of the heme degradation, we have examined the coupled oxidation started from the oxy forms of wild-type and mutant Mbs, and estimated the rate constants based on the absorbance change at an isosbestic point between the oxy and CO-Mbs (417

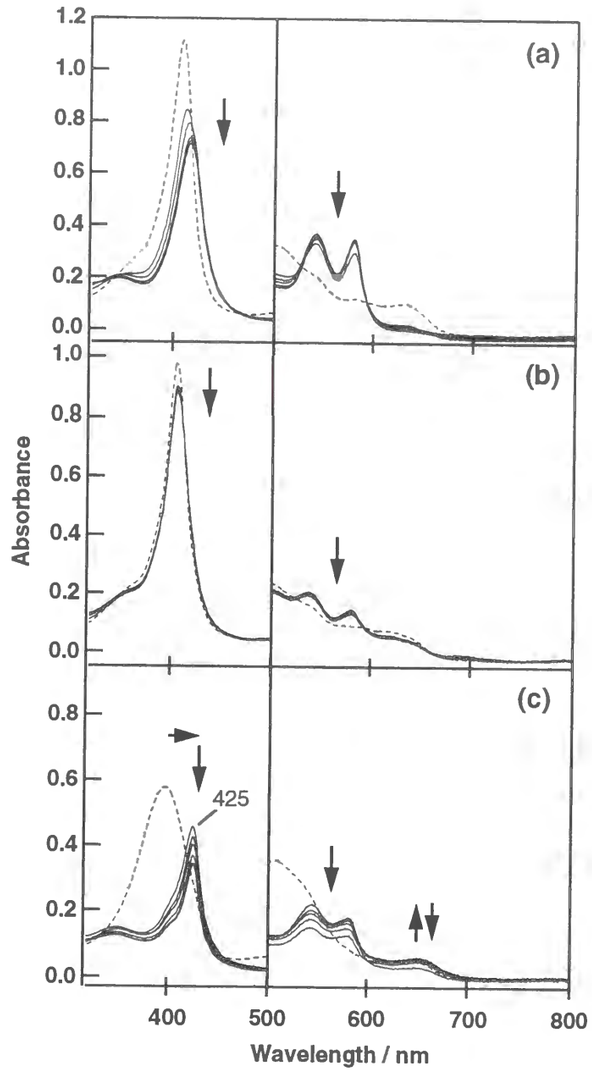

Figure 6. Electronic absorption spectral changes (320-850 nm) of metMbs (- - - - -) during coupled oxidation containing 1 mM ascorbate at 37°C: (a) wild-type, (b) I107D/H64L, and (c) I107H/H64L Mbs. The transitional spectra (——) are recorded at 1-h intervals.

nm for wild-type Mb, 414 nm for I107D/H64L Mb, and 419 nm for I107H/H64L Mb). As shown in Figure 7, the addition of ascorbate to wild-type and I107H/H64L oxyMbs causes a simple decrease of the Soret band in intensity. On the other hand, blue-shift of the Soret band to 406 nm in one hour and the subsequent slow decrease of the intensity are observed in the coupled oxidation of I107D/H64L oxyMb (Figure 7b). The spectrum of

I107D/H64L after one hour of the reaction is nearly identical with the spectrum observed an hour after the coupled oxidation of I107D/H64L metMb in the presence of ascorbate. These results also support that formation of the met form from the oxy form is much faster than the heme degradation. Faster autooxidation of I107D/H64L oxyMb than its formation from the met-form in the presence of ascorbate indicates the

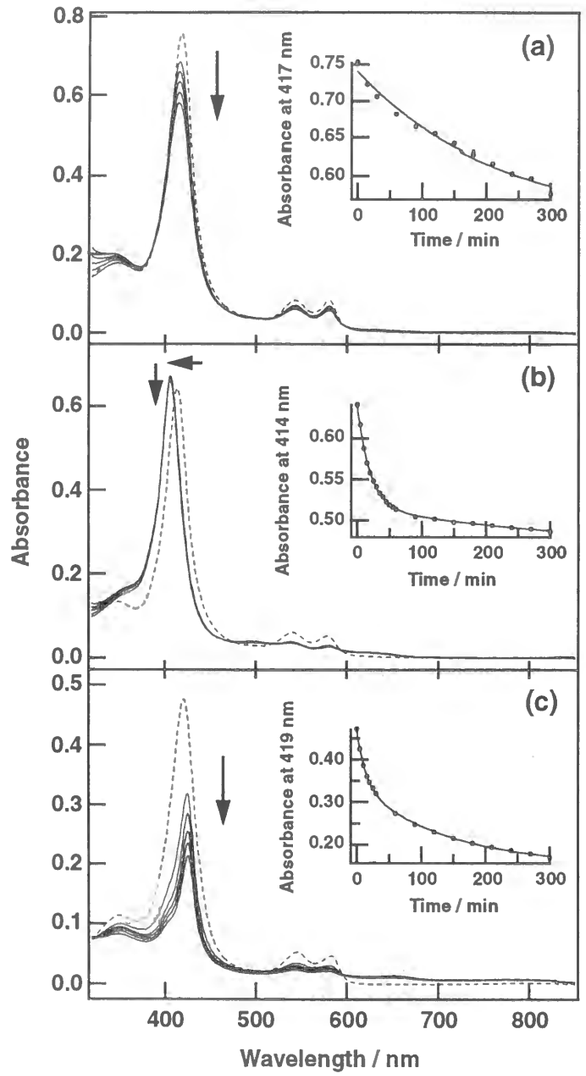

Figure 7. Electronic absorption spectral changes (320-850 nm) of oxy-ferrous Mbs (- - - - -) during coupled oxidation containing 1 mM ascorbate: (a) wild-type, (b) I107D/H64L, and (c) I107H/H64L Mbs. The transitional spectra (——) are recorded at 1-h intervals. (inset) absorbance change at the isosbestic point between the oxy- and CO-ferrous complexes.

equilibrium between the met and oxy-forms. This consideration is in good agreement with the time dependent spectral changes shown in Figures 6b and 7b, however, the autooxidation rate of I107H/H64L oxyMb (1.1×10^{-2} min^{-1}, Table 2) is smaller than the reduction rate of the met form (5.9×10^{-2} min^{-1}).

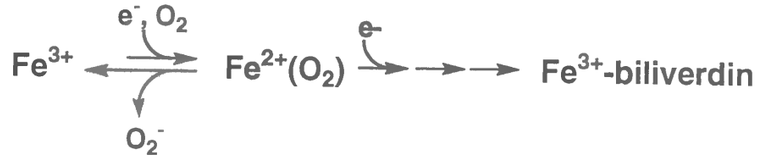

(1)

To examine whether the reduction of the met form of I107D/H64L is the rate determining or not, dithionite has been used as a reductant for the coupled oxidation of I107D/H64L oxyMb. The spectrum immediately after the addition of dithionite (0.1 mM) is identical to that obtained an hour after the coupled oxidation with ascorbate (Figure 8). These results indicate that the reproduction of the met form from the oxy form is not as simple as expected for usual autooxidation shown in eq (1). One of the possible schemes to explain these results is the involvement of the reduction of the oxy form to a peroxo-Fe(III) intermediate and the following release of peroxo anion as observed for Thr-252 mutants of P-450_{cam} (Scheme 1).[30]

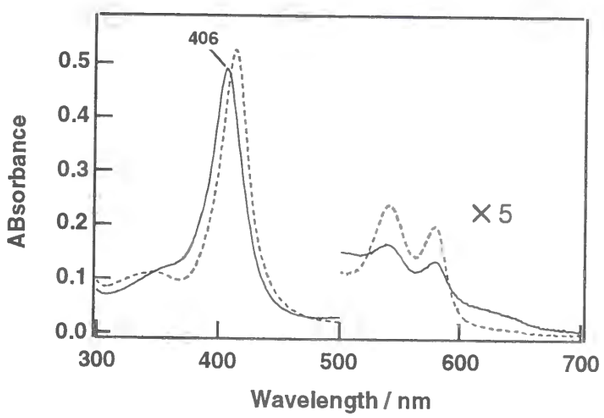

Figure 8. Electronic absorption spectra of I107D/H64L oxyMb (- - - - -) and the product immediately after the aerobic addition of dithionite (0.1 mM) to the oxyMb (——).

Scheme 1

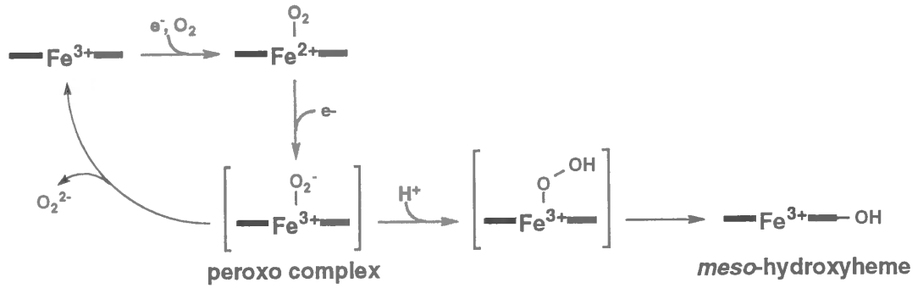

As already discussed, the appearance of the ν_{CO} of I107D/H64L CO-Mb at 1941 cm^{-1} (Table 3) is the indication of less interaction of the CO with aspartate-107 while that for the CO-inhibited heme-HO complex was observed at 1958 cm^{-1}, suggesting an anionic residue(s) interacting with the CO. The same consideration could be applicable to the NMR results providing the smaller Δ ppm of the 2-vinyl protons of I107D/H64L MbCN than that of the CN-bound heme-HO complex in the pH-titration. At the same time, very broad CO line for the CO-inhibited heme-HO complex is indicative of water molecule(s) being around the active site, and a carboxylate has been suggested to be located near the α-*meso*-position on the basis of NMR measurements.[9] Thus, the double mutation of Ile-107 to Asp as well as His-64 to Leu to mimic the distal site of heme-HO has allowed us to reproduce electronic absorption spectra, pH dependent chemical shifts of the 2-vinyl group, and low reduction potential of heme-HO. Upon the reduction of the oxy form of heme-HO and I107D/H64L Mb, putative ferric-peroxy intermediates[31] should be formed. In the case of heme-HO, water molecule, which may interact with the carboxylate to have proper position, serve as a proton donor to form hydroperoxy-ferric species to allow further heme degradation. On the other hand, Asp-107 is not able to control proton coupling and promotes the release of peroxo anion. These considerations are quite consistent with the Raman studies on the CO complexes and uncoupling system of the Thr-252 mutants of P-450_{cam} as shown in Figure 9.[30] In fact, Noguchi et al. observed that approximately 8–9 mol of dioxygen (theoretically 3 mol) and 11–12 mol of NADPH were consumed per mol of hemin lost due to an uncoupling to yield hydrogen peroxide suppressing the biliverdin formation during the HO-catalyzed heme degradation.[31]

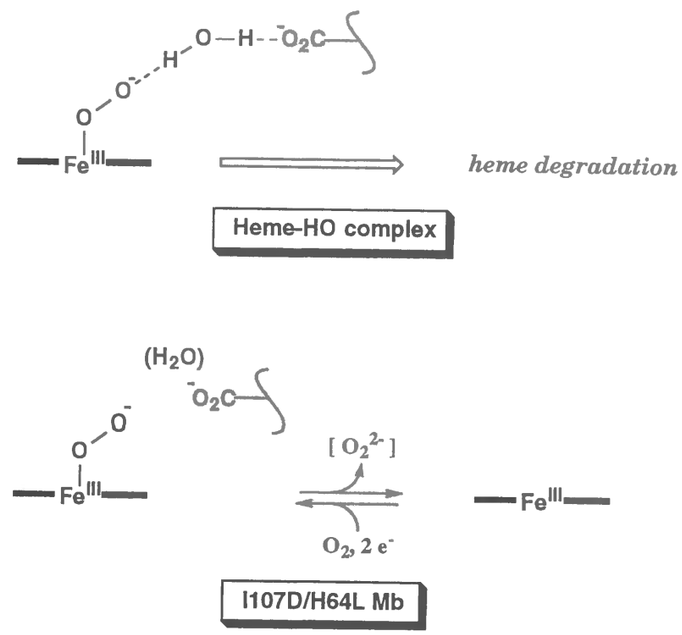

Figure 9. Schematic drawing of heme-HO complex and I107H/H64L Mb reactions.

Considering that a hydrogen bonding of a protic residue to the bound oxygen has been confirmed by ESR studies of the oxy cobalt heme-HO complex,[32] these results allow us to imagine a location of an anionic residue near the α-*meso*-position and protic residue near the heme iron in the distal site of the heme-HO complex. In this case, a biased electric field constructed by the negatively and positively charged residues could polarize the O-O bond of the O_2-bound complex, and enhance the *meso*-hydroxylation.

Conclusion

A Mb mutant bearing a negatively charged residue, Asp, in the distal site provided similar electronic absorption spectra to heme-HO of aquomet, cyanomet, oxy, and CO complexes. The Asp residue located far from the heme iron than His-64 stabilizes the oxy-form. The lower reduction potential is also observed for I107D/H64L Mb, and based on these spectroscopic properties except for the resonance Raman spectrum of the CO complex, the distal site with an anionic residue at position 107 well-

mimics those of heme-HO. Furthermore, it has been directly observed that protonation of the carboxylate side chain of Asp-107 near the α-*meso*-position affects the chemical shift of the 2-vinyl group, while it does not very much alter the distribution of π unpaired spin density on the heme periphery. However, I107D/H64L Mb shows the poor reactivity of the coupled oxidation, which is due to an uncoupling reaction to produce H_2O_2 (Scheme 1).

References

(1) (a) Tenhunen, R.; Marver, H. S.; Schmid, R. J. *Proc. Natl. Acad. Sci. U.S.A.* **1968**, *61*, 748. (b) Tenhunen, R.; Marver, H. S.; Schmid, R. *J. Biol. Chem.* **1969**, *244*, 6388-6394.

(2) Yoshida, T.; Kikuchi, G. *J. Biol. Chem.* **1978**, *253*, 4224-4229.

(3) Yoshida, T.; Noguchi, M.; Kikuchi, G. *J. Biol. Chem.* **1980**, *255*, 4418-4420.

(4) Yoshida, T.; Kikuchi, G. *J. Biol. Chem.* **1978**, *253*, 4230-4236.

(5) (a) Takahashi, S.; Wang, J.; Rousseau, D. L.; Ishikawa, K.; Yoshida, T.; Host, J. R.; Ikeda-Saito, M. *J. Biol. Chem.* **1994**, *269*, 1010-1014. (b) Takahashi, S.; Wang, J.; Rousseau, D. L.; Ishikawa, K.; Yoshida, T.; Takeuchi, N.; Ikeda-Saito, M. *Biochemistry* **1994**, *33*, 5531-5538. (c) Sun, J.; Wilks, A.; Ortiz de Montellano, P. R.; Loehr, T. M. *Biochemistry* **1993**, *32*, 14151-14157.

(6) Lemberg, R. *Rev. Pure. Appl. Chem.* **1956**, *6*, 1-23.

(7) Murakami, T.; Matsui, T.; Ozaki, S.; Watanabe, Y.; Morishima, I. *Chem. Commun.* in press.

(8) Antonini, E.; Brunori, M. *Hemoglobins and Myoglobins in Their Reactions with Ligands*; Elsevier: Amsterdam, 1971.

(9) Hernández, G.; Wilks, A.; Paolesse, R.; Smith, K. M.; Ortiz de Montellano, P. R.; La Mar, G. N. *Biochemistry* **1994**, *33*, 6631-6641.

(10) Springer, B. A.; Egeberg, K. D.; Sliger, S. G.; Rohlfs, R. J.; Mathews, A. J.; Olson, J. S. *J. Biol. Chem.* **1989**, *264*, 3057-3060.

(11) Makino, R.; Uno, T.; Sakaguchi; Ishimura, Y. *Oxygenase and Oxygen Metabolism*; Makino, R.; Uno, T.; Sakaguchi; Ishimura, Y., Ed.; Academic Press: New York, 1982, pp 467-477.

(12) Brantley, J., R. E.; Smerdon, S. J.; Wilkinson, A. J.; Singleton, E. W.; Olson, J. S. *J. Biol. Chem.* **1993**, *268*, 6995-7010.

(13) Quillin, M. L.; Arduini, R. M.; Olson, J. S.; Phillips Jr, G. N. *J. Mol. Biol.* **1993**, *234*, 140-155.

(14) Omata, Y.; Noguchi, M. *A Spectroscopic Study on the Intermediates of Heme Degradation by Heme Oxygenase*; Omata, Y.; Noguchi, M., Ed.; Springer Verlag: Keio University, 1997, pp 339-344.

(15) Harbury, H. A. *Proc. Natl. Acad. Sci. U.S.A.* , *54*, 1658-.

(16) (a) Moore, G. R.; Leitch, F. A.; Pettigrew, G. W.; Rogers, N. K.; Williams, G. *Frontiers in Bioinorganic Chemistry*; Xavier, A. V., Ed.: VCH, Weinheim, Federal Republic of Germany, 1986, pp 494-506. (b) Rees, D. C. *J. Mol. Biol.* **1980**, *141*, 323.

(17) Hildebrand, D. P.; Tang, H.-l.; Luo, Y.; Hunter, C. L.; Smith, M.; Brayer, G. D.; Mauk, A. G. *J. Am. Chem. Soc.* **1996**, *118*, 12909-12915.

(18) (a) Alben, J. O.; Caughey, W. S. *Biochemistry* **1968**, *7*, 175-183. (b) Caughey, W. S.; Alben, J. O.; McCoy, S.; Boyer, S. H.; Carache, S.; Hathaway, P. *Biochemistry* **1969**, *8*, 59-62.

(19) Li, T.; Quillin, M. L.; Phillips Jr, G. N.; Olson, J. S. *Biochemistry* **1994**, *33*, 1433-1446.

(20) Decatur, S. M.; Boxer, S. G. *Biochem. Biophys. Res. Commun.* **1995**, *212*, 159-164.

(21) Emerson, S. D.; La Mar, G. N. *Biochemistry* **1990**, *29*, 1545-1555.

(22) de Ropp, J. S.; Yu, L. P.; La Mar, G. N. *J. Bilmol. Nucl. Magn. Reson.* **1991**, *1*, 175-190.

(23) Cutnell, J. D.; La Mar, G. N.; Kong, S. B. *J. Am. Chem. Soc.* **1981**, *103*, 3567-3572.

(24) Krishnamoorthi, R.; La Mar, G. N. *Eur. J. Biochem.* **1984**, *138*, 135-140.

(25) Ramaprasad, S.; Johnson, R. D.; La Mar, G. N. *J. Am. Chem. Soc.* **1984**, *106*, 3632-3635.

(26) (a) Shulman, R. G.; Glarum, S. H.; Karplus, M. *J. Mol. Biol.* **1971**, *57*, 93-115. (b) Yamamoto, Y.; Nanai, N.; R., C.; Suzuki, T. *FEBS Lett.* **1990**, 113-116.

(27) Yamamoto, Y.; Suzuki, T. *Biochim. Biophys. Acta.* **1993**, *1163*, 287-296.

(28) Peyton, D. H.; La Mar, G. N.; Ascoli, F.; Smith, K. M.; Pandey, R. K.; Parish, D. W.; Bolognesi, M.; Burunori, M. *Biochemistry* **1989**, *28*, 4880-4887.

(29) Ito-Maki, M.; Ishikawa, K.; Mansfield Matera, K.; Sato, M.; Yoshida, T. *Arch. Biochem. Biophys.* **1995**, *317*, 253-258.

(30) (a) Imai, M.; Shimada, H.; Watanabe, Y.; Matsushima-Hibiya, Y.; Makino, R.; Koga, H.; Horiuchi, T.; Ishimura, Y. *Proc. Natl. Acad. Sci. U.S.A.* **1989**, *86*, 7823-7827. (b) Kimata, Y.; Shimada, H.; Hirose, T.;

Ishimura, Y. *Biochem. Biophys. Res. Commun.* **1995**, *208*, 96-102. (c) Shimada, H.; Watanabe, Y.; Imai, M.; Makino, R.; Koga, H.; Horiuchi, T.; Ishimura, Y. *The role of threonine 252 in the oxygen activation by cytochrome P-450cam: Mechanistic studies by site-directed mutagenesis.*; Shimada, H.; Watanabe, Y.; Imai, M.; Makino, R.; Koga, H.; Horiuchi, T.; Ishimura, Y., Ed.; Elsevier Science Publishers B.V.: Amsterdam, 1991; Vol. 66, pp 313-319. (d) Gerber, N. C.; Sligar, S. G. *J. Am. Chem. Soc.* **1992**, *114*, 8742-8743.

(31) (a) Noguchi, M.; Yoshida, T.; Kikuchi, G. *J. BioChem. (Tokyo)* **1983**, *93*, 1027-1036. (b) Wilks, A.; Torpey, J.; Ortiz de Montellano, P. R. *J. Biol. Chem.* **1994**, *269*, 29553-29556.

(32) private communication with H. Fujii.

PART V.

STRUCTURES OF HEME OXYGENASE

CHAPTER 1.

Substrate-Induced Conformational Change in Heme Oxygenase

Abstract

The conformational change of heme oxygenase (HO) induced by substrate binding has been examined by NMR, circular dichroism (CD), and fluorescence spectroscopies, and by urea-induced denaturation. Binding of CO-ferrous heme to HO affords two largely downshifted resonances of exchangeable protons in the proton NMR spectrum, and nearly the same chemical shifts are also observed for paramagnetic CN-ferric heme-HO, but not in the absence of the heme. The insensitivity of the resonances on the heme magnetism suggests that largely downshifts are originated from inter-segmental hydrogen bonds involving aromatic side chains of histidine, tryptophan, and/or tyrosine residue and are formed relatively far from the substrate-binding site upon the addition of heme to HO. The near-UV CD and the fluorescence emission spectra do not exhibit significant changes suggesting that the tryptophan and tyrosine residues are not involved in the observed hydrogen bond. Histidine residues are likely responsible for the hydrogen bondings. According to the urea-induced denaturation curves of HO and heme-HO, HO is thermodynamically more stable than heme-HO complex, and protects more hydrophobic residues from solvent. The heme binding also results in a decrease in helicity. A fluorescent probe for non-polar binding sites shows that the heme-binding site of HO is exposed to solvent relative to those of myoglobin and hemoglobin and is unlikely to be well-organized in the absence of heme. These results suggests that the heme binding to HO causes a global conformational change in HO including the destruction of a part of α-helix and the formation of the two inter-segmental hydrogen bondings, and could allow us to imagine that HO does not have so-called heme pocket by nature.

Introduction

Heme oxygenase (HO) is a microsomal enzyme which catalyzes the first key step in heme catabolism, the oxidative degradation of heme (iron-protoporphyrinIX) to biliverdin and carbon monooxide.[1] Though it has two known isoforms, referred to as HO-1 (33 kDa) and HO-2 (36 kDa),[2] it is generally assumed that their active sitea are similar and share a similar mechanism of action. HO-1 is inducible and is highly expressed in spleen and liver. HO-2 is constitutive and found primarily in brain. Heme oxygenase is not a hemoprotein by nature, but binds heme at the active site in a 1:1 ratio[3] and constrains it to an environment suitable for a site-specific ring opening. Normal catalytic turnover of the enzyme by utilizing NADPH and cytochrome P-450 reductase yields biliverdin *via* a sequence that is thought to involve α-*meso*-hydroxylation of the heme, aerobic fragmentation of the α-*meso*-hydroxyheme to verdoheme, and oxidative cleavage of verdoheme to the iron(III)-biliverdin complex.[4] The iron of the complex is removed when reduced by one electron, and then biliverdin is subsequently excreted from the binding site (Scheme 1).[5]

The enzyme-substrate complex has properties similar to those of hemoproteins with neutral histidine residue,[6] and exhibits ferric and

Scheme 1

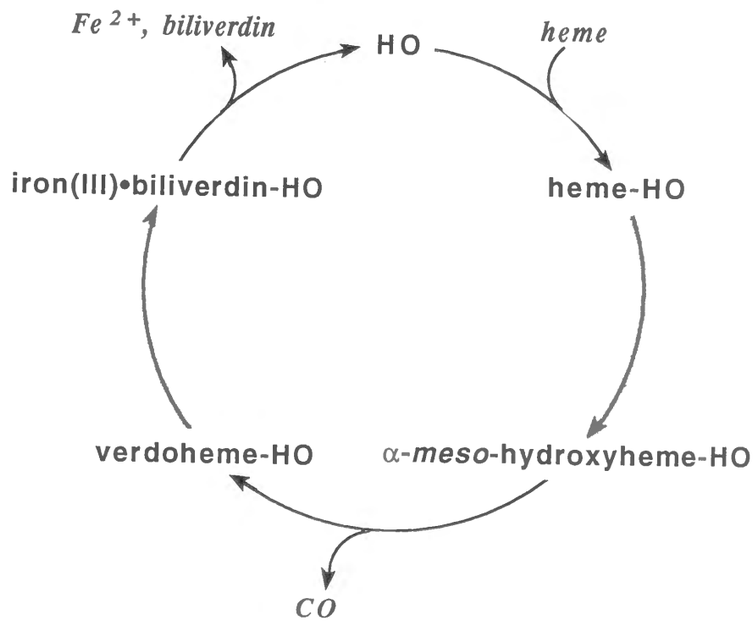

ferrous redox states, binding of exogenous inhibitory ligands such as CO or CN^-. According to the available information, the distal site of heme-HO has a protic residue interacting with dioxygen bound to the heme iron[7] and is moderately hydrophobic, which sugggests that heme is bound to the so-called heme pocket of heme-HO as observed for Mb and Hb. In addition, the heme binding site of heme-HO is suggested to be considerably exposed to solvent compared with those of Mb and Hb.[8] One of the unique properties of HO is heme binding as the substrate unlike hemoprotein. Although the amino acid sequences of some of HO are now known, no crystal structures of HO and heme-HO are available, consequently, little is known of their secondary and tertiary structure of both the enzyme and the enzyme-substrate complex.[9]

Studies on sperm whale apoMb have demonstrated that the heme group not only play a functional role but also allows Mb to adopt and maintain the correct native fold: disruption of the heme-protein interactions results in a structure that is ca. 25% less helical[10] and ca. 23 kJ less stable[11] than the holoprotein. Considering that HO does not contain heme by nature, the stabilizing mechanism of HO must be different from that of hemoproteins.

On the other hand, a substrate-induced conformational change is generally linked to the enzyme function. For example, hexokinase, which catalyzes the phosphorylation of D-glucose, contain two lobes separated by a cleft.[12] The glucose binding to the cleft makes the two lobes to come together, and then the cleft is closed.[12] Anderson et al. proposed that one of functions for the substrate-induced change was to orient catalytic groups or perhaps to exclude solvent for an efficient nucleophilic attack of the phosphoryl acceptor on the phosphoryl group to be transferred.[12] As described above, while HO can bind heme and the following three metabolites to the binding site, HO also releases the final metabolite, biliverdin. This function of HO would be related to the conformational differences between HO and the substrate- or metabolite-HO complex.

In the present study, circular dichroism (CD), ^{1}H-NMR, and fluorescence measurements, and urea-induced denaturation have been examined in order to gain insight into structural aspects of HO and heme-HO.

Experimental Section

Protein Preparation. A truncated DNA of heme oxygenase-1 gene encoding the soluble portion of rat heme oxygenase-1 which lacked the membrane binding domain (22 amino acids at the C-terminus) was inserted into the expression vector pBAce[13] followed by transfection into *E. coli* JM109. Preparation and purification of heme oxygenase-1 and a heme-bound enzyme complex were performed according to the method described elsewhere.[14]

Spectroscopy. All spectroscopic measurements were performed in 50 mM sodium phosphate buffer (pH 7.0) unless otherwise stated. Electronic absorption spectra were recorded on a Perkin Elmer Lambda 19 spectrometer.

Circular Dichroism (CD) spectra of HO and the heme-bound enzyme complex in far- and near-UV regions were measured with a JASCO J-720 at ambient temperature. Mean residue α-helical content was evaluated from the ellipticity at 222 nm using eq 1[16]:

$$\alpha\text{-helix}\,(\%) = -([\theta]_{222} + 2340)/30300 \qquad (1)$$

In the course of the CD measurements, nitrogen gas was purged into the cell to avoid incorporated chirality of dioxygen. All spectra were an average of 16 scans recorded at a speed of 100 nm/min and resolution of 0.2 nm. Light paths of sample cells were 1 mm for far-UV region and 10 mm for near-UV region.

Fluorescence emission measurements were performed on a Perkin Elmer LB50 emission spectrometer. The spectra were measured between 300 and 450 nm for the heme titration and between 400 and 600 nm for ANS (the magnesium salt of 1-anilino-8-naphthalene sulfonate) titration, and were an average of 4 scans recorded at a speed of 100 nm/min, operated with a slit width of 5 mm. The excitation wavelength was 280 nm and 295 nm with a slit at 280 nm for the heme titration, and 340 nm with a slit at 390 nm for the ANS titration.

Hyperfine-shifted ^{1}H-NMR spectra were recorded at 20°C on a Brucker DRX 500 spectrometer equipped with a SGI Indy workstation. The concentration of the samples were ca. 1 mM in both 90% ^1H_2O/10% ^2H_2O and 100% ^2H_2O. The solution pH values were measured before and after each run, using a Beckman Model 3550 pH meter equipped with a HORIBA 6029-10T electrode. The pH readings were uncorrected for the

isotope effect, and hence referred to as 'pH'. A ferric heme-bound enzyme complex was reduced with excess sodium dithionite under nitrogen atmosphere, and subsequent CO flushing afforded a CO-bound form of the complex. Peak shifts were referenced to the residual water signal which was calibrated against tetramithylsilane (TMS).

Titration of Heme Oxygenase with heme and ANS. A hemin solution was prepared according to the method reported before (Yoshida & Kikuchi, 1978). To 0.5–3 ml of an enzyme solution in each cell for various measurements was added 2.5 μl of the hemin or ANS solution at a time, and stood on ice for 5 min for equilibration.

Urea-Induced Denaturation Study. Denaturant solutions contained 50 mM sodium phosphate (pH 7.0), 0.5 mM NaCN, and various concentrations of urea. An aliquot of the concentrated enzyme or heme-bound enzyme complex solution was added to the 0.5-ml denaturant solution to keep the final protein concentration at 5 μM, and equilibrated for about six hours at 25°C. The denaturation of the enzyme and the heme-bound enzyme complex was monitored by changes in ellipticity at 222 nm. The fractional population of denatured form (f_D) under each condition was estimated by the equation,

$$f_D = ([\theta]_{222} - [\theta]_{222,D})/([\theta]_{222,N} - [\theta]_{222,D}) \quad (2)$$

where, $[\theta]_{222,N}$ and $[\theta]_{222,D}$ represent ellipticities at 222 nm in the native and denatured state, respectively.[16] values of $\Delta G_{N\text{-}U}$ for a two-state process were determined using the relation:

$$\Delta G_{N\text{-}U} = -RT \ln\{f_D/(1-f_D)\} \quad (3)$$

All plots of $\Delta G_{N\text{-}U}$ versus denaturant concentration were analyzed using the linear free energy model:

$$\Delta G_{N\text{-}U} = \Delta G^0_{N\text{-}U} - m_u[\text{urea}] \quad (4)$$

where m is the slope of the plot and $\Delta G^0_{N\text{-}U}$ is the extraporated value of $\Delta G_{N\text{-}U}$ at [urea] = 0 M.

Results

Heme Titration monitored by Various Spectroscopies. The spectrophotometric titration of HO with hemin has been carried out by stepwise addition of 2.5 μl of 2.8 mM heme at pH 7.0 (Figure 1). The increments of absorbance at 404 nm are plotted against the molar ratio of the heme added and the free HO which is supposed to be present in the sample cuvette (inset of Figure 1). The bent line around a 1:1 ratio coincides with the results observed for HO purified from pig spleen microsomes.[17]

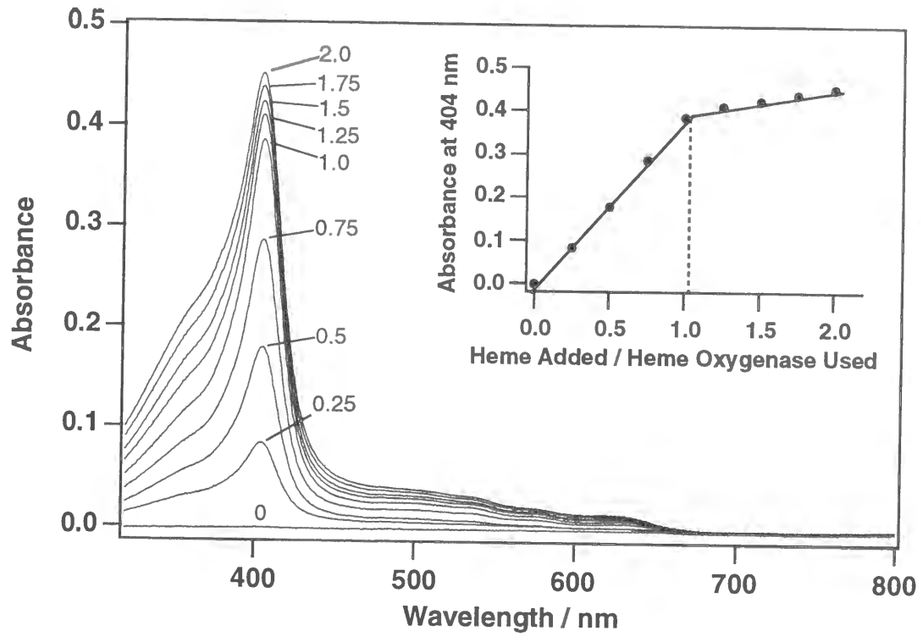

Figure 1. Electronic absorption spectral changes upon the stepwise addition of heme to HO. (*inset*) Absorbance change at 404 nm.

Figure 2 shows CD spectral changes upon the addition of 0.25 equiv each of heme to HO in the far-UV, near-UV regions where the CD reflects the secondary and tertiary structures of proteins, respectively. HO exhibits two negative broad peaks around 222 and 208 nm (Figure 2A). The CD_{222} which is sensitive to the α-helical content of proteins slightly decrease upon the addition of heme. This heme-induced decrease of the α-helical content is interesting because reconstitution of the apo forms of hemoproteins with heme usually induces recovery of the secondary structures.[10,11,18] The CD_{222} against the amount of added hemin shows

the similar saturation behavior as the absorbance change at the Soret band (inset of Figure2A).

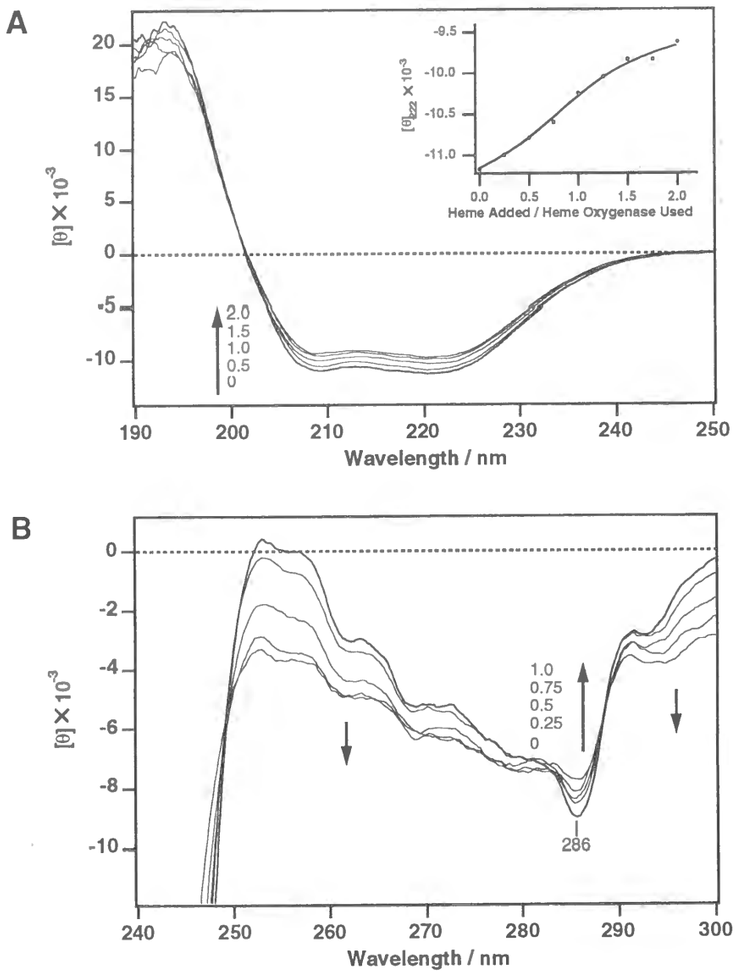

Figure 2. CD spectral changes in far-UV (panel A) and near-UV (panel B) region upon the stepwise addition of heme to HO. (*inset*) Ellipticity change at 222 nm.

We have measured the near-UV CD spectral changes upon the heme titration to examine whether or not the heme binding to HO causes change of tertiary structures. As shown in Figure 2B, HO shows fine structures at 250-280 nm and a negative peak at 286 nm which is the cotton effects of tyrosine and phenylalanine residues, and tryptophan

residue, respectively. The addition of heme to HO caused gradual changes these peak intensites without shift of the CD maxima.

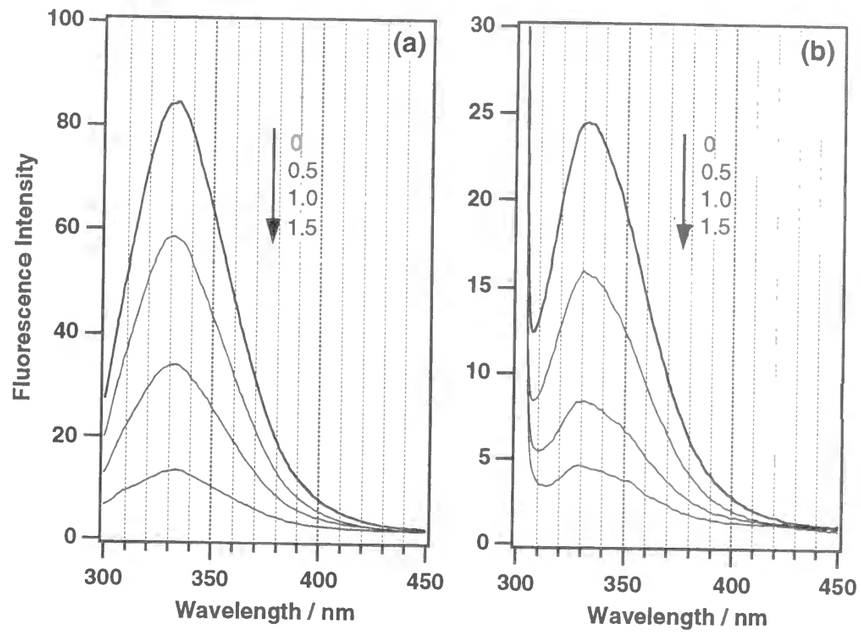

Figure 3. Fluorescence emission spectral changes for the titration of HO solution with increments of heme in the buffer. Excitation at 280 nm (panel A) and 295 nm with a slit at 280 nm (panel B).

Fluorescence spectroscopy of endogenous tryptophan and tyrosine residues has often been employed to monitor alterations of proteins by the substrate binding.[19] Since HO has two tryptophan and eleven tyrosine residues, we examined the intrinsic fluorescence properties in the heme titration. Upon excitation at 280 nm in which fluorescence arises from the exicitation of both trypotophans and tyrosines, a fluorescence emission maximum appears at 332 nm, suggesting that those residue are in slightly hydrophilic environment compared with that of apoMb (327±1 nm).[20] The addition of 1 equiv of heme decrease the fluorescence intensity (40 and 34 % in Figure 3a and 3b, respectively) due to the energy transfer from those residues to the heme, and does not cause any shift of the maximum. Upon excitation at 295 nm in which fluorescence arises from the excitation of only tryptophans, a fluorescence emission with the same maximum at 332 nm is observed (Figure 3b). There is only a minor blue

shift (approximately 1 nm) in the fluorescence spectrum upon the heme titration from 0 to 1.0 equiv, suggesting that there are no major changes in the average polarity of the regions surrounding the tryptophans. Further addition of 0.5 equiv of heme causes a blue shift by 2 nm relative to the emission maximum of 331 nm after the addition of 1 equiv to HO (Figure 3b).

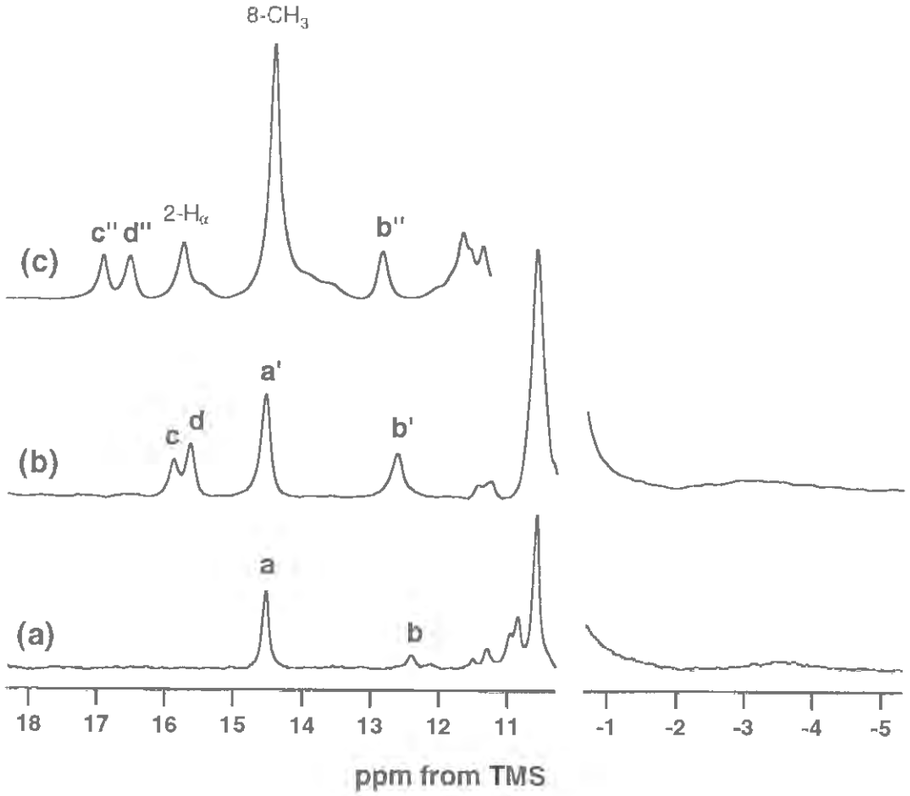

Figure 4. Proton NMR spectra of (a) HO and (b) the CO-ferrous heme-HO in 90% ^1H_2O/10% ^2H_2O at pH 7.0 and 20 °C.

Change upon the Heme Binding in Proton NMR Spectroscopy. Figure 4 shows the hyperfine-shifted regions of HO and the CO-ferrous heme-HO complex, both of which are diamagnetic, and the paramagnetic CN-ferric heme-HO complex in 90% H_2O/10% ^2H_2O, pH 7.0, at 20°C. Two largely downshifted resonances, peak a (14.5 ppm) and b (12.4 ppm), are observed for HO. The absence of these peaks in 100% ^2H_2O suggests that they arise from exchangeable protons. The difference in the resonance frequency between these signals and a bulk water signal dictates that

their hydrogen exchange rates should be $<< 3 \times 10^3$ s^{-1}. The shifts and hydrogen exchange rates of these protons resemble those of a histidine imidazole NH proton, tryptophan indole NH proton, and tyrosine phenol OH proton, which are buried in the protein matrix and possibly involved in an internal hydrogen bond. In the spectrum of the CO-ferrous heme-HO complex, four exchangeable proton resonances, peak c, d, a' and b', are observed at 15.9, 15.6, 14.5, and 12.6 ppm, respectively. While peak a'

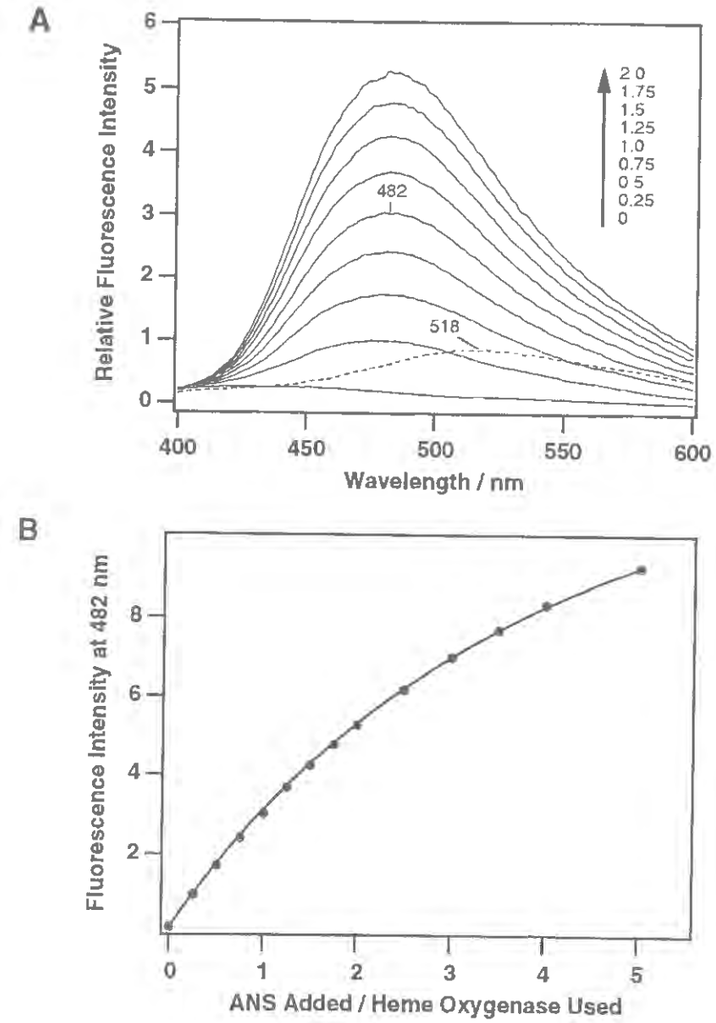

Figure 5. Fluorescence emission spectral changes for the titration of HO solution with increments of ANS in the buffer (panel A) and changes in fluorescence intensity at 482 nm (panel B). Broken line in panel A corresponds to the spectrum of 1 equiv of ANS in the absence of HO.

and b' exhibit nearly the same chemical shift to peak a and b for HO, peak c and d newly appear upon the heme binding. In the spectrum of the CN-ferric heme-HO complex (Figure 4c), three exchangeable proton resonances are also observed at 16.9, 16.5, and 12.9 ppm, and these chemical shifts are similar to those of peak c, d, and b' in Figure 4b. Furthermore, the broader line width of peak a' and b' than those of peak a and b is also observed, which corresponds to faster exchange of the protons for peak a' and b' with solvent.

Nature of Heme Binding Site of HO. Figure 5A shows the fluorescence emission spectral changes upon the addition of 1-anilino-8-naphthalene sulfonate (ANS), which is incorporated into the heme pocket of various apo forms of heme proteins in a highly specific and stoichiometric manner.[21] Therefore, its fluorescence serves as a sensitive probe for the nature of a heme environment. Excitation at 366 nm prevented any interference from intrinsic protein fluorescence or energy transfer from tryptophan. The emission maximum of an ANS-HO complex (477 nm) is significantly shifted from that of ANS in buffer (519 nm), but it exhibits the smaller blue shift than those of 454 nm for Mb and of 457 nm for Hb α subunit.[21] Furthermore, the fluorescence intensity of the ANS-HO complex is comparable to that of ANS in buffer. These results suggest that HO forms an apolar pocket as found for heme proteins, but the pocket of HO is exposed to solvent relative to those of Mb and Hb.

Fluorescence intensity at 477 nm is plotted against the molar ratio of heme added and the free HO which is supposed to be present initially in the same sample (Figure 5B). The intensity gradually leveled off but does not reach a plateau. Therefore, the association constant of ANS may be considerably low.

Urea-Induced Denaturation of HO and Heme-HO Complex. Curves in Figure 6a show the urea-induced denaturation of HO and a ferric heme-HO complex at pH 7.0 and 25°C. The transition curve for heme-HO shifts to the right side relative to HO. Linear relations between ΔG and [urea] are observed for both HO and heme-HO (Figure 6b). By applying Eq. 4, m_u, $\Delta G^0_{N\text{-}U}$ and the urea concentration where ΔG is equal to 0 (C_m) have been determined (Table 1). Though the heme binding gives rise to the increase in the C_m values, the $\Delta G^0_{N\text{-}U}$ values for the ferric heme-HO

complex (13.9 kcal/mol) is lower than that for HO (19.9 kcal/mol) due to the much lower m_u value of the ferric heme-HO complex.

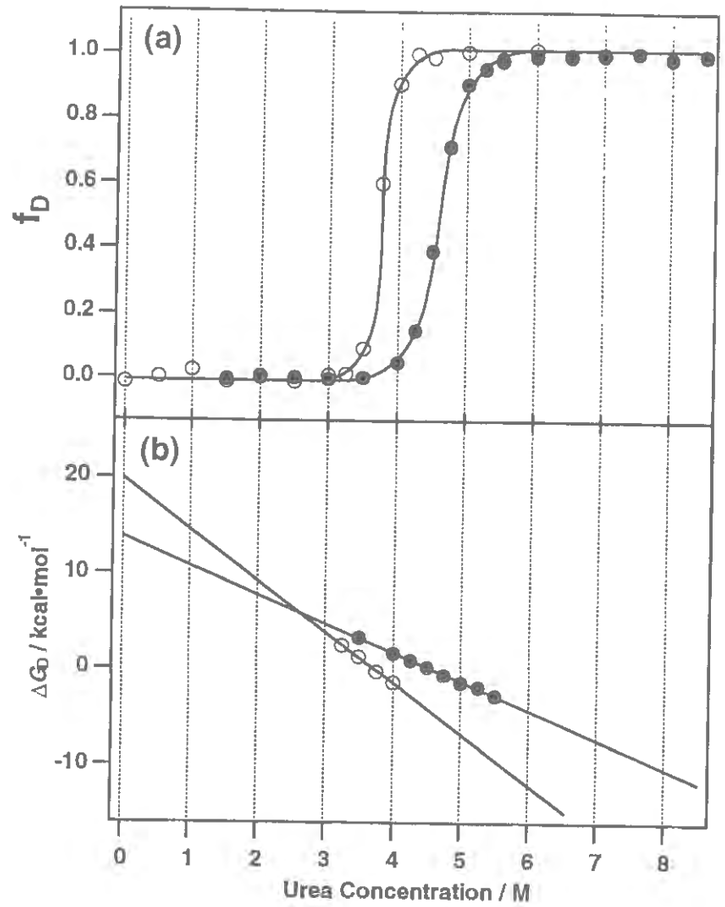

Figure 6. (a) Denaturation curves of HO and heme-HO by urea in the buffer containing 0.1 M NaCl at pH 7.0 and 25 °C. (b) Relationship between ΔG and [urea]. Symbols correspond to HO (○) and heme-HO (●).

Table 1. Thermodynamic Parameters for HO and heme-HO Unfolding at pH 7.0 and 25 °C [a]

	$\Delta G^0_{N\text{-}U}$ (kJ/mol)	m_u (kJ/mol per M)	C_m (M)
HO	19.9	5.33	3.73
heme-HO	13.9	3.02	4.59

[a] Both solutions contained 0.1 M NaCl.

Discussion

Substrate-induced conformational change of proteins such as hexokinase is well-known.[12] Some of them are characterized at the molecular level and link to specific events in the functional cycle. Conformational changes switch protein structures to the active conformation (e.g., induced fit[22]). Many conformational changes are not still well characterized. The present work demonstrates that the substrate binding to HO induces a unique conformational change and the transformation is closely related to the stability of HO and the mechanism discriminating heme and the following three metabolites from biliverdin and the other nonpolar compounds whose binding to HO inhibit the reaction.

Formation of the Inter-Segmental Hydrogen Bonds upon the Heme Binding to HO and Its Possible Roles. As shown in Figure 4b, two exchangeable proton resonances (c and d) are newly observed for the diamagnetic CO-ferrous heme-HO compared with HO. Since the paramagnetic CN-ferric heme-HO complex also affords the two exchangeable proton signals with similar chemical shifts, we could exclude the contribution of the porphyrin ring current effect to the chemical shifts. On the other hand, Yamamoto et al. observed large downshifted signals of exchangeable protons around 13 ppm from TMS for both apoMb and CO-ferrous Mb, and assigned those signals to the inter-segmental hydrogen-bonded protons of aromatic side chains, histidine imidazoles buried in the protein matrix.[23] Taking into acount that the hydrogen exchange rates for the signals c and d is $<< 3 \times 10^3\ s^{-1}$, we can assign these signals to histidine imidazole NH proton(s), tryptophan indole NH proton(s), and/or tyrosine phenol OH proton(s) under the inter-segmantal hydrogen bonding interaction.

From the sequence homology among the cDNAs for rat, human, mouse, rabbit, and chicken, His-25, 84, 119, and 132 of the rat enzyme is conserved,[24] and especially His-25 is identified to be the axial ligand of heme-HO.[25] The roles of the other three histidine residues was also examined by determining the enzymatic activities of mutant enzymes in which each of these residues was replaced by alanine.[25a] When the activities of equal amount of protein of the respective soluble fractions for heme breakdown were compared, H84A, H119A, and H132A mutant HO exhibited 41, 39, and 1 %, respectively, of wild-type HO.[25a] Ishikawa et al. suggested that substitution of His-84 or His-119 influenced the structure of

the active center and/or the interaction with P-450 reductase, but did not draw any conclusion from the result for H132A mutant HO because expression of the mutant protein was too low.[25a] Recent reexamination of H132A mutant HO provided that the extremely low activity is not due to the intrinsic property of the mutant, but to the involvement of a large amount of an inactive fraction easily given from H132A mutant HO, suggesting a similar activity to the wild-type HO.[26] Thus, the conserved His-132 was also proposed to play a structural role in stabilization of the HO protein. These observation could allow us to expect that these conserved histidine residues are responsible for the inter-segmental hydrogen bond buried in the protein matrix as observed in Figure 4b. Actually, apoMb is synergistically stabilized by such a inter-segmental-hydrogen bonds of His-24.[27]

This consideration would be supported by the near-UV CD and fluorescence results upon the heme binding to HO as follows. Changes in the protein tertiary structure can be monitored in its CD spectra in the near-UV region where the CD signals originate mainly from tryptophan, tyrosine, and phenylalanine residues.[28] HO with tryptophan and tyrosine shows a pronounced minimum at 286 nm, which indicates the existence of a defined tertiary structure of tryptophan and/or tyrosine residues. The addition of heme to HO induces a small change of the near-UV CD in intensity, which is the most likely to be caused by the heme bound to HO, and more importantly no shift of the near-UV CD. Hydrogen-bonded tryptophan is known to show a red-shifted CD signal relative to the intact tryptophan residue.[29] Thus, these results do not contradict the assignment of the two signals of heme-HO to the NH of histidine imidazole. NOESY and COSY experiments for the assignment are under investigation.

Rearrangement of the hydrogen bond in $\alpha 1$-$\beta 2$ subunit interface plays a crucila role in hemoglobin allostery.[30] Especially, the hydrogen bond formation between Tyr-42(C7)$\alpha 1$ and Asp-99(G1)$\beta 2$ in the surface has long-range effects on the heme electronic structure to stabilize the deoxy T quaternary structure.[31] Therefore, the hydrogen bond formed upon the heme binding to HO might moderately maintain the unstable heme-HO structure relative to the HO structure not to lose the heme.

Structural Insight into a Putative Substrate-Binding Site of HO. Heme clearly stabilizes intact Mbs and Hbs with respect to their

corresponding apoglobins. Binding of heme to Mb results in a increase of helicity, contraction of the resulting holoprotein, and a marked increase in resistance to denaturation.[10,11] The most pronounced change is the formation of the compact heme pocket due to recovery of the disordered helix F organizing the proximal site of holoMb.[31] This conformational change is reflected by the NMR spectrum representing that the inter-segmental hydrogen-bonded NH resonance of His-82(EF5) is considerably sharpened upon the binding of heme.[23a] On the other hand, heme-induced conformational change in HO is entirely different from that in apoMb in terms of these points. This is best described as the decrease of helicity and the thermodynamical destabilization upon the binding of heme to HO. We discuss the unique properties of HO in detail.

Since the m_u value of HO is much larger than that of heme-HO as shown in Figure 6, the $\Delta G^0_{N\text{-}U}$ value of HO is larger than that of heme-HO in spite of a smaller C_m value of HO. According to the current interpretation of m_u,[32] the binding of heme to HO seems to decrease the difference in exposed surface area between the denatured and native states, and this consideration indicates that HO packs more densely than heme-HO. This is supported by the fact that HO contains more α-helix than heme-HO and the inter-segmental hydrogen-bonded proton resonance at 14.5 ppm is much sharper for HO than heme-HO, that is, the proton of HO is in a more hydrophobic environment compared with that of heme-HO.

The fluorescence characteristics of naphthalensulfonates are useful probes of the polarity of protein binding sites.[33] In this study, we have used ANS to probe the chemical and physical properties of hydrophobic sites of HO. While ANS, when bound to HO, is in a slightly nonpolar environment as shown in Figure 5,[21] the association is extremely weak compared with those of apoMb and apoHb which form ANS-protein complexes by stoichiometric addition of ANS, and the emission maximum of 477 nm and the relatively low fluorescence intensity are expected for the core considerably exposed to solvent to cause efficient fluorescence quenching.[21] On the basis of the urea-induced denaturation studies and the properties of ANS bound to HO, we propose that HO does not have a well-organized hydrophobic core for the heme binding by nature, and thus gains a compact and rigid conformation for the tight side-chain packing to compensate lack of heme which stabilizes intact Mb and Hb with respect to their corresponding apoproteins.

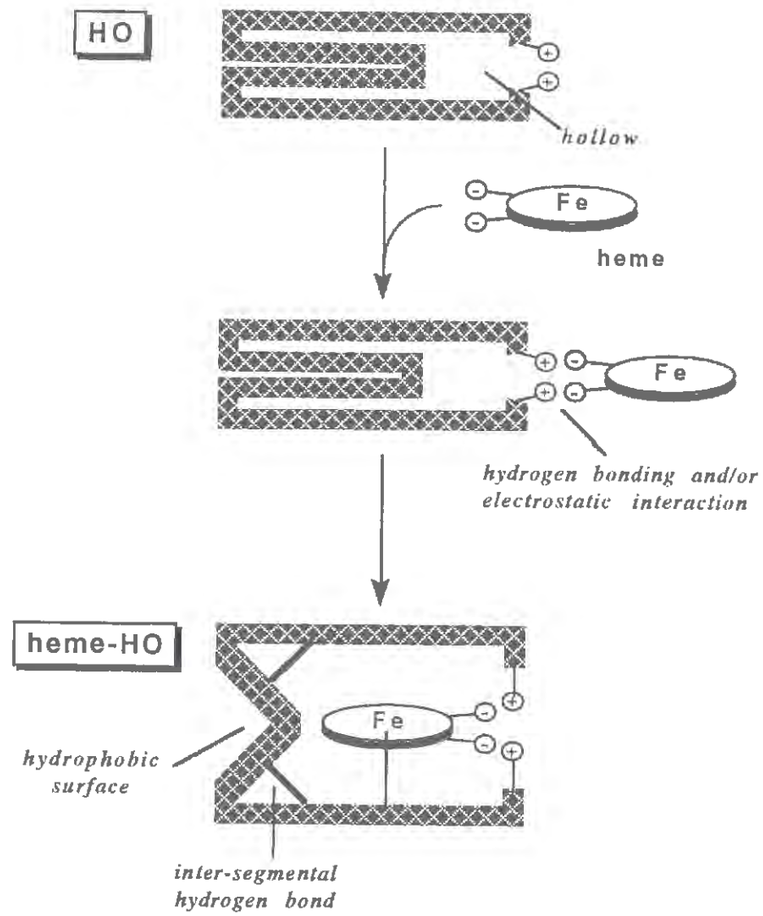

Figure 7. A possible schematic model for HO, illustrating the process of conformational reorganization involved in the substrate binding to HO.

Tomaro et al. reported that the presence of two vicinal propionic acid side-chains at C6 and C7 was essential for substrate activity and that a hemin with only one propionic acid residue at C5 was not a substrate of the enzyme at all due to the complete lack of interaction of the modified heme with HO.[34] These properties also support the absence of hydrophobic cores large enough to incorporate heme into HO because apoMb bearing such core binds a heme derivative even without two propionic acid residues interacting with Arg-45, Ser-92, and His-97 in holoMb.[35] Such specificity for the substrate might allow us to imagine the mechanism as illustrated in Figure 7. First of all, the substrate-induced conformational change in HO is triggered by hydrogen bonding and/or electrostatic interactions between the propionic acid side-chains of heme

and protic residues in the surface of HO. The subsequent formation of the inter-segmental hydrogen bond and destruction of a part of α-helix result in the construction of the substrate binding site, heme pocket, and heme is simultaneously incorporated to form heme-HO.

Comparison with Hemoproteins.

Considering the different roles of heme between HO and hemoproteins such as Mb and Hb, i.e., heme is the substrate and prosthetic group for HO and the prosthetic group for hemoproteins, physiological implication of the absence of the heme pocket in HO could be described as stabilization of the substrate-free enzyme and efficient excretion of biliverdin. In the digestion of Hb, heme in Hb is at first removed by serum albumin[36] and apohemopexin after red cell lysis to form loosely-folded apoHb.[18] The increased surface area exposed to solvent of apoHb is favorable to the access of proteases. Thus, the absence of the heme pocket in HO must prevent such an easy proteolysis in terms of decreasing of the surface area and fluctuation. Moreover, biliverdin, the end metabolite in the heme degradation catalyzed by HO, must be excreted from the binding site to prevent the product inhibition. Since biliverdin is incorporated into the heme pocket of apoMb to afford a biliverdin-apoMb complex, whose crylstal structure is almost the same as that of holoMb,[37] the presence of the heme pocket in HO is unfavorable to release biliverdin. In this case, the decreased interaction of biliverdin with HO due to the loss of the axial ligation of histidine residue would cause the transformation from "open" form to "close" form of HO, accompanied with the excretion of biliverdin.

Conclusion

In the present report, we studied global-scale structural changes upon the substrate binding to HO. The experimental results demonstrated that the heme binding to HO caused (i) the formation of the inter-segmental hydrogen bond possibly by histidine residues far from the binding site, (ii) the decrease of the α-helical content, and (iii) thermodynamical destabilization of HO. Further, it is suggested that HO does not have a complete substrate-binding site, so-called heme pocket, by nature. Taken together, these results demonstrate that HO gains its stability in terms of lack of large vacant cores as observed for apoMb and

more α-helix, which serve to form a tightly packed secondary structure, unlike hemeproteins stabilized by heme binding as the prosthetic group

References

(1) (a) O'Carra, P. *Porphyrins and Metaloporphyrins*; Elsevier: Amsterdam, 1975. (b)Kikuchi, G.; Yoshida, T. *Mol. Cell. Biochem.* **1983**, *53/54*, 163-183. (c) Maines, M. D. *FEBS Lett.* **1988**, *2*, 2557-2568.

(2) Maines, M. D.; Trakshel, G. M.; Kutty, R. K. *J. Biol. Chem.* **1986**, *261*, 411-419. (a) Muller, R. M.; Taguchi, H.; Shibahara, S. *J. Biol. Chem.* **1987**, *262*, 6795. (b) Cruse, I.; Maines, M. D. *J. Biol. Chem.* **1988**, *263*, 3348.

(3) (a) Yoshida, T.; Kikuchi, G. *J. Biol. Chem.* **1979**, *254*, 4487-4491. (b) Bonkovsky, H. L.; Healy, J. F.; Pohl, J. *Biochem. J.* **1990**, *189*, 155.

(4) Beale, S. I. *Chem. Rev.* **1993**, *93*, 785-802.

(5) Yoshida, T.; Kikuchi, G. *J. Biol. Chem.* **1978**, *253*, 4230-4236.

(6) (a) Takahashi, S.; Wang, J.; Rousseau, D. L.; Ishikawa, K.; Yoshida, T.; Host, J. R.; Ikeda-Saito, M. *J. Biol. Chem.* **1994**, *269*, 1010-1014. (b) Takahashi, S.; Wang, J.; Rousseau, D. L.; Ishikawa, K.; Yoshida, T.; Takeuchi, N.; Ikeda-Saito, M. *Biochemistry* **1994**, *33*, 5531-5538. (c) Sun, J.; Wilks, A.; Ortiz de Montellano, P. R.; Loehr, T. M. *Biochemistry* **1993**, *32*, 14151-14157.

(7) Fujii, H. submitted for publicaition.

(8) Hernández, G.; Wilks, A.; Paolesse, R.; Smith, K. M.; Ortiz de Montellano, P. R.; La Mar, G. N. *Biochemistry* **1994**, *33*, 6631-6641.

(9) McCoubrey, J., W. K.; Huang, T. J.; Mains, M. D. *J. Biol. Chem.* **1997**, *272*, 12568-12574.

(10) Harrison, S. C.; Blout, E. R. *J. Biol. Chem.* **1965**, *240*, 299-303.

(11) Griko, Y. V.; Privalov, P. L.; Venyaminov, S. Y.; Kutyshenko, V. P. *J. Mol. Biol.* **1988**, *202*, 127-138.

(12) (a) Bennett, J. W. S.; Steitz, T. A. *Proc. Natl. Acad. Sci. U.S.A.* **1978**, *75*, 4848-4852. (b) Anderson, C. M.; Zucker, F. H.; Steitz, T A. *Science* **1979**, *204*, 375-380.

(13) Craig III, S. P.; Yuan, L.; Kuntz, D. A. *Proc. Natl. Acad. Sci. U.S.A.* **1991**, *88*, 2500-2504.

(14) Omata, Y.; Noguchi, M. *A Spectroscopic Study on the Intermediates of Heme Degradation by Heme Oxygenase*; Omata, Y.; Noguchi, M., Ed.; Springer: Keio University, 1998, pp 322-327.

(15) Greenfield, N.; Fasman, G D. *Biochemistry* **1976**, *8*, 4108.
(16) Konno, T.; Morishima, I. *Biochim. Biophys. Acta.* **1993**, *1162*, 93-98.
(17) Yoshida, T.; Kikuchi, G. *J. Biol. Chem.* **1978**, *253*, 4224-4229.
(18) Leutzinger, Y.; Beychok, S. *Proc. Natl. Acad. Sci. U.S.A.* **1981**, *78*, 780-784.
(19) (a) Brandolin, G.; Dupont, Y.; Vignais, P V. *Biochemistry* **1985**, *24*, 1991-1997. (b) Martineau, P.; Szmelcman, S.; Spurlino, J. C.; Quiocho, F. A.; Hofnung, M. *J. Mol. Biol.* **1990**, *214*, 337-352. (c) Peerce, B. E. *J. Biol. Chem.* **1990**, *265*, 1737-1741. (d) Walmsley, A. R.; Petro, K. R.; Henderson, P. J. F. *Eur. J. Biochem.* **1993**, *215*, 43-54.
(20) Postnikova, G. B.; Komarov, Y. E.; Yumakova, E. M. *Eur. J. Biochem.* **1991**, *198*, 223-232.
(21) Stryer, L. *J. Mol. Biol.* **1965**, *13*, 482-495.
(22) Koshland, D. E. *The Enzyme*; Boyer, P. D.; Lardy, H.; Myrbäck, K. Ed.; Academic Press: New York, 1959; Vol. 1, pp 305-346.
(23) (a) Yamanoto, Y. *Eur. J. Biochem.* **1997**, *243*, 292-298. (b) Yamamoto, Y. *J. Biochem.* **1996**, *120*, 126-132.
(24) (a) Shibahara, S.; Müller, R. M.; Taguchi, H.; Yoshida, T. *Proc. Natl. Acad. Sci. U.S.A.* **1985**, *82*, 7865-7869. (b) Yoshida, T.; Biro, P.; Cohen, T.; Müller, R. M.; Shibahara, S. *J. Biochem.* **1988**, *171*, 457-461. (c) Kageyama, H.; Hiwasa, T.; Tokunaga, K.; Sakiyama, S. *Cancer Res.* **1988**, *48*, 4795-4798. (d) Evans, C.-O.; Healey, J. F.; Greene, Y.; Bonkovsky, H. L. *Biochem. J.* **1991**, *273*, 659-666.
(25) (a) Ishikawa, K.; Sato, M.; Ito, M.; Yoshida, T. *Biochem. Biophys. Res. Commun.* **1992**, *182*, 981-986. (b) Ito-Maki, M.; Ishikawa, K.; Mansfield Matera, K.; Sato, M.; Yoshida, T. *Arch. Biochem. Biophys.* **1995**, *317*, 253-258. (c) Sun, J.; Loehr, M.; Wilks, A.; Ortiz de Montellano, P. R. *Biochemistry* **1994**, *33*, 13734-13740. (d) Wilks, A.; Sun, J.; Loehr, T. M.; Ortiz de Montellano, P. R. *J. Am. Chem. Soc.* **1995**, *117*, 2925-2926.
(26) Mansfield Matera, K.; Zhou, H.; Taiko Migita, C.; Hobert, S. E.; Ishikawa, K.; Katakura, K.; Maeshima, H.; Yoshida, T.; Ikeda-Saito, M. *Biochemistry* **1997**, *36*, 4909-4915.
(27) Barrie, D.; Hughson, F. M.; Baldwin, R. L. *J. Mol. Biol.* **1994**, *237*, 588-601.
(28) Siligardi, G.; Drake, A. F.; Mascagni, P.; Rowlands, D.; Brown, F.; Gibbons, W. A. *Eur. J. Biochem.* **1991**, *199*, 545-551.
(29) Strickland, E. H.; Billups, C.; Kaye, F. *Biochemistry* **1972**, *11*, 3657-3662.

(30) Imai, K.; Fushitani, K.; Miyazaki, G.; Ishimori, K.; Kitagawa, T.; Wada, Y.; Morimoto, H.; Morishima, I.; Shih, D. T.-b.; Tama, J. *J. Mol. Biol.* **1991**, *218*, 769-778.
(31) (a) Cocco, M. J.; Lecomte, J. T. J *Biochemistry* **1990**, *29*, 11067-11072. (b) Cocco, J. M.; Kao, Y.-H.; Phillips, A. T.; Lecomte, J. T J *Biochemistry* **1992**, *31*, 6481-6491. (c) Houghson, F. M.; Wright, P. E.; Baldein, R. L. *Science* **1990**, *249*, 1544-1548. (d) Lecomte, J T. J.; Kao, Y.-H.; Cocco, M. J. *Proteins: Struct. Funct. Genet.* **1996**, *25*, 267-285. (e) Cocco, M. J.; Lecomte, J. T. J. *Protein Sci.* **1994**, *3*, 267-281. (f) Jennings, P. A.; Wright, P. E. *Science* **1993**, *262*, 892-896.
(32) (a) Pace, C. N. *Methods in Enzymology.*; Academic Press, 1986; Vol. 131, pp 266-280. (b) Alonso, D. O. V.; Dill, K. A. *Biochemistry* **1991**, *30*, 5974-5985. (c) Schellman, J. A. *Biopolymers* **1978**, *17*, 1305-1322. (d) Schellman, J. A. *Biopolymers* **1987**, *26*, 549-559.
(33) (a) Pokar, N.; Lah, J.; Salobir, M.; Macek, P.; Gorazd, V. *Biochemistry* **1997**, *36*, 14345-14352. (b) Kirby, E. P.; Steiner, R. F. *J. Biol. Chem.* **1970**, *245*, 6300-6306. (c) Colonna, G.; Balestrieri, C.; Bismuto, E.; Servillo, L.; Irace, G. *Biochemistry* **1982**, *21*, 212-215.
(34) Tomaro, M. L.; Frydman, R. B.; Frydman, B.; Pandey, R. K.; Smith, K. M. *Biochim. Biophys. Acta.* **1984**, *791*, 342-349.
(35) (a) Takano, T. J. *J. Mol. Biol.* **1977**, *110*, 537-568. (b) Evans, S. V.; Brayer, G. D. *J. Mol. Biol.* **1990**, *213*, 885-897. (c) Hunter, C. L.; Lloyd, D.; Eltis, L. D.; Rafferty, S. P.; Lee, H.; Smith, M.; ; Mauk, A. G. *Biochemistry* **1997**, *36*, 1010-1017.
(36) Bunn, H. F.; Jandl, J. H. *J. Biol. Chem.* **1968**, *243*, 465.
(37) Wagner, U. G.; Muller, N.; Schmitzberger, W.; Falk, H.; Kratky, C. *J. Mol. Biol.* **1995**, *247*, 326-337.

PART VI.

SUMMARY AND GENERAL CONCLUSIONS

In the present thesis, I have aimed to elucidate molecular mechanisms of O_2 activations and oxygenations by P-450 and heme oxygenase (HO). For these purposes, I have focused on the electronic structure and functions of reaction intermediates proposed in the catalytic cycle of the enzymes by utilizing synthetic iron porphyrin complexes and mutant proteins. The results of the studies are summarized below.

Part II described the electronic structure, reactivity, and formation mechanism of a new high-valent iron porphyrin complex as a model for a possible reaction intermediate in the catalytic cycle of P-450. While the active species responsible for the oxidative metabolism of foreign compound by P-450 has been considered to be a high-valent oxo-iron porphyrin complex equivalent to Compound I (oxo-ferryl porphyrin cation radical, $O=Fe^{IV}Por^{+\bullet}$), the detailed electronic structure has not been resolved yet. In Chapter 1, I have described the preparation, characterization, and reactivity of the oxo-perferryl porphyrin complex ($O=Fe^{V}Por$) at -90 °C by using sterically hindered iron porphyrin complexes to prevent oxidative self-destruction of the complex. The electronic absorption and NMR data for the new reaction intermediate demonstrated a non-oxidized porphyrin ring, thus, very different from Compound I. Iodometric titration of the complex supported the two-electron oxidation from the ferric complex, and more importantly the S=3/2 system was confirmed by the ESR measurement. Thus, the most likely description for the new reaction intermediate is a high spin complex of either $O=Fe^{V}Por$ or $\bullet O\text{-}Fe^{IV}Por$ which is oxidized by two electrons from the iron-oxo unit. Finally, the resonance Raman result established the iron-oxo unit bearing a double bond character, suggestive of the $O=Fe^{V}Por$ rather than $\bullet O\text{-}Fe^{IV}Por$. Further, the oxo-perferryl complex was found to have high reactivity enough to perform epoxidation of olefins even at -90 °C. Thus, it is of importance to elucidate the factors switching Compound I to the oxo-perferryl porphyrin complex and its implication to the active intermediate of P-450. Thus, we focused on the mechanism regulating the formation of the reaction intermediates. As electron-withdrawing ability of the substituents bound to the porphyrin ring decreased, the reaction intermediate was found to change from the oxo-perferryl porphyrin complex to the oxo-ferryl porphyrin cation radical, accompanied with lowering of the redox potential of the $Fe^{III}Por/Fe^{III}Por^{+\bullet}$ couple. These results suggest that lower HOMO (a_{2u}) level of the porphyrin ring is necessary for the formation of the oxo-perferryl complex. Further, oxidation of the ferric porphyrin complex having strong electron-

withdrawing substituents in the absence of methanol afforded the oxo-ferryl porphyrin cation radical, which was converted to the oxo-perferryl porphyrin by the addition of methanol. The axial ligation of methoxide, which could destabilize HOMO of the iron (d_{xz} and d_{yz} orbitals), was also found to control the structure of the reaction intermediate. Therefore, these two effects eventually turn upside down the energy levels between the ring HOMO and the iron HOMO, and the higher level of the iron HOMO than that of the ring HOMO would be essential for the formation of oxo-perferryl complex.

Part III described a suicidal *meso*-oxidation related to the *meso*-hydroxylation catalyzed by heme oxygenase (HO) and the detailed reaction mechanism. Since α-*meso*-hydroxyheme is extremely reactive to be rapidly converted to a further metabolite, verdoheme, it has been difficult to examine the details of its formation. Thus, I have attempted to construct a model reaction equivalent to the *meso*-hydroxylation by employing less-sterically hindered iron porphyrin complexes to permit a suicidal oxidation of the complexes, and examine the detailed reaction mechanism. The suicidal *meso*-oxygenation of the complex has been successfully observed in the presence of a small amount of trifluoroacetic acid at -70 °C to afford a *meso*-monooxygenated isoporphyrin complex which is a putative precursor of α-*meso*-hydroxyheme. The oxygenation described in Chapter 1 is the first example of a synthetic model of the α-*meso*-hydroxylation catalyzed by heme oxygenase. The mechanism for the formation of the isoporphyrin complex was described in Chapter 2. Electronic absorption spectra recorded at 2-min interval demonstrated the formation of an intermediate during the reaction. The time-dependent absorbance change at the isosbestic point between the intermediate and the isoporphyrin complex showed a sigmoidal curve with an initial induction. These results are well interpreted as the pre-equilibrium between the starting complex and an oxidant-bound complex, which are spectroscopically indistinguishable, during the induction period followed by the O-O bond cleavage of the iron bound peracid to afford isoporphyrin complex *via* the intermediate. Furthermore, it was also suggested that the O-O bond of the oxidant cleaved in heterolytic fashion, and the leaving anionic group made a nucleophilic attack on a *meso*-carbon. Therefore, I propose that the heterolysis of the O-O bond of a ferric hydroperoxy complex ($Fe^{III}\text{-}OOH$) gives the isoporphyrin *via a nucleophilic addition* of hydroxide to a *meso*-carbon, and the following deprotonation of the

isoporphyrin complex at the *meso*-carbon led to the formation of α-*meso*-hydroxyheme.

As described in Part III, heme oxygenase regioselectively hydroxylates the α-*meso*-carbon of heme to yield α-*meso*-hydroxyheme in the first catalytic reaction. The regulation mechanism remains undetermined. In Chapter 1 of Part IV, sperm whale myoglobin (Mb) mutants were constructed by the double substitution of amino acid residues in the distal site to relocate the distal histidine-64 by position 29 (B10), 43 (CD1), and 107 (G8), and it was examined whether or not the regioselectivity was regulated by the arrangement of the distal histidine perturbing the orientation of the iron bound dioxygen in the HO-type model reaction. As the result, almost complete regulation of the regioselectivity was observed in the HO-model reaction of a H64L/L29H Mb mutant bearing the distal histidine located too far from the heme iron to directly interact with the bound dioxygen, and the Mb mutant afforded biliverdin IXγ as the major product. Since the environment near the α-*meso*-carbon of a H64L Mb mutant is as sterically open as that of wild-type Mb exclusively and gives biliverdin IXα in the HO-model reaction, the regioselectivity observed for the H64L/L29H Mb mutant seems not to be regulated by steric effect near the active site. Furthermore, the same Mb mutant was degraded most rapidly among all Mb mutants. Since the considerably polarized distal site was observed only for the Mb mutant like heme-HO, I proposed an indirect effect, e.g. a biased polarity, for the mechanism regulating not only the regioselectivity but also the reactivity in the heme degradation.

Heme-HO exhibits distinct spectroscopic features in comparison with Mb, while they share neutral histidine as the axial ligand which has the major effect on the electronic structure of heme. For instance, the unique property of HO appears in the NMR contact shift pattern characteristic of spin density delocalized primarily at the pyrrole positions adjacent to the α-*meso*-position and the large pH-dependence of the contact shift pattern. In Chapter 2 of Part IV, the Mb mutant having aspartic acid near the α-*meso*-position was prepared and effects of the carboxylate side chain on the active site structure of Mb and the HO-type heme degradation were examined. Various oxidation and ligation states of the Mb mutant showed spectroscopic properties nearly identical to those of heme-HO. Further, it was observed that protonation of the carboxylate side chain of the mutant shifted the 2-vinyl resonances near the α-*meso*-position like heme-HO. Thus, the Mb mutant bearing a carboxylate side chain near the α-meso-

carbon spectroscopically well-mimics the active site of heme-HO. However, the Mb mutant showed poor reactivity of the HO-model heme degradation, which would be rationalized by an uncoupling of the reaction to release H_2O_2 from the heme iron without the *meso*-hydroxylation. These results suggest that the location of a carboxylate side chain in HO must be strictly defined near the α-*meso*-position to efficiently hydroxylate the α-*meso*-position.

In Part V, an unique conformational change of HO was observed upon the substrate (heme) binding to HO by proton NMR, circular dichroism, and fluorescence spectroscopies. First of all, inter-segmental hydrogen bonds involving an exchangeable proton of aromatic side chains were formed at the sites relatively far from the substrate-binding site upon the addition of heme to HO. Further, HO is thermodynamically destabilized by making heme-HO complex. The heme binding also results in a decrease in helicity. By use of a fluorescent probe of non-polar binding site, it is found that the heme-binding site of HO is highly exposed to solvent relative to those of myoglobin and hemoglobin and is unlikely to be well-organized in the absence of heme. These results could allow us to imagine that a part of the α-helix of HO is destroyed and the two inter-segmental hydrogen bonds are subsequently formed to complete a hydrophobic core for heme uptake, and the increased amount of helicity of HO compared with that of heme-HO would serves stabilization of HO in the absence of heme which is known to stabilize intact myoglobin and also the other hemeproteins compared with their apo proteins.

As mentioned above, mechanisms regulating the diverse functions of the heme-containing monooxygenases were extensively studied by utilizing the structurally manipulated synthetic complexes and myoglobin mutants. The model approaches allow us to not only clarify the electronic structure and formation mechanism of unstable reaction intermediates but also provide significant insight into the structure-function relationships of the heme-containing monooxygenases. The advantage for the use of synthetic model complexes in organic solvents is the possibility to carry out the reaction at low temperature. By contrast, synthetic model complexes are not suitable to mimic a function of enzymes regulated by single or a few amino acid residues near the active site. Site-directed mutagenesis of structurally well-characterized proteins rather makes it possible to explore roles of selected single amino acid residue in the active site. Therefore, many active site mutants of Mb have been constructed to mimic the function and heme environmental structure of the resting

state, but have been hardly applicable to evaluate the influence of the electronic structure of unstable reaction intermediates, whose subtle differences determine the subsequent oxygenations as observed in this thesis, on the functions because of their insolubility in organic solvents. Recently, it has been shown that homogeneous solutions of enzymes in organic solvents can be prepared by the covalent modification of free amino groups on the protein's surface with poly(ethylene glycol). Especially, Mb have been successfully modified in this way to afford pegylated Mb nearly identical to intact Mb in the secondary structure. Therefore, pegylated Mb mutants with desired functions could provide more comprehensive insight into not only the whole regulation of O_2 activations and oxygenations by heme-containing monooxygenases but also structure-function relationships of heme enzymes. I believe that the present conclusions and suggestions certainly contribute to develop an area in bioinorganic chemistry.